Non-Darcy Flow Through Synthetic Porous Media and Development of Non-Darcy Coefficient Correlations

Abadelhalim Elsanoose, BEng, MEng

A thesis submitted to the School of Graduate Studies in partial fulfillment of the requirements for the degree of Doctor of Philosophy

Faculty of Engineering and Applied Science

Memorial University of Newfoundland

St. John's, Newfoundland, Canada A1B 3X5.

May 2023

Abstract

The flow in porosity is one of the hot research topics involved in many engineering applications, so there has been extensive research in this field. The flow in porous media is either Darcy or non-Darcy, depending on the flow velocities. Therefore, the need for a study that effectively: presents an experimental study that captures the complexity of the non-Darcy flow and calculates the non-Darcy coefficient is crucial. This study provides a comprehensive radial flow experimental method focusing on the non-Darcy flow in porous media. The study outlines samples preparation, updating the experimental setup, and analyzing the experimental data. The porous media samples were prepared from sand collected from local sources. The sand was dried, sieved, and classified into different grain sizes. The sand was mixed with an appropriate amount of epoxy; seven samples were prepared. A perforation was drilled in the center of each sample, and the perforation was considered the outlet. The experimental setup has been updated to be suitable for conducting single and multiple-phase flow experiments. Pressure sensors and three flow lines for water, gas, and oil with non-return valves were added. Three gas, water, and oil flowmeters were installed and connected to the DAQ. In this study, three experiments were carried out, the first using water as a working fluid, the second for compressible flow using air, and finally, multiple flows by mixing water and air. A radial flow experiment was conducted to investigate the existence of non-Darcy flow and calculate the non-Darcy "inertia" coefficient on seven cylindrical perforated synthetic porous media samples. Nonetheless, it was found that the non-Darcy flow exists even in the very low flow rate deployed in this study. Three criteria were used to detect the existence of non-Darcy flow:

Reynolds number Re, pressure forces vs. inertia forces curve, and hydraulic gradient vs. velocity. Reliable correlations for estimating the non-Darcy coefficient are introduced in this study, one of which considered tortuosity a vital parameter. The correlations resulted from analyzing the beta values obtained from experiments for two types of fluids on a wide range of flow rates and compared to other correlations reported in the literature. In Addition, an experimental and numerical study of multi-phase flow in porous media near a perforation was conducted. The effect of properties on the flow, such as porosity and permeability, are crucial for increasing oil and gas production. The numerical validation of the two-phase flow experimental results was using ANSYS software. The investigation confirms that the flow rate of water mainly determines the steady state, while the flow rate of air primarily affects the unstable stage. The equations reached in this study can be relied upon in the Forchheimer equation, which is widely used in industrial applications to calculate the pressure drop in the oil and gas industry. The limitations of this study are the use of only two types of fluids and the number of samples. This study may be more comprehensive if more fluids are used and samples with less permeability and porosity than the current samples.

This dissertation is dedicated to my parents

My late father, Mohammed Elsanoose, who was my idol, to my mother, Maryam Massry, your endless love, prayers, and support is the light of my life.

My wife

Hafsa Mraiky, who was there for me throughout this journey, it couldn't have been done without your support

&

My kids

Fatima, Khadija, and Ibrahim, for their endless love and support

Acknowledgment

I would like to express my gratitude to my supervisory committee, who guided me throughout this project. I would also like to thank my supervisor Prof. Faisal Khan for his support, guidance, and courage, which offered deep insight into the study. I would also like, at this critical moment, to express my deep gratitude and thanks to my former supervisor, the late Professor John Shirokoff. I would also like to express my appreciation to Professor Mohammad Azizur Rahman for his guidance, ideas, and broad lines that were the basis for this research, as well as his assistance in completing research papers and covering the costs of publishing some of them. Thanks and gratitude go to Professor Amer Aborig for his generous efforts and support throughout completing this study. He was with me step-by-step through the conduct of laboratory experiments, starting with preparing samples and then checking the properties of all samples with Edison's aid. Professor Amer Aborig was the direct supervisor of the fluid flow experiments, and thanks to his efforts, the results became a reliable reality.

I would like to express my gratitude to Dr. Stephen Butt for providing the experimental setup and reviewing the manuscripts. Further, I do not forget to extend my thanks to Dr. Syed Imtiaz, who provided a place for the experimental design, and Dr. Edison Sripal, who helped us measure the index properties for synthetic samples.

Contents

List of Tables

List of Figures

Nomenclature

β	non-Darcy flow coefficient, m^{-1}
φ	porosity, adimensional
μ	fluid viscosity, Pa s
ρ	fluid density, kg m^{-3}
ρ_p	air density at the air compressor
Q_p	volumetric flow rate
β	non-Darcy coefficient
φ	Porosity
τ	Tortuosity
ρ	Density
υ	viscosity
α_q	Volume fraction
γ	Porosity
ρ_q	Phase density
$\overline{\overline{\tau}}$	Stress tensor related to viscous flow
$\overline{\overline{\tau_q}}$	Phase shear stress
υ	Viscosity of water
k	Permeability
kr	Relative permeability

A	flow area, m^2
c	zRT/M, J
M	molecular weight
P	pressure, Pa
q	volumetric flow rate, $m^3\ s^{-1}$
Qm	mass flow rate, kg s^{-1}
T	temperature, K
u	seepage velocity, Darcy's velocity, m s^{-1}
v	fluid velocity, superficial velocity, m s^{-1}
z	compressibility coefficient
v	Fluid velocity
P	Pressure
g	Gravity
i	Hydraulic gradient
f	Friction factor
re	Shape factor efficiency
R	Hydraulic mean radius
Re	Reynolds number
Sw	Water saturation
a, b	Are constants calculated experimentally
$\vec{F}_{pq}^{D}$	Drag force for non porous flows/region

$\vec{F}_{pq}^{TD}$ Turbulent dispersed force

$\vec{F}_q$, $\vec{F}_q^L$ *and* $\vec{F}_q^{vm}$ External body, lift, and virtual mass exchange forces

M.P.D. Mean pour diameter

M.I.P. Mercury intrusion porosimetry

Chapter 1

1. Introduction and overview

1.1 Introduction

The flow in porous media gained much attention at the beginning of the emergence of the oil and gas industry. Fluid flow and transport in porous media are of fundamental importance to various systems of scientific interest and application. The flow and the pressure drop data are essential for understanding the nature of the flow in porous media [1]. A well's productivity and life span depend on the flow behavior and pressure data; depending on that data, decisions can be made on whether the well needs to be injected with fluids that help increase the reservoir pressure [2]. Other fields, such as extracting water from the ground, civil engineering, multiphase flow in packed bed reactors, and agricultural irrigation, all deal with the flow in porous media. Studying the flow in porous media is also essential in other engineering fields, such as drying biological materials and biomedical studies [3].

The flow in porous media is a complex phenomenon where various parameters interfere with the process. Each porous media has its own singularity defined by its porous geometry and unique nature. To understand the flow in porous media, we need fluid mechanics, chemistry, rheology, petroleum engineering, etc. [4]. The flow in porous media differs from that in pipes by overlapping properties such as permeability, porosity, and tortuosity. In addition, the flow in porous media becomes complex if various physical property changes and chemical reactions occur. Properties that could change during the flow include viscosity, surface tension, phase state, concentration, and temperature [5].

The French engineer Darcy was the first who present an equation describing the flow in porous media when he needed to know the amount of sand required to filter a certain amount of water, so he obtained this information in the laboratory. Through those laboratory experiments, he introduced the famous Darcy equation. Darcy's equation can describe the flow and calculate the pressure gradient in the oil industry. However, as the flow approaches the well, the pressure decreases, the flow accelerates, and the most significant pressure drop occurs [5].

Darcy simplified his equation by assuming that the viscous forces are much greater than the inertia forces and, therefore, the inertia forces can be neglected. This assumption may be possible in the slow flow. However, with more deep experimental investigation and field measurements, it became clear to the researchers that inertial forces are essential, and the relationship between pressure gradient and fluid velocity becomes nonlinear even if the velocity is slow in many cases [6]. In general, non-Darcy Flow is the flow that has a non-linear relationship between flow rate and pressure difference and cannot be described by Darcy's law.

In order to address the additional pressure and drop, the Forchheimer equation was introduced. The additional term includes the Forchheimer or non-Darcy coefficient [7]. It is an empirical value whose physical meaning has not yet been accurately defined, but it represents the inertial resistance in a porous medium and depends on the pore geometry and fluid properties. Different mechanisms have been presented to explain the non-Darcy phenomenon described in the Forchheimer equation, and it was attributed to turbulence [8]. However, since the 1970s, many researchers concluded that the non-Darcy flow is not due

to turbulence but to inertial effects, as they found that the non-Darcy flow occurs even at a low Reynolds number [9]. It can be concluded that the non-Darcy flow is a universal phenomenon in oil and gas reservoir development and affects most aspects of reservoir engineering analysis, such as reservoir parameter estimation, reservoir development planning, and reservoir performance prediction. Field flow and pressure data are not usually available. Still, fortunately, this data can be collected in the Lab using artificial or real samples with different properties in terms of permeability and porosity

This study presented a novel experiment for studying the non-Darcy flow in porous media using radial flow and cylindrical large synthetic porous media and the two-phase flow behavior. The current study also produced novel correlations that calculated the non-Darcy coefficient β. Moreover, this study will help clarify and understand the flow behavior in the porous media.

This study provides an extensive investigation into the effect of the properties of porous media on the non-Darcy flow. Among those critical properties is tortuosity, which many researchers neglect due to the difficulty of calculating it mathematically and the lack of appropriate devices to measure it.

There are differences between the non-Darcy coefficient correlations that available in the literature. These differences are attributed to several reasons such as permeability, porosity, and tortuosity are the three major players in the correlations, the porous media pore geometry, the flow direction and the size and the geometry of the samples. Also, most of these studies, only incompressible fluids were used, and the experimental runs were few [10].

The Radial Flow Facility used in this experiment is unique in its design, as the flow enters the samples radially, which is the closest to reality. In addition, the design allows high pressures and flow rates during the experiment.

Non-Darcy flow in porous media is studied by recording pressure and flow data under various conditions. This data makes it possible to determine the point at which the flow begins to transform from a Darcy flow to a non-Darcy flow.

The main investigative procedures of experimental and numerical analysis have been used in this study to reach the following objectives:

1. Propose a technique for preparing synthetic samples that can be applied to this study and oil and gas production research.
2. Characterization of the non-Darcy flow by providing intensive investigation of the significant parameters that affect the flow, such as the permeability porosity and, most importantly, the tortuosity.
3. Accurately calculating the non-Darcy coefficient β using compressible fluid (air), where calculating the density and the viscosity is crucial during the experimental runs.
4. Introduce non-Darcy coefficient β correlations; these correlations were reached by conducting 381 experiments on two types of fluids (water and air). In total, 14 β points were reached.
5. Introducing a new correlation for the non-Darcy coefficient that includes the sample's tortuosity, which is not common in the literature.

6. Studying the effect of two-phase flow conditions and sample properties (the liquid and gas flow rate, liquid viscosity, permeability, and porosity) on the injection build-up pressure and the time needed to reach a steady-state flow condition.

1.2 Methodology

1.2.1 Sample preparation

The experimental setup was designed to deal with a specific size of the samples. The first of these difficulties was finding a source that could cut samples of the required sizes; the other most crucial thing is the properties of those samples in terms of porosity and permeability [11]. The properties index of the samples plays an essential role in conducting the experiments. The samples must have a suitable gradient in the values of porosity and permeability to test the effect of these properties on the flow, for example when the value of permeability is small, what is the impact on the flow, and how do the pressure drop values change when the permeability increases. The capability of the experimental setup to inject the fluid through the samples depends on the sample's permeability and porosity; for example, the real samples, which have very low permeability, need a pump with high pressure that may not be available in the lab. Thus, the prepared synthetic permeable samples are suitable for the experimental setup. The sand was collected, considering that the grains' size is diverse, which allowed the preparation of several samples with different properties indexes. The next stage was drying the sand in an

oven at high temperatures to facilitate the sieving process and ensure that the small grains did not stick to the large ones.

Figure 1. Part of the sieving process results

The sieving process resulted in eight sizes; used each size to manufacture a sample so that the samples were homogeneous. After sieving and classifying the sizes of the grains, the manufacturing process starts with mixing the sand with specific quantities of epoxy enough to give the samples the required hardness; at the same time, the pores are not blocked with epoxy.

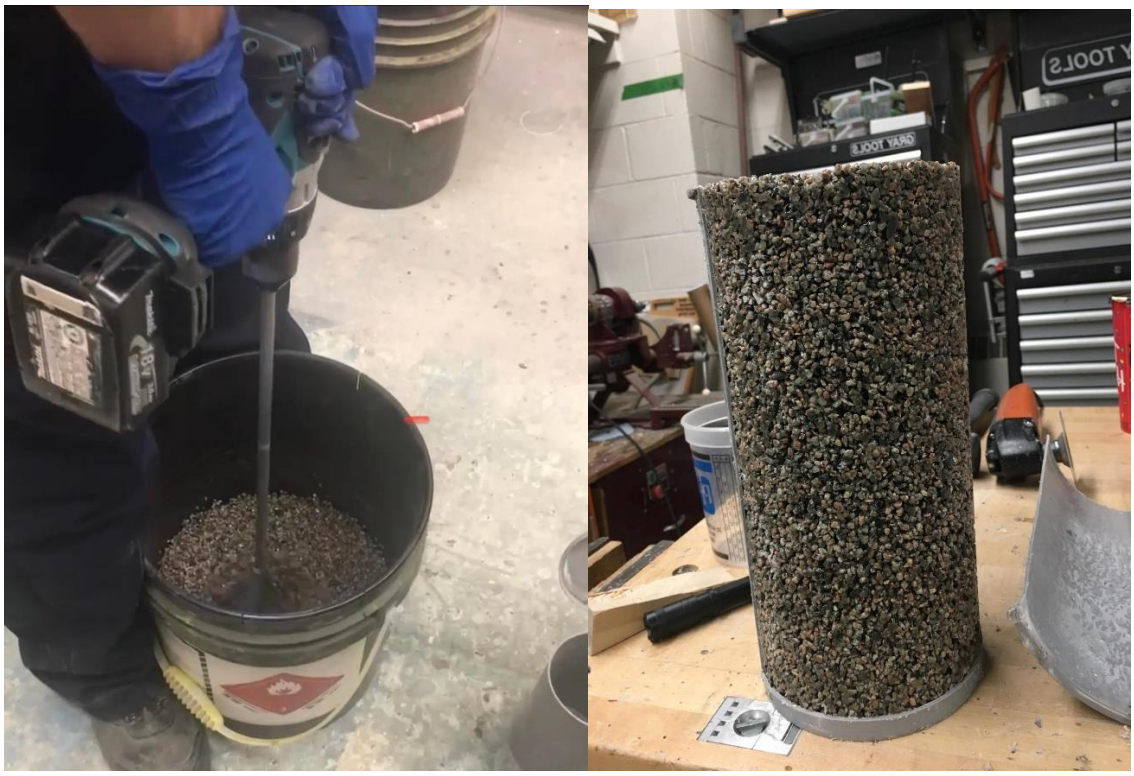

Figure 2. Mixing the sand with specific quantities of epoxy

The mixture was then poured into a cylindrical plastic container with a height of 31.8 cm and a diameter of 15.54 cm. A vibrator was used to ensure no voids or holes in the samples. The samples are then left to dry for 24 hours. In the drilling lab, a perforation is drilled in the sample's center and used as an outlet during the flow experiments.

Figure. 3 Drilling a perforation in the drilling Lab.

1.2.2 Measurement of the Properties of the Sample

Mercury Intrusion Porosimeter (MIP) is a powerful technique wildly used to evaluate porosity, permeability, tortuosity, pore size distribution, and characterization of a wide variety of solids and materials. Permeability is the quality or state of being permeable—able to be penetrated or passed through, especially by a liquid or gas. The instrument, known as a porosimeter, employs a pressurized chamber to force mercury into the voids in a porous substrate. As pressure is applied, mercury fills the larger pores first [12]. As pressure increases, the filling proceeds to smaller and smaller pores. Both the inter-particle pores (between the individual particles) and the intra-particle pores (within the particle itself) can be characterized using this technique.

Mercury Intrusion Porosimeter (MIP) was used at the University of Memorial of Newfoundland labs to characterize and analyze the synthetic samples' pore morphology and index properties. The index properties, including permeability, porosity, median pore diameter, and tortuosity, are listed in “Table 2. Chapter 3”.

1.2.3 Grain Size and the Index Properties for the Samples

There is a direct relationship between the particle size and the properties of the manufactured porous media. The size and shape of the grains, whether rounded or angular, for example, determine the porosity of the porous media [13]. Screening the grains and classifying them into sizes is one of the critical steps in manufacturing porous media. Manufacturing a sample by mixing more than the size of the grains may change the direct relationship between the grain size and the properties of the porous media. When combining several sizes of grains, the smaller grains fall into the pore, and the spaces narrow [14]. As a result, the direct relationship, as in Figures 4/6, is inverse, or there may be no relationship, depending on the proportions of mixing small grains with large ones and compaction.

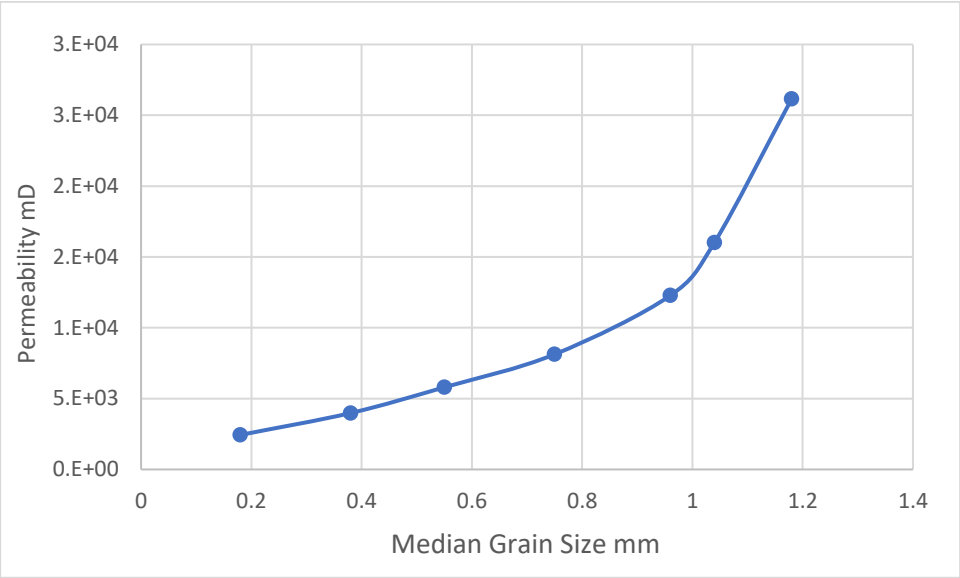

Figure 4. Effect of median grain size on Permeability

Figure 4 illustrates the relationship between the size of the grains and the permeability of the porous media samples; it can be seen that the permeability is directly proportional to the size of the grains. The greater the grain size, the greater the permeability, and vice versa; that is true only if one size is used to manufacture each sample.

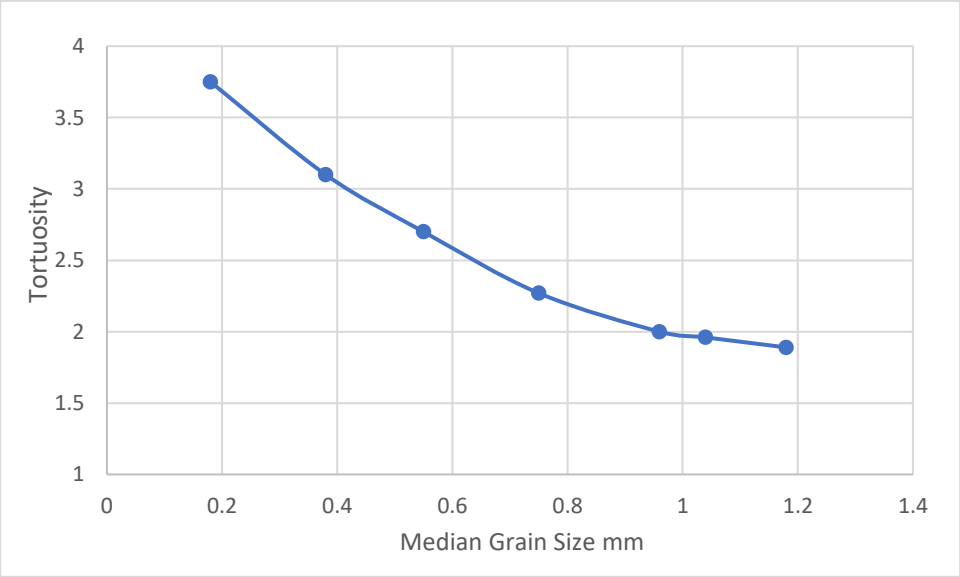

Figure 5. Effect of median grain size on tortuosity.

Tortuosity is an intrinsic property of a porous material usually defined as the ratio of actual flow path length to the straight distance between the ends of the flow path. In contrast to the permeability, the tortuosity is inversely proportional to the grain size. Figure 5.1 shows that the tortuosity value decreases with the increase in median grain size. However, the median pore size increases with the median grain size Figure 6.

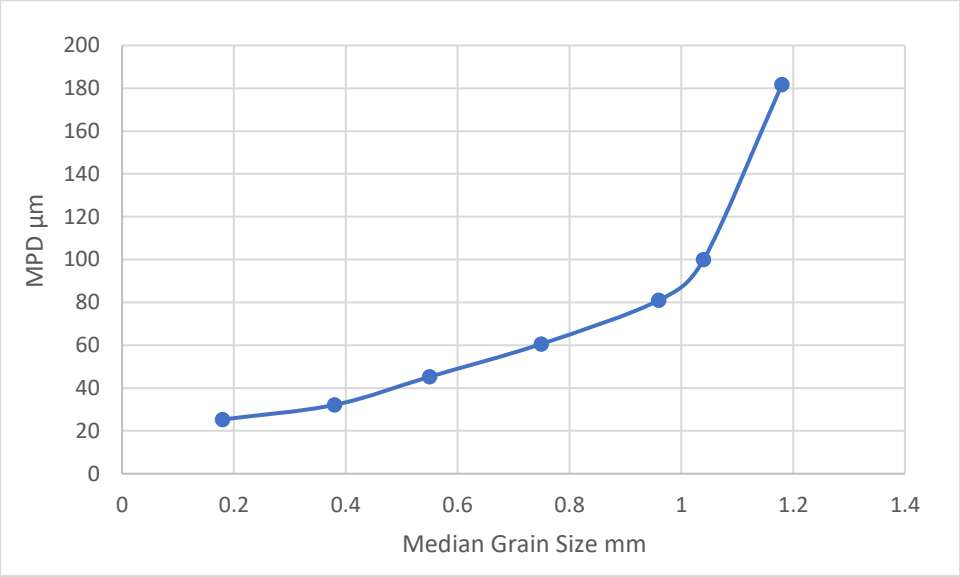

Figure 6. Effect of median grain size on mean pore diameter.

1.2.4 Experimental Method

In the present study, we updated the experimental setup initially designed and built by Ahammad et al. [15] as a radial flow cell (RFC) to work with three-phase gas, water, and oil in a cylindrical sample. The RFC, constructed at Memorial University of Newfoundland's Drilling Technology Lab, was created to carry out experiments under wellbore conditions. Figure.2.3 “Chapter 2” shows the setup, which features the three main sections: flow lines extending from inlet to outlet; this component consists of flow meters,

pressure gauges, inlet, and outlet flow boundary, flow control valve, pumps, and temperature meters. Switching from a control panel can alter the flow lines for divergent flow. An inner chamber for holding samples and a Data Acquisition (DAQ) system. Experiments on perforation methods have primarily relied on rather simplistic assumptions, such as those presented by Rahman et al. [16]. Moreover, due to laboratory constraints, most experimental investigations have neglected key reservoir characteristics, such as thermal effects, drawdown pressure, and actual reservoir pressure.

In the experimental portion of this work, we injected a measured volume of a single-phase (water or air) or two-phase (air/water) into our core sample. We also used a geotechnical radial flow test setup to measure the samples' differential pressure and flow rate, with air and water radially injected into cores within the following boundary conditions. The outer side of the sample is considered an inlet, while the perforation surface is an outlet.

1.2.5 Numerical Procedure

ANSYS 18.1 FLUENT (3D) was used to simulate the multiphase flow pattern in the porous media. For the multi-phase flow model, the volume of fluid method coupled with the RNG k-ε turbulence model has been applied to solve the turbulent air-water flow pattern. The Volume Of Fluid method (VOF) is designed for immiscible fluids where it can predict the situation of the interface between the immiscible fluids during the flow time. The k-ε turbulence model is the most common turbulent model used in computational fluid dynamics. The k-ε turbulence model derived from Reynolds Averaged Navier Stokes (RANS) equations is often applied for simulating multiphase flows, with greater or lesser

success rates inaccuracy. Fig. 5 shows the geometry of the area surrounding the perforation; the geometry of a cylindrical core sample with a perforated hole at the center is used for the numerical simulations. The sample dimensions are 30.48 cm high, 15.24 cm radius, 2.54 cm radius of the perforation, and 25.4 the depth of the perforation.

1.3 Uncertainty Analysis

The approach proposed by Kline and McClintock [17] has been employed to calculate the uncertainty in the experiment's measurements. This technique is often called the root-sum squared (RSS) method. The uncertainty in the results can be estimated from the uncertainties in the primary measurements. Assume that experimental measurement of independent variables, $V_1, V_2, , V_3, \dots, V_n$ are taken, then replicate measurement's mean value V_m may be expressed as

$$V_m = \frac{V_1, V_2, , V_3, \dots, V_n}{n} = \frac{\sum_{i=1}^{n} V_i}{n} \tag{1}$$

In statistical parlance, the term "uncertainty" is associated with a measurement that refers to the expected variation of the value derived from an average of several readings from the true mean of the data set or readings. In other words, the uncertainty can be considered the standard deviation of the data set's mean [18]. The formula for uncertainty can be derived by summing squares of deviation of each variable from the norm, then dividing the result by the product of the number of readings and the number of readings minus one, and then computing the square root of the outcome [19]. Mathematically, the Uncertainty Formula is represented as, Where

$$U = \sqrt{\frac{\sum_{i=1}^{n}(V_i - V_m)}{n * (n-1)}} \quad (2)$$

Where U is the uncertainty, V_i is a reading, V_m

The uncertainty in the experimental measurements of temperature, pressure, and flow rate are summarized in Table 1. Furthermore, the uncertainties in the properties of the working fluid are $\pm 0.5\%$.

Table 1. Uncertainty in Measurements

Measurement	**Uncertainty**
Airflow Rate $[m^3/s]$	± 0.1
Water Flow Rate $[m^3/s]$	$\pm 0.05\%$
Pressure [Pa]	$\pm 0.08\%$

The first strategy involved replacing our sensor with a trusted and more accurate one, after which we checked the measurement readings at the same flow boundary conditions and 210 compared them against earlier readings. In the second strategy, we employed both manual and theoretical calculations. Manual calculations were obtained by collecting and then measuring liquid quantities at the outlet and calculating the time needed. The calculated flow rate results were then compared against the meter readings for the flow rates.

1.4 Contributions

This study's main contributions are to present a novel experimental technique by creating prototype synthetic samples that mimic near-wellbore conditions and a numerical model that can predict the pressure of two-phase flow more accurately. Earlier methods to predict the non-Darcy coefficient and characterization of non-Darcy flow remain relatively impractical from an applicability perspective when considered for use in different reservoir types. This lack of practical applicability is caused by issues around non-Darcy coefficient correlation units accuracy, geometrical effects, and the nature of the experiments. Therefore, this study will comprehensively analyze non-Darcy fluid flow in the near-wellbore region and find new correlations that calculate the non-Darcy coefficient considering the tortuosity.

1.5 Industrial applications

Flow in porous media has many engineering applications starting from the petroleum industry, civil engineering, groundwater extraction and agricultural engineering, and many other fields. For example, understanding the nature of fluid flow in porous media is essential in determining oil tanks' productivity and lifespan. Typical porous media applications include catalytic and chromatographic reactions, packed absorption and distillation towers, ion exchange columns, and packed filters.

1.6 Organization of the thesis

This thesis has five chapters. The first chapter describes the introduction, the literature review, objectives, methodology, contributions, industrial applications, and thesis organization.

In chapter 2, Experimental Investigation of Single Flow Through Porous Media Around Perforation Tunnel

In chapter 3, Estimating of Non-Darcy Flow Coefficient in artificial Porous Media

In chapter 4, Characterization of a non-Darcy flow and a new correlation of the non-Darcy coefficient

In chapter 5, Investigation of Multiphase Flow in Porous Media Around Perforation Tunnel Near Wellbore Region, Experimental and Numerical Study.

In chapter 6 Conclusion and future work

References

[1] Daïan, Jean-François. Equilibrium and Transfer in Porous Media 2: Transfer Laws. London, UK: ISTE, 2014.

[2] Dullien, F. A. L. Porous Media: Fluid Transport and Pore Structure. Second edition. Oxford: Elsevier Science, 1991.

[3] Adler, Pierre M., Jean-François. Thovert, and Valeri V. Mourzenko. Fractured Porous Media. Oxford: Oxford University Press, 2013.

[4] Feder, Jens, Eriik Grude Flekkøy, and Alex Hansen. Physics of Flow in Porous Media. Cambridge, United Kingdom ; New York, NY: Cambridge University Press, 2022.

[5] Allen, Myron B., G. A. Behie, J. A. Trangenstein, G. A. (Grace Alda) Behie, and J. A. (John Arthur) Trangenstein. Multiphase Flow in Porous Media: Mechanics, Mathematics, and Numeric. New York ;: Springer-Verlag, 1988.

[6] Greenkorn, Robert Albert. Flow Phenomena in Porous Media: Fundamentals and Applications in Petroleum, Water, and Food Production. New York: M. Dekker, 1983.

[7] Szymkiewicz, Adam. "Modelling Water Flow in Unsaturated Porous Media: Accounting for Nonlinear Permeability and Material Heterogeneity." GeoPlanet: Earth and Planetary Sciences, 1. Aufl., vol. 9, Springer-Verlag, 2013,

[8] Dejam, Morteza, Hassan Hassanzadeh, and Zhangxin Chen. "Pre-Darcy Flow in Porous Media." Water Resources Research 53, no. 10 (2017): 8187–8210.

[9] Jia, Zejiang, Zhengfu Ning, Guanghui Yang, Wentong Zhang, Zhilin Cheng, and Zhu Mao. "Experimental Investigation on the Effect of Solid–Liquid Interface Charge Transport on Natural Porous Media Flow." Transport in Porous Media 143, no. 3 (2022): 579–98.

[10] Matyka, MacIej, Arzhang Khalili, and Zbigniew Koza. "Tortuosity-Porosity Relation in Porous Media Flow." Physical Review. E, Statistical, Nonlinear, and Soft Matter Physics 78, no. 2 (2008): 026306–026306.

[11] Babakhani, Peyman, Jonathan Bridge, Ruey-an Doong, and Tanapon Phenrat. “Parameterization and Prediction of Nanoparticle Transport in Porous Media: A Reanalysis Using Artificial Neural Network.” Water Resources Research 53, no. 6 (2017): 4564–85.

[12] Wyrzykowski, Mateusz, René Kiesewetter, Josef Kaufmann, Robert Baumann, and Pietro Lura. “Pore Structure of Mortars with Cellulose Ether Additions – Mercury Intrusion Porosimetry Study.” Cement & Concrete Composites 53 (2014): 25–34.

[13] Civan, Faruk. Porous Media Transport Phenomena. Hoboken, N.J: Wiley, 2011.

[14] Ho, Clifford K., and S. W. Webb. Gas Transport in Porous Media. Edited by Clifford K. Ho and S. W. (Stephen W.) Webb. Dordrecht: Springer Netherlands, 2006.

[15] Ahammad, M. J., Rahman, M. A., Butt, S. D., & Alam, J. M. (2019a). An experimental development to characterize the Flow phenomena at THE Near-Wellbore Region. ASME 2019 38th International Conference on Ocean, Offshore and Arctic Engineering. Glasgow, Scotland, UK: Volume 8: Polar and Arctic Sciences and Technology; Petroleum Technology.

[16] Kline, S., and F. Mcclintock. "Describing Uncertainties in Single-Sample Experiments." Mechanical Engineering 75 (1953): 3-8.

[17] Rahman, M. A. (2008). Scale-up of perforation process from laboratory model to bottom hole dimensions. Journal of Porous Media, 11(1), 19-34.

[18] Gupta, S. V. Measurement Uncertainties: Physical Parameters and Calibration of Instruments. Berlin, Heidelberg: Springer Berlin Heidelberg, 2012.

[19] Pintelon, R., P. Guillaume, and J. Schoukens. “Uncertainty Calculation in (operational) Modal Analysis.” Mechanical Systems and Signal Processing 21, no. 6 (2007): 2359–73.

Chapter 2

Experimental Investigation of Single Flow Through Porous Media Around Perforation Tunnel

Preface

A version of this chapter has been published in Conference TFEC-2022-40935. I am the primary author of this manuscript, along with co-authors Dr. Abobaker, Dr. Faisal Khan, Dr. Rahman, Dr. Amer Aborig, and Dr. Butt. Dr. Butt assisted in the design of the setup. I proposed the idea and concept and prepared the samples with assistance from Dr. Amer and Abobaker; they also helped conduct the experiments. However, I collected and analyzed the experimental data. Dr. Aziz evaluated the methodology and reviewed the manuscript. I wrote the original manuscript, and Dr. Aziz reviewed the manuscript and suggested amendments that significantly impacted this manuscript.

2.1 Abstract

The flow near-well reservoir region during injection or production is not fully understood. This flow needs to be characterized and its origins fully understood, as it is critical for a well's productivity. This study investigates the existence of non-Darcy flow by testing a wide range of flow rates for compressible and incompressible. The difference in pressure squared and mass flow rate calculated from the volumetric flowmeter set at the injection pump) would generate a straight line, indicating the linear behavior of Darcy flow. However, the test results to check the flow's nonlinearity showed that the trend depicted is not linear. One of the assumptions that could justify such a deviation from linearity is that permeability does not change with flow rate. Lastly, the mass flow rate is constant across the core. Still, the volume flow rate can change even threefold (mainly due to different pressure gradients), leading to similar changes in density and viscosity to a certain extent.

2.2 Introduction

Since the Darcy equation was introduced, it has gained a lot of attention as the Darcy equation describes the flow in porous media, especially with the discovery of oil. According to Darcy's law, the pressure drop is entirely determined by the viscous resistance between the surface of the fluid and the solid [1]. However, some experiments on low-velocity flow in low-permeability porous media prove an additional loss in pressure exists. Excess pressure drop induced by inertial effects limits Darcy's law's applicability for modeling fluid flow through porous media at low and high velocities [2]. Many researchers have found that the pressure gradient in a low flow velocity regime is higher than what Darcy's law estimates. This low-velocity non-Darcy flow phenomenon exists in low and extra-low permeability reservoirs near-wellbore regions. The permeability of a real sample obtained from reservoirs is low that it practically cannot measure a minimal steady-state flow rate in a Lab experiment [3]. Generally, low-velocity non-Darcy flow is affected by the interaction forces between the fluid and tight pores in small pressure gradients and low velocities. The interaction forces can be referred to as the boundary layer effect. The fluid within a pore can be divided into boundary fluid and inner free fluid. The boundary fluid has a relatively higher density and viscosity [4]. The inertia resistance factor, or the so-called factor β, a parameter in the Forchheimer equation for quantifying the non-Darcy flow effect, is routinely measured for proppant packs.

The non-Darcy flow in porous media occurs if the flow velocity becomes large enough so that Darcy's law for the pressure gradient and the flow velocity is no longer applicable [5]. According to the oil and gas industry convention, the β factor is generally

deduced experimentally from the slope of the Forchheimer graph (i.e., the plot of the inverse of the apparent permeability $1/k_{app}$ vs. a dimensional pseudo-Reynolds number($\rho V/\mu$). The apparent permeability K_{app} is defined as [6]:

$$\frac{1}{K_{app}} = -\frac{\nabla P}{\mu V} = \frac{1}{K} + \beta \frac{\rho V}{\mu} \quad (1)$$

Both Darcy's law and the Forchheimer equation originated empirical equations driven from experiments. It is generally agreed that Darcy's law describes the laminar flow regime with zero inertia, whereas the Forchheimer equation represents the laminar flow regime with inertia effect [7]. The transition from the Darcy flow regime to the Forchheimer regime can usually be observed based on pressure drop and flow-rate measurements. However, local flow investigations in pore space are necessary to determine the range of applicability for the Forchheimer equation and explore the flow behaviors beyond the Forchheimer regime. Experimental results on identifying flow regimes using local measurement techniques such as electrochemical microprobes are then reviewed [8]. Fritz [9] studied the non-Darcy flow experimentally, where nitrogen was injected horizontally at various flow rates in several directions into a Berea sandstone core sample. The experimental results found that when the flow rate was low, the fluid flow followed Darcy's Law, and when the flow rate was high, the fluid flow departed away from the linear relationship between the differential pressure and the flow rate. However, that opinion has been doubted as many experimental studies found that the pressure losses are higher than Darcy's Equation. Many researchers have long been interested in clarifying the physical reason for nonlinearity. Early descriptions attributed the nonlinearity to the occurrence of turbulence. However, experiments have indicated that when the macroscopic velocity gradually increases, the

nonlinear phenomena appear much before the turbulence in porous media flow occurs [10]. Thus, it can be concluded that flow regime changes may not initiate deviations from Darcy's law if the inertia force is neglected. This paper reports a laboratory study in which the existence of non-Darcy flow in compressible and incompressible flow is investigated. Three synthetic samples were used in this study, and air and water were used in the flow experiments.

2.3 Experimental procedure:

The experiments begin with preparing the samples by mixing the sand and epoxy in appropriate quantities. Three samples of the proper size were prepared to fit into the experimental setup chamber, figure 1. The sample dimensions are 30.48 cm high and 15.54 cm in diameter, and a perforation tunnel has a 25.54 cm depth and 2.54cm diameter. A cylindrical perforation is considered the flow outlet. Mercury Intrusion Porosimetry (MIP) was used to characterize and analyze the synthetic samples' pore morphology and index properties. The index properties include permeability, porosity, median pore diameter, and tortuosity table 1. In the flow test, the air compressor is connected to the setup, ensuring no leakage in the lines and connecting all pressure sensors to the DAQ. Radial flow facility Fig. 2 has been updated with five pressure sensors that have been calibrated with pressure sensors from other experiments. Two pressure sensors were placed on the inlet and outlet, and the rest was placed on the fluid mixing lines.

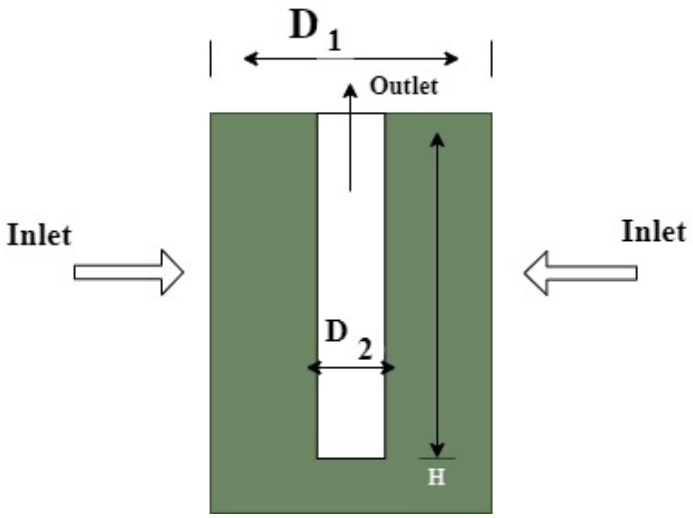

Figure 1. Schematic Drawing of the Samples.

The flow rate ranged from 3 to 50 LPM, the samples were tested one by one, and all pressure and flow data were recorded.

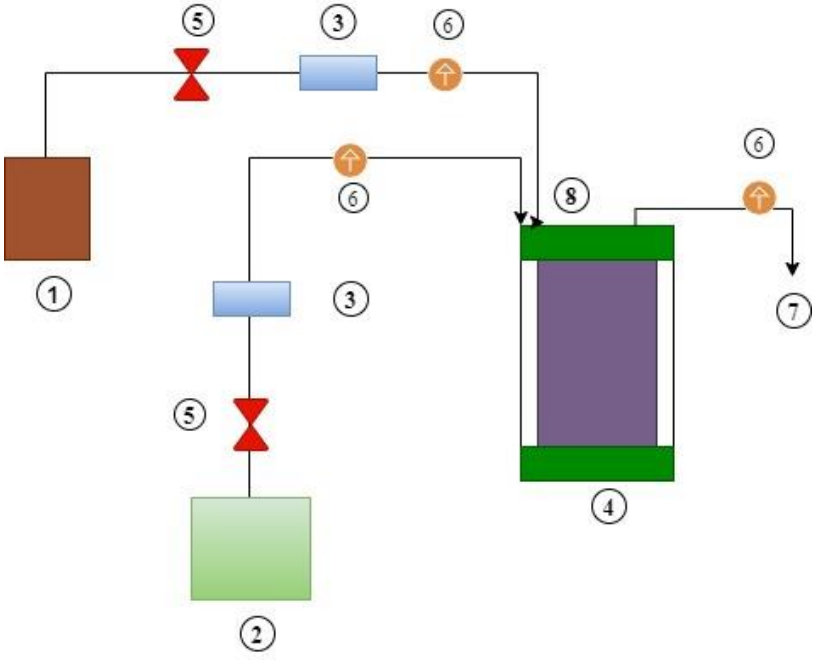

Figure 2 shows the experimental setup. (1) water pump. (2) air compressor. (3) flow meters. (4) sample chamber. (5) Non-Return valve. (6) pressure sensors. (7) Out-Let. (8) In-Let

2.4 Experimental results and analysis

We tested three cores in this experiment; the results are shown in Fig. 3, 4, 5, and 6. The flow rate and pressure gradients in the rectangular coordinate system are the abscissa and ordinate, respectively. The figure shows that the pressure gradient and flow rate have a better linear relationship when the flow rate is low. As the flow rate increases, the curve departs from linearity and tilts towards the pressure gradient axis, i.e., there is an obvious non-Darcy.

2.5 Compressible flow

Equation (1) is considered for a compressible flow, and the air is an ideal gas. The density is a function of pressure and temperature in the case of compressible flow. Assuming mass flow rate (Qm), gas density (ρ), and volumetric flow rate (q) can be expressed as follow:

$$Q_m = \rho q \qquad \rho = \frac{MP}{zRT} \tag{2}$$

Where p=pressure, A=cross-sectional area of fluid flow, v=fluid velocity. Then it is possible to derive the following expression M=molecular weight, z=compressibility factor, R=gas constant, T=temperature. For gases, the Equation is best expressed in terms of mass velocity Q_m= ρv because the mass velocity is constant when the cross-section is constant; the Forchheimer equation can be written in the following form [10]

$$\frac{P_1^2 - P_2^2}{\frac{zRTQ_m\mu}{M\pi h}} = \frac{1}{K} ln \frac{r_2}{r_1} + \frac{\beta Q_m}{2\pi h\mu} \left(\frac{1}{r_1} - \frac{1}{r_2}\right) \tag{3}$$

Equation (4) describes the non-Darcy flow in porous media, flow data, air compressibility, and other parameters obtained at the operating pressure and temperature. The properties of

porous media are usually calculated in several ways; one of the most widely used is Mercury Intrusion Porosimetry (MIP). The permeability and porosity of the three samples were calculated in Memorial University laboratories. Three small pieces were taken from each sample; those small pieces were tested, and the results of those tests are recorded in the following table (1). The measurement accuracy is ± 2%.

Table (1) The index properties for the samples

Sample No.	The index properties for the samples			
	Permeability (mD)	Porosity (%)	Tortuosity	Median pore diameter (μm)
Sample1	2035.95	21.5	3.62	25.31
Sample2	3981.50	26.2	3.19	32.14
Sample3	6292.66	27.3	2.82	45.27

The other important parameter that must be calculated in Equation (4) is β or the non-Darcy flow coefficient. Many equations in the literature are used to calculate β, derived from laboratory experiments or field data. There are many differences between these equations Because each was extracted using a different sample type. One of the widely used correlations is Geertsma's equation.

$$\beta = \frac{0.005}{k^{0.5} \times \varphi^{5.5}} \tag{4}$$

Where k and are permeability and porosity respectively.

The following table contains the calculated values for the non-Darcy coefficient; the values were calculated using the corresponding permeability and porosity from Table (1).

Table (2) non-Darcy coefficient

Sample No	β
Sample1	440041.83
Sample2	153871.68
Sample3	122395.33

Results and Discussion

By considering the validity of Darcy's law and assuming M, R, T, A, and k as constants, they are then plotting the difference of pressure squared ($P_2^2 - P_1^2$) vs. $Q_m \mu$ (where Qm mass flow rate calculated from the volumetric flow rate set at the injection pump) would generate a straight line, indicating the linear behavior of Darcy flow. Fig. 3 shows the results of a test performed to check the nonlinearity of flow. The trend depicted in Fig. 3 is not linear. Thus, non-Darcy flow behavior exists in the flow rate range used in this experiment. In particular, the data obtained in this experiment better fit a second-order polynomial. One of the assumptions that could justify such a deviation from linearity is that permeability does not change with flow rate. Lastly, the mass flow rate is constant across the core. Still, the volume flow rate can change even threefold (mainly due to different pressure gradients), leading to similar changes in density and viscosity to a certain extent.

This expansion can also change the temperature locally and affect density, volume, and viscosity locally.

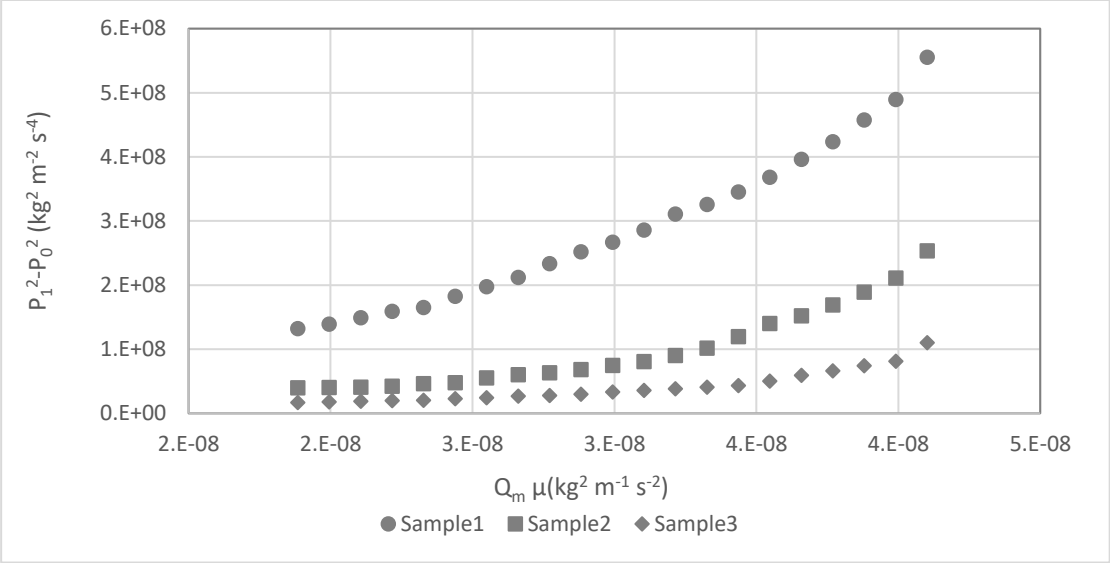

Figure (3) Results of a test performed on natural sand samples to check the nonlinearity of Darcy flow.

Figure 4. shows the deviation of Darcy's data from Darcy's law compared to the experimental data; we see that as the flow rate increases, the experimental data tend to deviate from the linear relation, implying a deviation from Darcy's law. Though Darcy recognized in a first approximation a linear relationship between the flow rate and the pressure drop, he was also well aware of deviations and tried to ascribe their origin to some experimental flows.

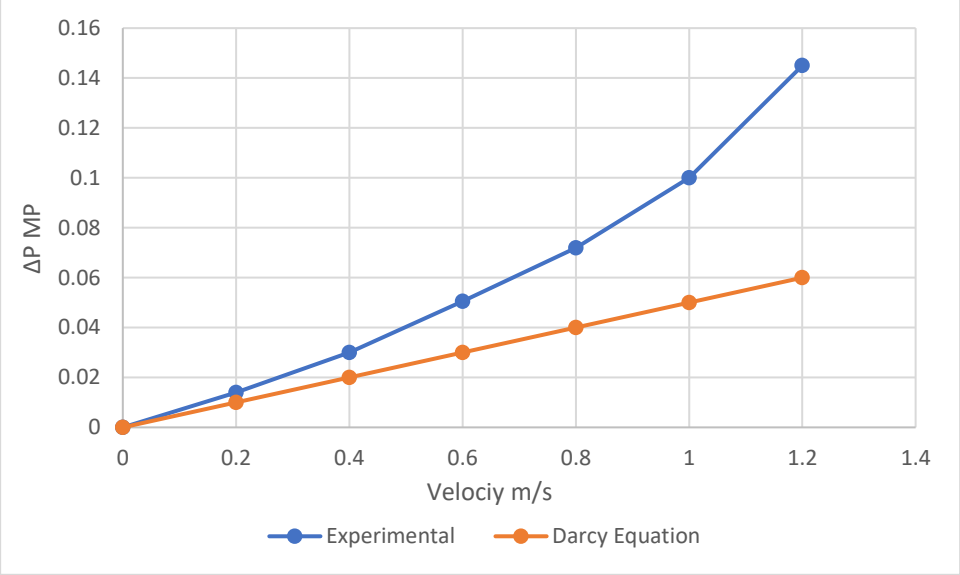

Figure 4. Deviation of Darcy's data from Darcy's law. Experimental data

Figure. 5 illustrate the departure Forchheimer equation from the experimental data. Forchheimer, in his equation, corrected the shortcomings of Darcy's equation as he added a term to calculate the inertia force. There is a deviation between the experimental Forchheimer equation data. This difference can be attributed to the method of calculating the La-Darcy coefficient, as there is a significant difference between the equations available in the literature.

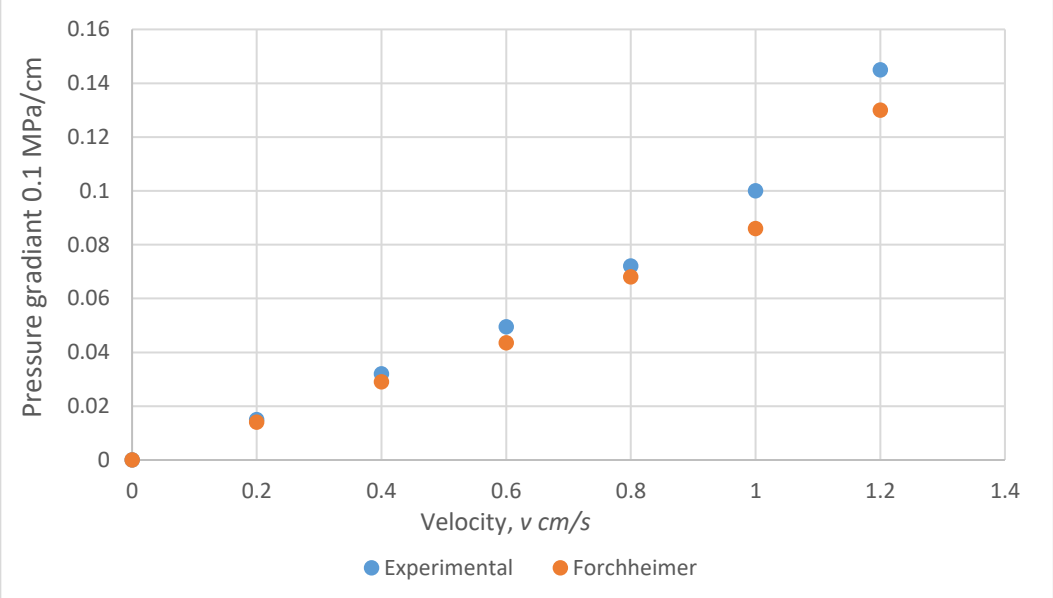

Figure 6 Pressure gradient vs . velocity, Comparison Forchheimer equation and the experimental results.

2.6 Compressible Flow Test

The fluid inertia, pressure gradient, and viscous resistance pressure gradient ratio is the Forchheimer number defined in (7). Therefore, the Forchheimer number is the ratio of inertial resistance and viscous resistance, with the same physical meaning as the Reynolds number for the flow in pipes. The Reynolds number for identifying the turbulent flow in a pipeline was adapted to describe a non-Darcy flow in porous media. Atmakidis [12] defined the Reynolds number as follows:

$$Re = \frac{\rho D_p v}{\mu} \tag{5}$$

where D_p is the diameter of the particles. The parameter $(\sqrt{\frac{k}{\emptyset}})$ has also been proposed instead of the particle diameter, and the Reynolds number was defined as follows [5]:

$$Re = \frac{v\rho}{\mu}\sqrt{\frac{k}{\emptyset}} \tag{6}$$

Where the critical Reynolds number is over the range of 0.022 to 0.29, the Forchheimer number has been proposed as the critical parameter to estimate the conversion from Darcy flow to non-Darcy flow, and it is expressed as follows:

$$F_o = \frac{k\beta\rho v}{\mu} \tag{7}$$

The fluid inertia pressure gradient and the viscous resistance pressure gradient ratio is the Forchheimer number defined in (8). Therefore, the Forchheimer number is the ratio of inertial resistance and viscous resistance, with the same physical meaning as the Reynolds number. The inertia coefficient (β) in the case of immobile saturation, many correlations exist, like Geertsma's can be used to calculate (β) [13]

$$\beta = \frac{1}{k^{0.5}\emptyset^{5.5}} \tag{8}$$

The characteristics and flow conditions of liquid and porous media directly affect the seepage; we should consider the properties of the porous media, such as porosity and permeability. Moreover, characteristic length ($\sqrt{\frac{k}{\emptyset}}$) can be used to represent the characteristics of the porous media and can be convenient for field applications. For fluid flow in porous media, the resistance coefficient *f* is the function of the Reynolds number Re, i.e., *f* = F (Re). The experimental data can be dimensionless according to the following relationship [14]:

$$Re = \frac{q\rho\sqrt{\frac{k}{\emptyset}}}{\mu A\emptyset} \tag{9}$$

$$f = \sqrt{\frac{k}{\emptyset}}\frac{\Delta P}{\rho(L)}\left(\frac{\emptyset A}{q}\right) \tag{10}$$

The resistance coefficient and its corresponding Reynolds number can be calculated by inserting the value of the flow rate or pressure gradient and the parameters of fluids and samples into the above formulas 9 and 10 for sample 3. The Reynolds number and resistance coefficient are set as the abscissa and ordinate, respectively, in the double logarithmic coordinate system, and their relationship curve is shown in Fig. 6.

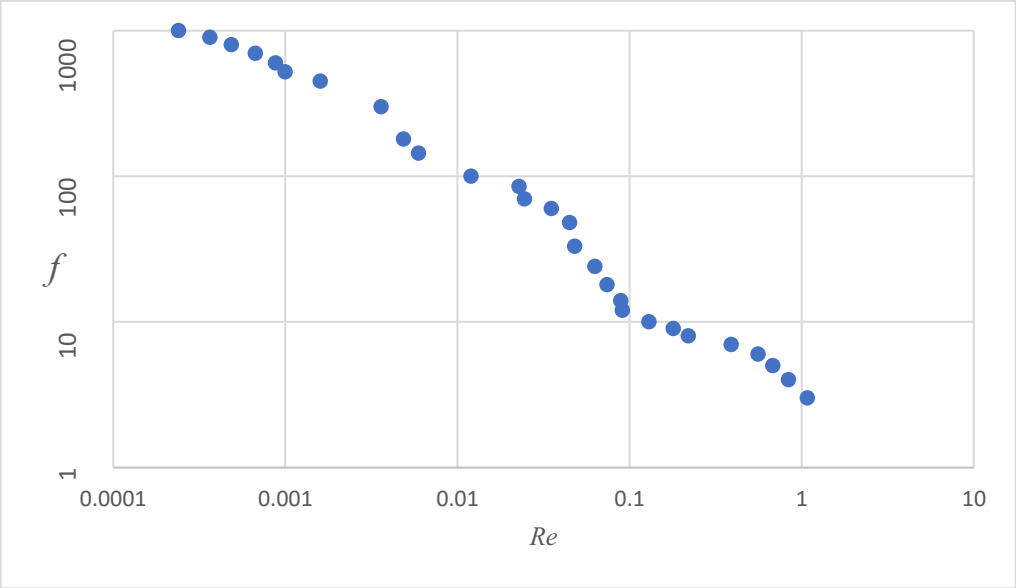

Figure 6 Curve of the resistance coefficient versus the Reynolds number “sample 3.

The curve of resistance coefficient versus Reynolds number can generally be divided into two parts. The first is when the lower flow rate represents a Darcy flow, which represents Re from 0.0001 to 0.1. As the Reynolds number increases above 0.1, the slope of the curve rises, indicating that the flow is moving away from Darcy's law.

2.7 Conclusion

1. Three cylindrical synthetic samples with perforations have been used to investigate the existence of non-Darcy flow by testing a wide range of flow rates for compressible and incompressible.

2. The existence of a non-Darcy flow regime has been confirmed for all the investigated samples by means of the ($P_1^2 - P_2^2$) vs. $Q_m\mu$ plot. Thus, non-Darcy flow behavior exists in the flow rate range used in this experiment. In particular, the data obtained in this experiment better fit a second-order polynomial. The implication for the petroleum industry is to handle the extrapolation of laboratory-derived low-pressure gas permeability to field conditions, involving correction for gas slippage.

3. A Darcy flow occurs when the Reynolds number is less than the critical Reynolds number. A non-Darcy flow occurs when the Reynolds number is above the critical Reynolds number.

References

[1] A. Elsanoose, E. Abobaker, F. Khan, M. A. Rahman, A. Aborig and S. D. Butt, "Estimating of Non-Darcy Flow Coefficient in Artificial Porous Media," Energies, vol. 15, no. 3, p. 1197, 2022.

[2] Aljalahmah, F. A. (2014). Experimental characterization of the Barree and Conway (2004) single-phase non-Darcy flow model in various hydraulic fracturing sands. ProQuest Dissertations Publishing.

[3] Xiong, Y., Yu, J., Sun, H., Yuan, J., Huang, Z., & Wu, Y. (2017). A New Non-Darcy Flow Model for Low-Velocity Multiphase Flow in Tight Reservoirs. Transport in Porous Media, 117(3), 367–383.

[4] Lai, B., Miskimins, J. L., & Wu, Y.-S. (2012). Non-Darcy Porous-Media Flow According to the Barree and Conway Model: Laboratory and Numerical-Modeling Studies. SPE Journal (Society of Petroleum Engineers (U.S.): 1996), 17(1), 70–79.

[5] Lai, Bitao. (2010). Experimental Measurements and Numerical Modeling of High-Velocity Multiphase Non-Darcy Flow Effects in Porous Media. ProQuest Dissertations Publishing.

[6] Pang, M., Zhang, T., Guo, Y., & Zhang, L. (2021). Re-crushing process and non-Darcian seepage characteristics of broken coal medium in coal mine water inrush. Scientific Reports, 11(1), 11380–11380.

[7] Shi, W., Yang, T., & Yu, S. (2020). Experimental Investigation on Non-Darcy Flow Behavior of Granular Limestone with Different Porosity. Journal of Hydrologic Engineering, 25(8), 6020004.

[8] Teitel, M. (2011). On the applicability of the Forchheimer equation in simulating flow through woven screens. Biosystems Engineering, 109(2), 130–139.

[9] Moutsopoulos, K. N., & Tsihrintzis, V. A. (2005). Approximate analytical solutions of the Forchheimer equation. Journal of Hydrology (Amsterdam), 309(1), 93–103.

[10] Fritz, M., Lima, E. A. B. F., Oden, J. T., & Wohlmuth, B. (2018). On the unsteady Darcy-Forchheimer-Brinkman equation in local and nonlocal tumor growth models.

[11] WHITAKER, S. (1996). The Forchheimer equation: A theoretical development. Transport in Porous Media, 25(1), 27–61.

[12] Zhou, J., Chen, Y., Wang, L., & Cardenas, M. B. (2019). Universal Relationship Between Viscous and Inertial Permeability of Geologic Porous Media. Geophysical Research Letters, 46(3), 1441–1448.

[13] Atmakidis, T., & Kenig, E. Y. (2009). CFD-based analysis of the wall effect on the pressure drops in packed beds with moderate tube/particle diameter ratios in the laminar flow regime. Chemical Engineering Journal (Lausanne, Switzerland: 1996), 155(1), 404–410.

[14] Geertsma, J. (1974). Estimating the Coefficient of Inertial Resistance in Fluid Flow Through Porous Media. Society of Petroleum Engineers Journal, 14(5), 445–450.

[15] Wei, Q., Zhou, H., & Yang, S. (2020). Non-Darcy flow models in porous media via Atangana-Baleanu derivative. Chaos, Solitons and Fractals, 141.

[16] J. Geertsma, "Estimating the Coefficient of Inertial Resistance in Fluid Flow through Porous Media," SPEJ , pp. 445 - 450, 1974.

Chapter 3

Estimating of non-Darcy flow coefficient in artificial porous media

Preface

A version of this chapter has been published in Energies 2022, 15, 1197. I am the primary author of this manuscript, along with co-authors Dr. Abobaker, Dr. Faisal Khan, Dr. Rahman, Dr. Amer Aborig, and Dr. Butt. Dr. Butt assisted in the design of the setup. I proposed the idea and concept and prepared the samples with assistance from Dr. Amer and Abobaker; they also helped conduct the experiments. However, I collected and analyzed the experimental data. Dr. Aziz evaluated the methodology and reviewed the manuscript. I wrote the original manuscript, and Dr. Aborig, Dr. Faisal Khan, and Dr . Aziz reviewed the manuscript and suggested amendments that had a significant impact on enriching this manuscript.

3.1 Abstract.

This study conducted a radial flow experiment to investigate the existence of non-Darcy flow and calculate the non-Darcy "inertia" coefficient; the experiment was performed on seven cylindrical perforated synthetic porous media samples. Two hundred thirty-one runs were performed, and the pressure drop was reported. The non-Darcy coefficient β was calculated and compared with those available in the literature. The results showed that the non-Darcy coefficient decreased nonlinearly and converged on a value within a specific range as the permeability increased. Nonetheless, it was found that the non-Darcy flow exists even in the very low flow rate deployed in this study. The existence of a non-Darcy flow was confirmed for all the investigated samples. The Forchheimer numbers for airflow at varied flow rates are determined using experimentally measured superficial velocity, permeability, and non-Darcy coefficient.

3.2 Introduction

Darcy's (1856) law has been widely applied in experiments and simulations, and it states that the discharge is proportional to the hydraulic gradient. However, this type of flow model is only appropriate for low velocity, steadiness, and laminar flow. In the case of nonlinear behavior, the Forchheimer equation is used, which has the non-Darcy "inertia" coefficient β that can be calculated in the laboratory. The flow of fluids through porous media plays a crucial role in understanding the interaction of fluids flow with the porous media. Since the flow in porous media differs from that of other types of flow, it was necessary to develop a different approach. Darcy's law describes the behavior of fluid flow in porous media. According to Darcy's law, the pressure gradient is linearly proportional to the velocity of the porous media fluid. The Darcy Equation (1) is an empirical equation based on experimental water flow through packed sands at low velocity, Zeng [1]:

$$-\boldsymbol{gradP} = \boldsymbol{\mu/k}\,\vec{\boldsymbol{u}} \tag{1}$$

Where $gradP =$ pressure, $\mu =$ fluid viscosity,$u =$ Darcy's velocity, the volumetric flow rate per unit flow area, $k =$ permeability of the medium. Many efforts have been made to derive the Darcy Equation theoretically via different approaches. Using the volumetric averaging theory, Stephen et al. [2] derived the permeability tensor for the Darcy Equation under low velocities. Following a continuum approach, Hassnizadeh et al. [3] developed a set of equations to describe the macroscopic behavior of fluid flow through porous media. In the case of converting these equations into linear equations, a suitable equation results that work for the flow of porous media at low velocities. Through experiments carried out by many researchers and a lot of real field data, it can be concluded that Darcy's Equation

works in low velocities. Excess pressure drop induced by inertial effects limits Darcy's law's applicability for modeling fluid flow through porous media at high velocities [4]. Various terms, such as non-Darcy, turbulent, inertial, high-velocity, etc., have been used to address the linear Darcy Equation's deviation. Many efforts have been made to adjust the Darcy Equation. Forchheimer (1901) added a second order of the velocity term to represent the inertial effect and corrected the Darcy Equation into the Forchheimer Equation [5]:

$$-\Delta P = \frac{\mu}{k}\vec{v} + \beta\rho|\vec{v}|\vec{v} \quad (2)$$

Where ΔP is the pressure drop, μ is the fluid viscosity, β is the non-Darcy coefficient ρ is the fluid density. Non-Darcy behavior has shown a significant influence on well performance. Researchers prefer to use the term "turbulent" or "non-Darcy flow" to describe the viscous flow at high velocities near the wellborn region, such as Kadi et al. [6]. This flow behavior is considered a non-Darcy flow rather than turbulent Belhaj et al. [7]; the gas slippage and inertial flow lead to non-Darcy behavior. If they are not taken into account, they will undoubtedly cause measurement errors. These result from the flow of fluid particles through the throats of twisted rocks of various sizes. In a steady Darcy flow, there is an increase in pressure and no corresponding increase in fluid flow velocity [8].

In addition, when the liquid particles pass through the throat of smaller pores, their velocity increases and slows down when they pass through large pores' throats, which leads to a dissipation of inertial energy and an increase in pressure Katz et al., [9]. Holditch et al. [10] presented a numerical model to study the non-Darcy effect on effective fracture conductivity and gas well productivity. They found that the non-Darcy effect could reduce

fracture conductivity by 20% and gas productivity by 50%, the same conclusion reached by [11] and [12].

In the reservoir, and especially the area near the well during injection or production, deviations from the linear Darcy's Equation often occur due to the high flow velocity as the pressure differentials are large and affect the inertia force [13]. The non-Darcy coefficient in wells is usually determined by analyzing the multi-rate pressure test results, but such data are not always available. The permeability, porosity, and pore size distribution are crucial in the Equation for predicting the non-Darcy coefficient developed by many researchers. In addition, the permeability heterogeneity and wettability are directly related to the effect of capillary number on viscous fingering patterns in porous media. Shiri et al. [14,15] studied the fault zone and discontinuity and investigated the impact of wettability and permeability heterogeneities in the fluid front and preferential flow pathway. In the fault zone, they found that the pattern of the fault zone and the adjacent layer was different when the fault zone permeability was less or more than that of the vicinity layer, the sweep efficiency, and the fingering pattern. This phenomenon reduces the displacement efficiency of the capillary trap mechanism. In addition, they concluded that the wettability difference between all the model components led to oil being cut off in wet oil regions. Faez et al. [16] studied the effect of fracture geometry on permeability; their results concluded that increased fracture orientation would exponentially increase permeability. Namdari et al. [17] investigated the effect of the discontinuity direction on fluid flow in porous rock masses; they used a hybrid FVM-DFN and streamlined simulation approach. The study

results indicated that the FVM-DFN hybrid method is effective if it uses the streamlined simulation to study the fluid flow in a large model with discontinuity.

Many equations of non-Darcy coefficients based on mathematical models were presented; for example, [18–25] introduced a mathematical model to evaluate the fracture length and the non-Darcy coefficient. Using the model and the data from variable-rate tests from low-permeability hydraulically fractured wells, they were able to determine the non-Darcy coefficients.

Belhaj et al. [7] derived a diffusivity equation by replacing the Equation derived from Darcy's law. The new Equation based on Forchheimer's Equation and Darcy's Equation also added a term to capture the effect of the high velocity. Liu et al. [23] plotted equation (4) Table 1 developed by Geertsma (1974) against the data obtained by [26–29]. They found that Equation (4 Table 1) was inaccurate. While suspecting tortuosity may influence data from limestone and sandstone samples measurements, Coles et al. [24] proposed two equations (13, Table 1) to calculate the non-Darcy coefficient with the same porosity method, where β is expressed in 1/ft and K in MD. Comparing equations (12) and (13) with equations developed by other investigators, the flow enters the exponents for porosity in equations (12) and (13) in Table 1 are positive instead of negative in other equations.

Li et al. [30] used a mixture of reservoir simulators and experimental procedures to investigate the non-Darcy flow in Berea sandstone cores, where nitrogen was injected at various flow rates in several directions. Comparing differential pressures from simulations with their counterparts from experiments, they found a β for Berea sandstone. By rearranging Cornell's experimental results, Janicek et al. [9] suggested the non-Darcy

coefficient equation for fluid flowing through sandstone, limestone, and dolomite porous media. Tek et al. [31] used experimental data to generate an equation to evaluate β for any porous media system and come up with a correlation, but the tortuosity was not considered (8 Table 1). Yuedong et al. [32] investigated sample displacement experimental data based on the dimensionless analysis method. They built a new mathematical model to describe the seepage of high and high-production reservoirs and formed the following conclusions. Whether high-velocity non-Darcy flow occurs is determined by the flow velocity value and the displacement medium (fluid) combined action, porous media, and external driving force. Studying the flow in porous media is understanding the flow behavior, and it is more challenging to inspect the fluid behavior in rock and simulate large-scale models.

Table (1) List of Non-Darcy correlations available in the literature

Eq N	**Ref No**	$\boldsymbol{\beta\ m^{-1}}$
1	[25]	$\beta = \frac{4.8 \times 10^{12}}{k^{1.176}}$
2	[33]	$\beta = \frac{4.24 \times 10^{4}}{k^{0.5} \times \varphi^{1.5}}$
3	[19]	$\beta = \frac{1.81 \times 10^{8}}{k^{1.25} \times \varphi^{0.75}}$
4	[27]	$\beta = \frac{0.005}{k^{0.5} \times \varphi^{5.5}}$
5	[34]	$\beta = \frac{6.15 \times 10^{10}}{k^{1.55}}$
6	[23]	$\beta = \frac{8.91 \times 10^{8} \tau}{k \times \varphi}$
7	[32]	$\beta = \frac{1.047 \times 10^{2}}{\varphi^{6.77} \times k^{0.5}}$

8	[31]	$\beta = \frac{5.5 \times 10^{9}}{\varphi^{0.75} \times k^{1.25}}$
9	[35]	$\beta = \frac{4.52 \times 10^{4}}{\varphi^{1.5} \times k^{0.5}}$
10	[36]	$\beta = \frac{1.386 \times 10^{7}}{\varphi^{1.15} \times k^{0.85}}$
11	[37]	$\beta = \frac{1.55 \times 10^{4} \tau^{3.35}}{\varphi^{0.98} \times k^{0.29}}$
12	[37]	$\beta = \frac{2.49 \times 10^{11} \varphi^{0.537}}{k^{1.79}}$
13	[24]	$\beta = \frac{1.07 \times 10^{12} \varphi^{0.449}}{k^{1.79}}$

We have previously performed both single-phase and two-phase flow studies in near-wellbore regions. Single-phase flow experiments in heterogeneous core samples by Shachi et al. [38] and two-phase flow modeling homogeneous core samples [39] were performed. We have also completed several studies related to foam flow in heterogeneous core samples without the presence of oil [40,41]. We have also created synthetic core samples and a perforation tunnel to conduct single-phase flow experiments and model a per-oration tunnel [42–45]. This study is based on the non-Darcy flow performed at steady radial pressure gradient-flow rate in large cores at a high airflow rate. The available experimental studies use relatively small samples without perforation and a linear low flow rate range. This study utilizes the Radial Flow Facility "RFC." The RFC allows for performing a radial flow experiment on perforated samples, which is very rare in the literature; also, in addition, the size of the samples is large enough to allow the flow to develop fully.

3.3 Formulation

Equation (2) is considered for a compressible flow, and the air is an ideal gas. The density is a function of pressure and temperature in the case of compressible flow. Assuming mass flow rate ($\boldsymbol{Q_m}$), gas density ($\boldsymbol{\rho}$), and volumetric flow rate ($\boldsymbol{q}$) can be expressed as follows:

$$Q_m = \rho q \tag{1}$$

$$\rho = \frac{MP}{zRT} \tag{2}$$

$$q = Av \tag{3}$$

where $\boldsymbol{p} =$ pressure, $\boldsymbol{A} =$ cross-sectional area of fluid flow, and $\boldsymbol{v} =$ fluid velocity. Then, it is possible to derive the following expression: $\boldsymbol{M} =$ molecular weight, $\boldsymbol{z} =$ compressibility factor, $\boldsymbol{R} =$ gas constant, and $\boldsymbol{T} =$ temperature. For gases, the Equation is best expressed in terms of mass velocity $\boldsymbol{Qm} = \boldsymbol{\rho v}$ because the mass velocity is constant when the cross-section is constant. By substituting Equations (3), (4), and (5) in Equation (2) for radial flow, we obtain:

$$-\frac{M}{ZRT}\int_{P_1}^{P_2} PdP = \frac{Q_m\mu}{2\pi hk}\int_{r_1}^{r_2}\frac{dr}{r} + \frac{\beta Q_m^2}{4\pi^2h^2}\int_{r_1}^{r_2}\frac{dr}{r^2} \tag{4}$$

where $\boldsymbol{r_1}$ is the perforation radius, $\boldsymbol{r_2}$ Sample radius and $\boldsymbol{h}$ is the sample height, the integration of Equation (6) will result in the following Equation:

$$\frac{P_1^2 - P_2^2}{\frac{z2RT}{M}} = \frac{Q_m\mu}{2\pi hK} ln\frac{r_2}{r_1} + \frac{\beta Q_m^2}{4\pi^2h^2}\left(\frac{1}{r_1} - \frac{1}{r_2}\right) \tag{5}$$

The last alternative to estimate is $\boldsymbol{\beta}$ to rearrange the Forchheimer Equation in the following form:

$$\frac{P_1^2 - P_2^2}{\frac{zRTQ_m\mu}{M\pi h}} = \frac{1}{K} ln \frac{r_2}{r_1} + \frac{\beta Q_m}{2\pi h\mu} (\frac{1}{r_1} - \frac{1}{r_2}) \tag{6}$$

The experimental data of ($\frac{\boldsymbol{P_1^2 - P_2^2}}{\frac{\boldsymbol{zRTQ_m\mu}}{\boldsymbol{M\pi h}}}$) and ($\frac{\boldsymbol{Q_m}}{\boldsymbol{2\pi h\mu}} (\frac{\boldsymbol{1}}{\boldsymbol{r_1}} - \frac{\boldsymbol{1}}{\boldsymbol{r_2}})$) were obtained in the laboratory and utilized linear regression, concluding that the factor $\boldsymbol{\beta}$ is constant for the range of flow rates, as in Figure 5.

3.4 Experimental Procedure

The experimental procedure was divided into two stages; the first stage was the preparation of samples from sand and epoxy and then conducting flow experiments on the Radial Flow Cell Facility. The experimental process is briefly described as follows. First, the experiments started at a low flow rate, and then the flow rate increased until the non-Darcy flow occurred. The air compressor has a large flow rate and continuously works for an extended period. High-velocity flow experiments have been performed on synthetic samples to simulate the airflow in the near-wellbore region. The samples are cylindrical with 15.54 cm in diameter, and the perforation has a 25.54 depth and 2.54 cm in diameter, as shown in Figure 2.

Figure 1 Seven synthetic samples.

3.4.1 Preparation of the Samples

Seven synthetic samples were created in Memorial University laboratories. Both Aziz and Ahmed et al. [46] made samples in the labs to produce samples using sand and epoxy. Lately, seven synthetic sand samples were created from sand collected from Nova Scotia, Canada, in the Memorial University of Newfoundland laboratory. The sand was dried in the civil engineering lab using a hot-air oven at 110 C. The sieving process resulted in six different sand sizes ranging from 0.18 mm to 1.18 mm. The sand of different sizes mixed with epoxy in different quantities; the mixture is then placed in a plastic container for four stages, using an electric vibrator to ensure grain distribution with the epoxy glue, and then they lift to dry and consolidate for 24 h, as shown in Figure 2. The sample dimensions are 30.48 cm high and 15.54 cm in diameter, and a perforation tunnel has a 25.54 cm depth and 2.54 cm diameter Abobaker et al. [47].

There are many available ways to measure the properties of the samples. Mercury Intrusion Porosimetry (MIP) is one of the most widely used ways at the University of Memorial of Newfoundland labs to characterize and analyze the synthetic samples' pore morphology

and index properties. The index properties include permeability, porosity, median pore diameter, and tortuosity, which are listed in the following Table 2.

Table 2. The Index Properties for the Samples

Sample No.	The Index Properties for the Samples			
	Permeability (mD)	**Porosity (%)**	**Tortuosity**	**MPD (µm)**
Sample 1	2035.95	21.5	3.62	25.31
Sample 2	3981.50	23.4	3.19	32.14
Sample 3	6292.66	26.31	2.82	45.27
Sample 4	8127.04	27.94	2.27	60.6101
Sample 5	12,281.50	29.3	2.10	81
Sample 6	16,320.24	31.2	1.96	100
Sample 7	26,151.72	33.2	1.7765	181.7485

3.5 Performing the Flow Experiments

At this stage, seven synthetic porous media samples were prepared; the next step was to conduct the flow experiments. RFC Figure 2 Ahamed et al. [46] has been updated to be suitable for conducting multi-phase flow experiments, as five pressure sensors have been calibrated with pressure sensors from other experiments. Two pressure sensors were placed on the inlet and outlet, and the rest was placed on the fluid mixing lines. With help from

the university's technical department, an air flowmeter was repaired and successfully calibrated. In addition, another two lines were added to make the experiment ready to perform experiments on a three-phase flow. The experiment begins by placing the sample in the cylinder and connecting the air compressor with the injection lines. The pressure sensors and flow meters are connected to the data acquisition to monitor the flow rate and record the pressure data during the experiment. The airflow rate ranged from 3 to 99 L per minute. The outlet inserted into the pack measured line pressures without end effects. Note that the flow entered the sample radial direction of gas flow to avoid spurious readings due to gas impinging on or accelerating off the probes (pitot effects).

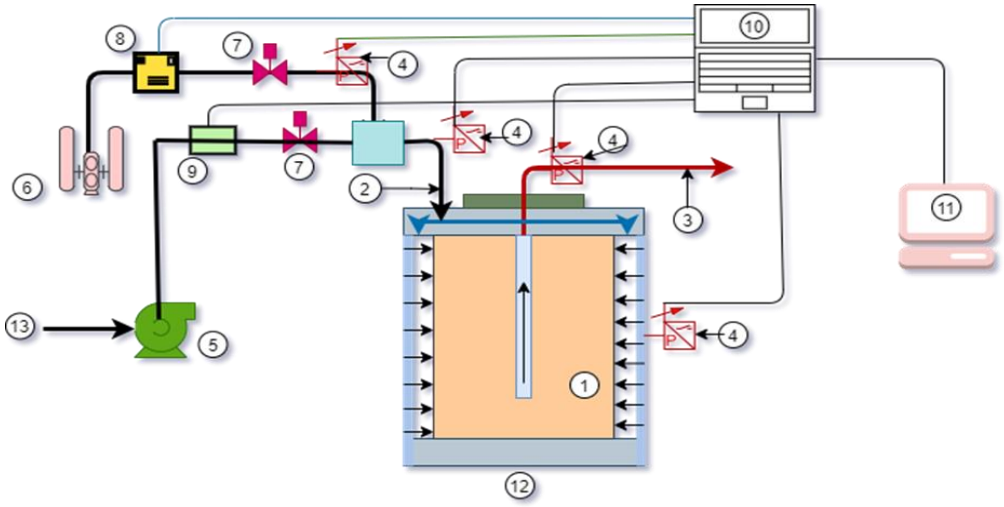

Figure 2. Schematic diagram of the experiment RFC facility: 1. Sample, 2. Inlet, 3. Outlet, 4. Pressure Sensors, 5. Water pump, 6. Air compressor, 7. non-Return valves, 8. Airflow meter, 9. Water flowmeter, 10. Data Acquisition, 11. Computer, 12. Samples Chamber, 13. Waterline.

The experimental run starts by installing the sample in the samples chamber (12 Figure 2) and then locking the lid tightly to prevent leakage. The pressure sensors and the flowmeters are then connected to the Data Acquisition inlet, where each sensor has a specific channel. Lab View transferred all the data for each run from the flowmeters and the pressure sensor

to digital numbers and charts. The flow starts by adjusting the air compressor at a certain pressure and putting the flow rate control valve at the needed flow rate. The flow enters the sample radially Figure 2; the outlet is installed at the top of the sample perforation. The flow rate range was between 3 and 99 LPM; at each run, the pressure and flow data were converted to an Excel table and then later analyzed.

3.6 Non-Darcy Flow Regime

If Darcy's law is considered assuming the air properties and k are constants and the term $(P_2^2 - P_1^2)$ plotted versus $(Qm\,\mu)$ would create a straight line. Figures 3 and 4 show the results of a test performed to check the nonlinearity of flow. Figures 3 and 4 show that the lines are not straight, indicating the presence of non-Darcy flow. Equations of the second degree can describe these lines.

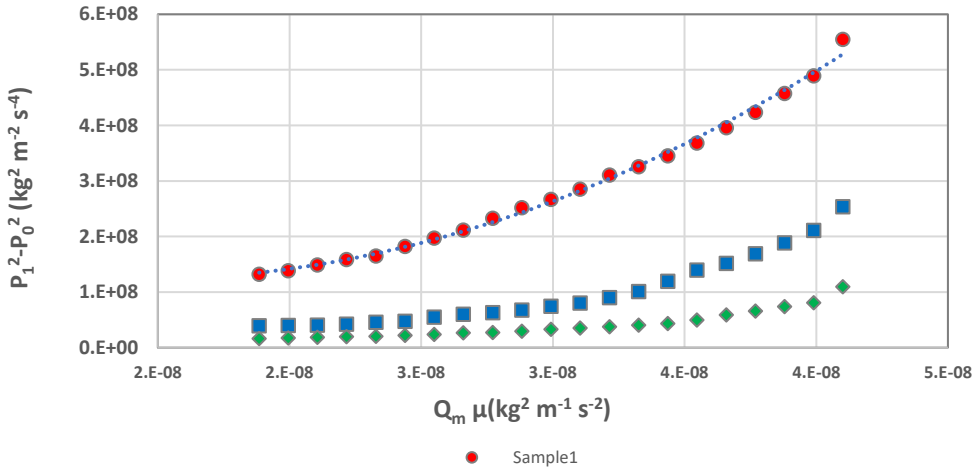

Figure 3. The nonlinearity of Darcy flow check of samples 1, 2, and 3.

A pressure loss occurs during the flow of air through the samples, which decreases the volumetric flow rate, but the mass flow rate remains constant. These changes in pressure and volumetric flow change air properties such as density and viscosity.

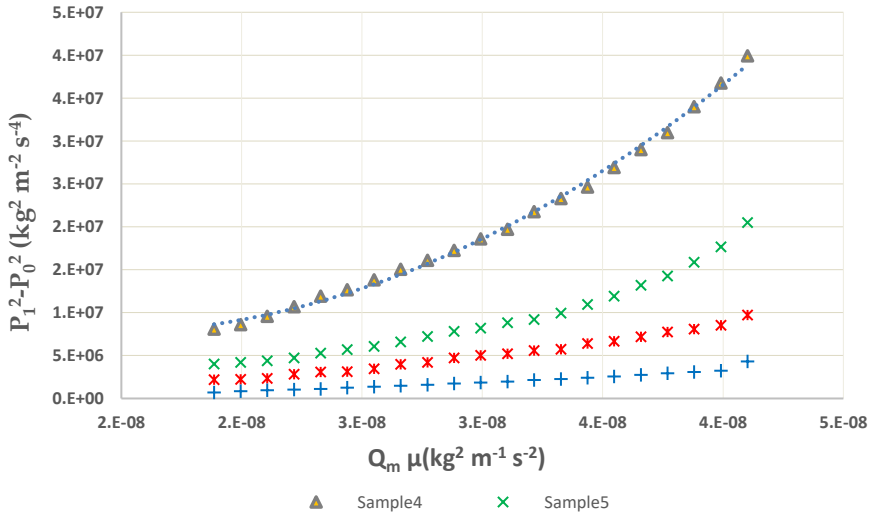

Figure 4. The nonlinearity of Darcy flow check of samples 4, 5, and 6.

4.6.1 Calculating Non-Darcy Coefficient β

A key to applying the Forchheimer Equation is to estimate a value for β. Methods developed to calculate β are based on experimental work, correlations, and the Forchheimer Equation. To determine (β) experimentally, the procedure is first to measure each of the core samples' absolute permeability and then apply a series of increasing pressure differentials across each sample by flowing fluid through the core plugs at ever-increasing rates. Knowing the flow rates and pressure differentials across the sample, the inertial resistance coefficient can be directly calculated using linear regression of the Forchheimer Equation (8). Figures 5, 6, and 7 are the results of the flow experiments. The experimental data of ((P_1^2-P_2^2)/((zRTQ_m μ)/Mπh)) and Q_m/2πhμ(1/r_1 -1/r_2) were obtained in our laboratory and utilized linear regression as in Figures 5, 6, and 7.

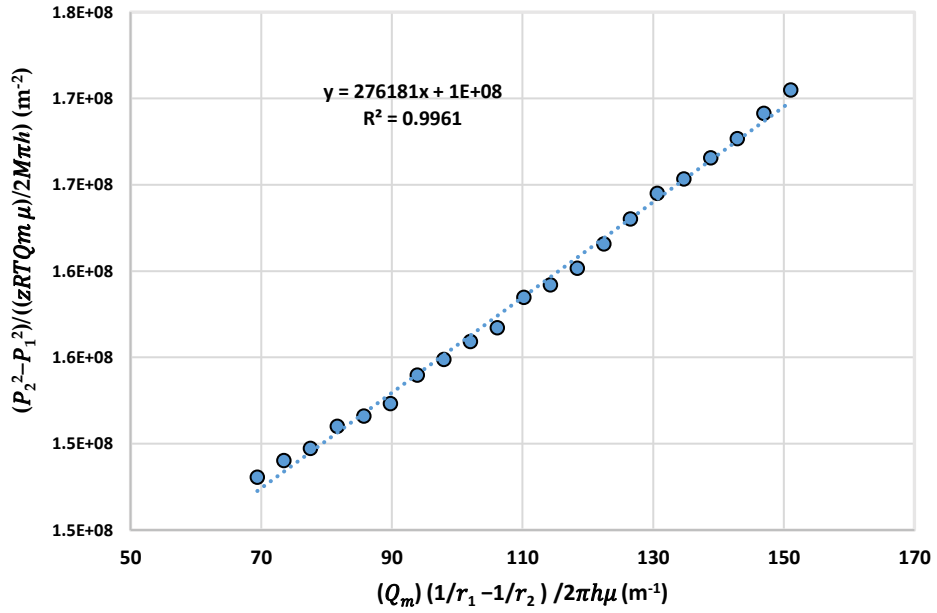

Figure 5. Calculating the non-Darcy β. Permeability = 2, Darcy.

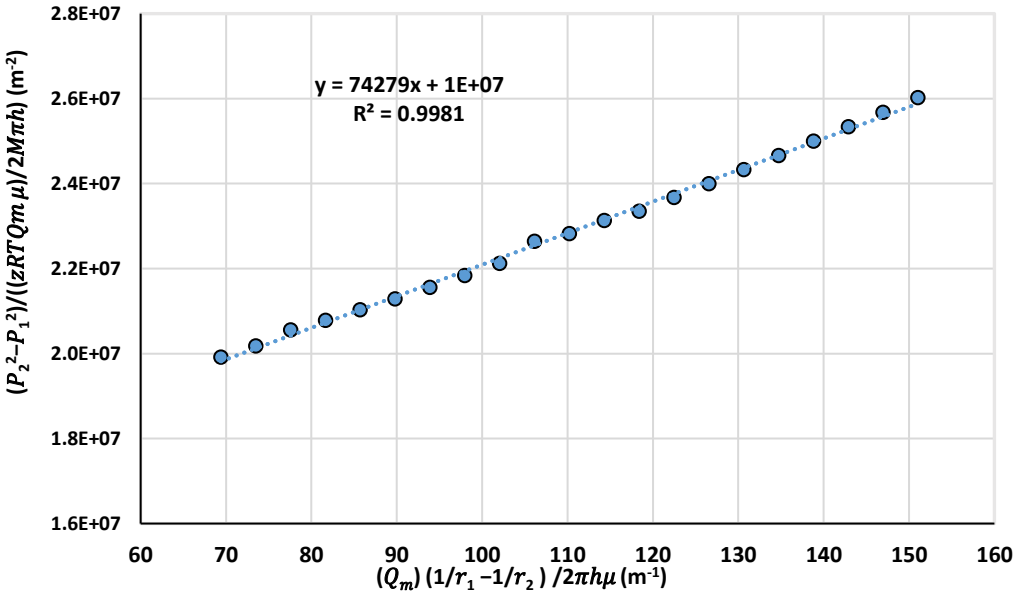

Figure 6 Calculating the non-Darcy β. Permeability = 12 Darcy**.**

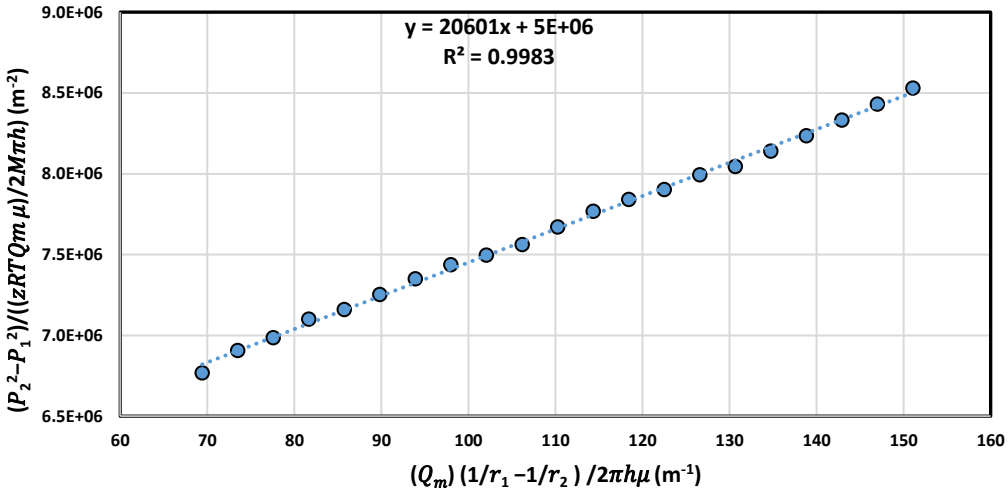

Figure 7 Calculating the non-Darcy β. Permeability = 26 Darcy.

Table 3 contains the calculated values for the non-Darcy coefficient. The non-Darcy coefficient was compared with values obtained from models available in the literature. The closest result to the current study is the Geertsma [27] model; the difference's value is about 0.6 to 4.0%. It is clear from the table that there is a large discrepancy between the results obtained from this study and the results of previous studies. This discrepancy can be attributed to several reasons, the first of which is the size and nature of the samples. Studies use small samples during which the flow cannot reach full development. The sample sizes in the literature reviewed in this study ranged from 2.5 cm x 6 cm up to 4 cm x 8 cm. The other possible reason is that the current study benefits from the radial flow and the perforation, which is the outlet of the flow. As Zeng et al. [1] and others mentioned, the flow accelerates due to pressure differences when approaching the perforation, thus increasing the velocity and turbulence. The results obtained from the experiment were

compared with previous studies in which the porous media used was similar to the current study samples.

Table 3. Non-Darcy coefficient calculated from the current experimental.

Sample No	β cm^{-1}	Geertsma [27]	Tek [31]
Sample 1	276,180.32	440,041.83	14,556.91
Sample 2	210,821.61	153,871.68	5708.06
Sample 3	169,710.87	122,395.33	2954.77
Sample 4	119,204.17	29,141.28	1957.57
Sample 5	73,103.274	17,068.78	1117.16
Sample 6	38,663.54	10,077.68	742.99
Sample 7	19,589.15	4165.19	377.27

3.6.2 Effect of Permeability, Porosity, Median Pore Diameter

Figure 8 reveals the variation of the non-Darcy according to the permeability from the modified Forchheimer plot of each synthetic sample. The plot illustrates the direct effect of permeability on the non-Darcy coefficient; with permeability increases, the non-Darcy coefficient decreases dramatically. These results show that the non-Darcy behavior is more severe in low-permeability porous media. That can be explained as the pressure drop increases with the permeability decrease. Thus, the superficial velocity rises and leads to a

more turbulent flow. The curvature of the aspect of decline is definite by increased permeability. Some previous studies proposed defining the Equation of the non-Darcy coefficient with permeability. They attempted linear regression analysis on the experimental data set of the coefficient despite the curvature noted of transition [27].

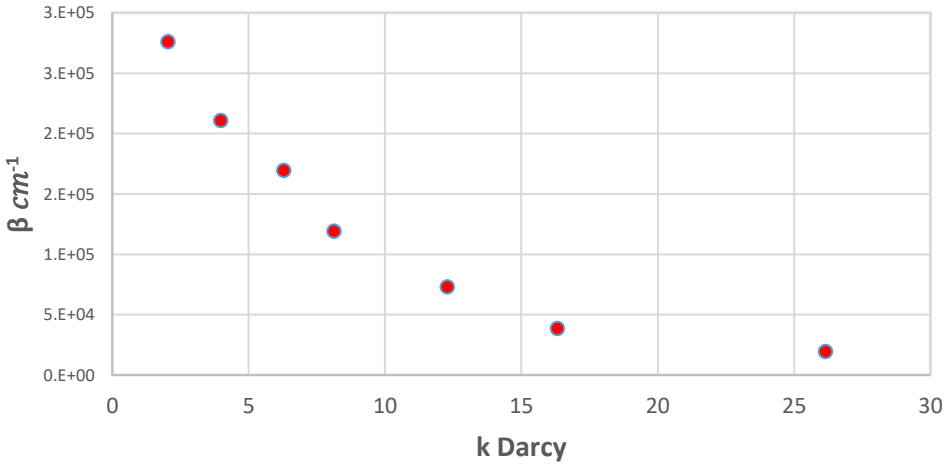

Figure 8. The effect of permeability inertia coefficient β**.**

It can be seen from Figure 9 that the non-Darcy coefficient decreases with the increase of median pore diameter. The non-Darcy coefficient decreases slowly in the bigger pore diameters, and that is because the flow cross-section area is larger in the porous media with a large pore.

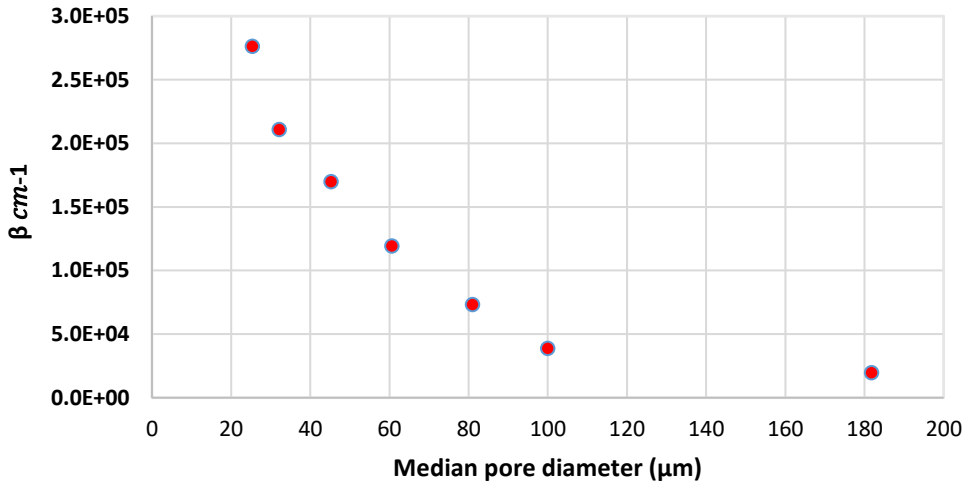

Figure 9. The effect of Median pore diameter on inertia coefficient β**.**

Figure 10 shows the non-Darcy coefficient versus the tortuosity of the samples. The graphs indicate that the non-Darcy coefficient is directly proportional to the tortuosity. The non-Darcy coefficient increases with the increase in tortuosity. The higher the tortuosity, the higher the flow path, increasing inertia.

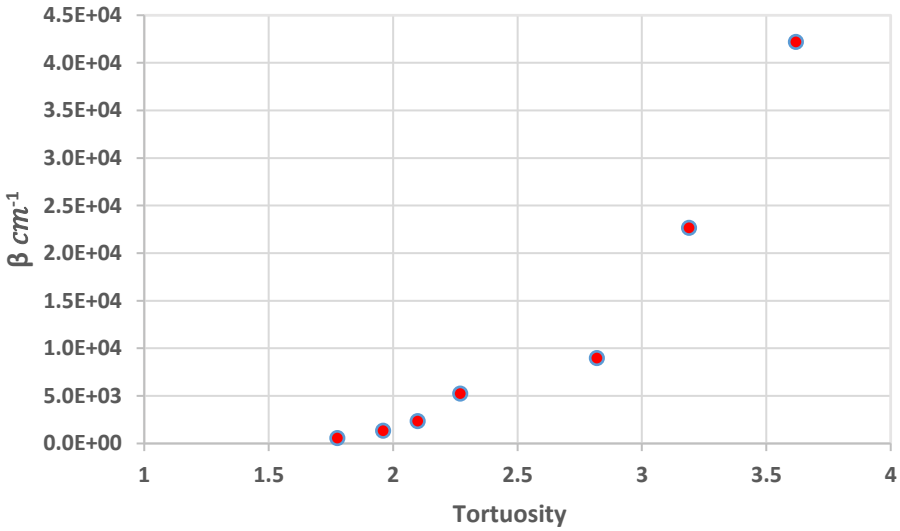

Figure 10. The effect of tortuosity on inertia coefficient β.

3.6.3 Forchheimer Number Fo

Forchheimer number Fo, is the ratio of pressure drop caused by fluid-solid interactions to that by viscous and inertia resistances, which is used instead of the Reynolds number, which indicates when nonlinear effects occur, is given as the following:

$$F_o = \beta k \rho v / \mu \tag{9}$$

Where $\boldsymbol{v}$ is the Darcy velocity, the superficial velocity. $\boldsymbol{v}$ for the sample is calculated for each flow rate as follows: Assuming there is no loss of air in the flow system due to leakage, reaction, or any other reasons, the mass flow rate in the air compressor is the same as that in the core sample at flow equilibrium, though the volumetric flow rates can be different due to the change in pressures. On the other hand, the mass flow rate equals the product of the density and the volumetric flow rate. Similar to the calculation of $\boldsymbol{z}$ and $\boldsymbol{\mu}$, the $\boldsymbol{\rho}$ density of air in the sample is calculated using the pressure data[1]. This behavior implies that the superficial velocity alone, as in the Reynolds number, is not a criterion for identifying the non-Darcy flow behavior; therefore, the Forchheimer number can be calculated. Analyzing the data in Table 4. it can be observed that Fo increases nonlinearly with the flow rate increase. The nonlinearity increases in the $\boldsymbol{Fo}$ indicate that the superficial velocity is not the only reason. However, interestingly, when comparing $\boldsymbol{Fo}$ with permeability, it is noticed that the divergence in $\boldsymbol{Fo}$ values is more significant with the increase in permeability values at the same velocity. That conclusion is consistent with the non-Darcy behavior is more severe in low permeability porous media.

Table 4. Forchheimer Number *Fo*

Forchheimer Number Fo				
Q LPM/s	Sample 3	Sample 4	Sample 5	Sample 7
3	0.0682	0.0573	0.0124	0.0073
9	0.2041	0.1708	0.0369	0.0146
15	0.3389	0.2829	0.0613	0.0218
21	0.4729	0.3938	0.0854	0.0291
27	0.606	0.5033	0.1093	0.0362
33	0.738	0.6116	0.1329	0.0434
39	0.869	0.7185	0.1564	0.0506
45	1.000	0.8243	0.1797	0.0578
51	1.129	0.9288	0.2027	0.0649
57	1.258	1.032	0.2256	0.0720
63	1.386	1.134	0.2483	0.0791
69	1.512	1.235	0.2707	0.0862
75	1.638	1.335	0.2929	0.0932

81	1.764	1.434	0.3150	0.1003
87	1.888	1.531	0.3369	0.1073
93	2.0116	1.628	0.3586	0.1143
99	2.1344	1.723	0.3801	0.1213

3.7 Conclusions

This study conducted a radial flow experiment to investigate the existence of non-Darcy flow and calculate the non-Darcy "inertia" coefficient. Seven synthetic samples were used. The flow rate of the air ranged from 3 LPM to 99 LPM, and in total, 231 runs were conducted.

Using the mean of pressure square difference versus $\boldsymbol{Q_m\mu}$ plot the non-Darcy behavior conformed. This resulted in lines better fitting to a polynomial.

The non-Darcy coefficient β was calculated for each sample from the experimental results of the pressure gradient and using linear regression. The β measurement results were between 276,180.32 $\boldsymbol{cm^{-1}}$ and 19,589.15 $\boldsymbol{cm^{-1}}$.

The non-Darcy coefficient decreases with the median pore diameter and porosity increase. When the median pore diameter at 25.31 μm non-Darcy coefficient β 276,180.32 $\boldsymbol{cm^{-1}}$ and at median pore diameter 181 μm, non-Darcy coefficient β = 19,589.15 $\boldsymbol{cm^{-1}}$.

Forchheimer numbers for airflow at varied flow rates are determined using experimental permeability and non-Darcy coefficient data. The non-Darcy flow were

References

[1] Zeng, Z.; Grigg, R. A Criterion for Non-Darcy Flow in Porous Media. Transp. Porous Media 2006, 63, 57–69.

[2] Whitaker, S. Advances in the theory of fluid motion in porous media. Ind. Eng. Chem. 1969, 61, 14–28.

[3] Hassnizadeh, M.; Gray,W. General conservation equations for multi-phase systems: 1. Averaging procedure. Adv. Water Resour. 1979, 2, 131–144.

[4] Green, C.T.; Stonestrom, D.A.; Bekins, B.A.; Akstin, K.C.; Schulz, M.S. Percolation and transport in sandy soil under a natural hydraulic gradient. Water Resour. Res. 2005, 41.

[5] Forchheimer, P.Wasserbewegung durch Boden. Z. Ver. Dtsch. Ing. 1901, 45, 1781–1788.

[6] Kadi, K.S. Non-Darcy Flow In Dissolved Gas-Drive Reservoirs. In Proceedings of the SPE Annual Technical Conference and Exhibition, Dallas, TX, USA, 24–27 September 1980.

[7] Belhaj, H.; Agha, K.; Nouri, A.; Butt, S.; Vaziri, H.; Islam, M.R. Numerical Modeling of Forchheimer's Equation to Describe Darcy and Non-Darcy Flow in Porous Media. In Proceedings of the SPE Asia Pacific Oil and Gas Conference and Exhibition, Jakarta, Indonesia, 9–11 September 2003.

[8] Rushing, J.; Newsham, K.; Fraassen, K.V. Measurement of the Two-Phase Gas Slippage Phenomenon and Its Effect on Gas Relative Permeability in Tight Gas Sands. In Proceedings of the SPE Annual Technical Conference and Exhibition, Denver, CO, USA, 5–8 October 2003.

[9] Katz, D.; Cornell, D.; Vary, J.; Kobayashi, R. Handbook of Natural Gas Engineering; Mcgraw-Hill Book Company: New York, NY, USA, 1959.

[10] Holditch, S.A.; Morse, R.A. The Effects of Non-Darcy Flow on the Behavior of Hydraulically Fractured Gas Wells. J. Pet. Technol. 1979, 28, 1169–1179.

[11] Guppy, K.H.; Cinco-Ley, H.; Ramey, H.J. Pressure buildup analysis of fractured wells producing high flow rates. J. Pet. Technol. 1982, 34, 2656–2666.

[12] Martins, J.P.; Milton-Tayler, D.; Leung, H.K. The Effects of Non-Darcy Flow in Propped Hydraulic Fractures. In Proceedings of the SPE Annual Technical Conference and Exhibition, New Orleans, LA, USA, 23–26 September 1990.

[13] David, C.; Donald, K. An analysis of high-velocity gas flow through porous media. Ind. Eng. Chem. 1953, 10, 2145–2152.

[14] Shiri, Y.; Hassani, H. Two-component Fluid Front Tracking in Fault Zone and Discontinuity with Permeability Heterogeneity. Rud. -Geol. -Naft. Zb. 2021, 36, 19–30.

[15] Shiri, Y.; Shiri, A. Numerical Investigation of Fluid Flow Instabilities in Pore-Scale with Heterogeneities in Permeability and Wettability. Rud. -Geol. -Naft. Zb. 2021, 36, 143–156.

[16] Faez, M.; Ramezanzadeh, A.; Ghavami-Riabi, R.; Tokhmechi, B. The evaluation of the effect of fracture geometry on permeability based on laboratory study and numerical modelling. Rud. -Geol. -Naft. Zb. 2021, 36, 155–164.

[17] Namdari, S.; Baghbanan, A.; Hashemolhosseini, H. Investigation of the effect of the discontinuity direction on fluid flow in porous rock masses on a large-scale using hybrid FVM-DFN and streamline simulation. Rud. -Geol. -Naft. Zb. 2021, 36, 49–59.

[18] Ergun, S. Fluid flow through packed column. Chem. Eng. Prog. 1952, 48, 89–94.

[19] John, J.; Donald, K. Applications of unsteady state gas flow calculations. In Proceedings of the Research Conference "Flow of Natural Gas from Reservoirs", Ann Arbor, MI, USA, 30 June–1 July 1955.

[20] Cooke, C.J. Conductivity of Fracture Proppants in Multiple Layers. J. Pet. Technol. 1973, 25, 1101–1107. [CrossRef]

[21] Macdonald, I.F.; El-Sayed, M.S.; Mow, K.; Dullien, F.A.L. Flow through Porous Media The Ergun Equation Revisited. Ind. Eng. Chem. Fundam. 1979, 18, 199–208.

[22] Kutasov, I.M. Equation Predicts Non-Darcy Flow Coefficient. Oil Gas J. 1993, 91, 66–67.

[23] Liu, X.; Civan, F.; Evans, R. Correlation of the Non-Darcy Flow Coefficient. J. Can. Pet. Technol. 1995, 34, PETSOC-95-10-05.

[24] Coles, M.E.; Hartman, K.J. Non-Darcy Measurements in Dry Core and the Effect of Immobile Liquid. In Proceedings of the SPE Gas Technology Symposium, Calgary, AB, Canada, 15–18 March 1998.

[25] Pascal, H.; Quillian, R.G. Analysis Of Vertical Fracture Length And Non-Darcy Flow Coefficient Using Variable Rate Tests. In Proceedings of the SPE Annual Technical Conference and Exhibition, Dallas, TX, USA, 24–27 September 1980.

[26] Cornell, D.; Katz, D.L. Flow of Gases through Consolidated Porous Media. Ind. Eng. Chem. 1953, 45, 2145–2152.

[27] Geertsma, J. Estimating the Coefficient of Inertial Resistance in Fluid Flow Through Porous Media. Soc. Pet. Eng. J. 1974, 14, 445–450.

[28] Evans, E.; Evans, R. Influence of an Immobile or Mobile Saturation on Non-Darcy Compressible Flow of Real Gases in Propped Fractures. J. Pet. Technol. 1988, 40, 1345–1351.

[29] Whitney, D.D. Characterization of the Non-Darcy Flow Coefficient in Propped Hydraulic Fractures. Master's Thesis, University of Oklahoma, Norman, OK, USA, 1988.

[30] Li, D. Analytical Study of theWafer Non-Darcy Flow Experiments. In Proceedings of the SPEWestern Regional/AAPG Pacific Section Joint Meeting, Anchorage, AK, USA, 8–10 May 2002.

[31] Tek, M.R.; Coats, K.H.; Katz, D.L. Turbulence on Flow of Natural Gas Through Porous Reservoirs. J. Pet. Technol. 1962, 14, 799–806.

[32] Yao, Y.; Li, G.; Qin, P. Seepage features of high-velocity non-Darcy flow in highly productive reservoirs. J. Nat. Gas Sci. Eng. 2015, 27, 1732–1738.

[33] Core, J. Using the Inertial Coefficient, B, To Characterize Heterogeneity in Reservoir Rock. In Proceedings of the SPE Annual Technical Conference and Exhibition, Dallas, TX, USA, 27–30 September 1987.

[34] Li, D.; Svec, R.K.; Engler, T.W.; Grigg, R.B. Modeling and Simulation of the Wafer Non-Darcy Flow Experiments. In Proceedings of the SPEWestern Regional Meeting, Bakersfield, CA, USA, 8–10 March 2001.

[35] Thauvin, F.; Mohanty, K.K. Network Modeling of Non-Darcy Flow Through Porous Media. Transp. Porous Media 1998, 31, 19–37.

[36] Shachi, S.; Yadav, B.K.; Rahman, M.A.; Pal, M. Migration of CO2 through Carbonate Cores: Effect of Salinity, Pressure, and Cyclic Brine-CO2 Injection. J. Environ. Eng. 2020, 146, 04019114.

[37] Ahammad, M.J.; Alam, J.; Rahman, M.; Butt, S.D. Numerical simulation of two-phase flow in porous media using a wavelet-based phase-field method. Chem. Eng. Sci. 2017, 173, 230–241.

[38] Sajjad Rabbani, H.; Osman, Y.; Almaghrabi, I.; Azizur Rahman, M.; Seers, T. The Control of ApparentWettability on the Efficiency of Surfactant Flooding in Tight Carbonate Rocks. Processes 2019, 7, 684.

[39] Ding, L.; Cui, L.; Jouenne, S.; Gharbi, O.; Pal, M.; Bertin, H.; Rahman, M.A.; Romero, C.; Guérillot, D. Estimation of Local Equilibrium Model Parameters for Simulation of the Laboratory Foam-Enhanced Oil Recovery Process Using a Commercial Reservoir Simulator. ACS Omega 2020, 5, 23437–23449.

[40] Rahman, M.; Mustafiz, S.; Koksal, M.; Islam, M. Quantifying the skin factor for estimating the completion efficiency of perforation tunnels in petroleum wells. J. Pet. Sci. Eng. 2007, 58, 99–110.

[41] Rahman, M.; Mustafiz, S.; Biazar, J.; Koksal, M.; Islam, M. Investigation of a novel perforation technique in petroleum wells Perforation by drilling. J. Frankl. Inst. 2007, 344, 777–789.

[42] Zheng, L.; Rahman, M.; Ahammad, M.J.; Butt, S.D.; Alam, J. Experimental and Numerical Investigation of a Novel Technique for Perforation in Petroleum Reservoir. In Proceedings of the SPE International Conference and Exhibition on Formation Damage Control, Lafayette, LA, USA, 19–21 February 2016.

[43] Abobaker, E.; Elsanoose, A.; Khan, F.; Rahman, M.A.; Aborig, A.; Noah, K. A New Evaluation of Skin Factor in InclinedWells with Anisotropic Permeability. Energies 2021, 14, 5585.

[44] Ahammad, J.; Rahman, A.; Butt, S.; Alam, M. An Experimental Development to Characterise the Flow Phenomena at the Near-Wellbore Region. In Proceedings of the ASME 2019 38th International Conference on Ocean, Offshore and Arctic Engineering, Glasgow, UK, 9–14 June 2019.

[46] Abobaker, E.; Elsanoose, A.; Rahman, M.A.; Aborig, A.; Zhang, Y.; Sripal, E. Investigation-the-Effect-Mixing-Grain-Size-and- Epoxy-Glue-Content-on-Index-Properties-of-Synthetic-Sandstone-Sample. In Proceedings of the Canadian Society for Mechanical Engineering International Congress, Charlottetown, PE, Canada, 21–24 June 2020.

Chapter 4

Characterization of a Non-Darcy Flow and Development of New Correlation of NON-Darcy Coefficient

Preface

A version of this chapter has been published in Energies 2022, 15, 1197. I am the primary author of this manuscript, along with co-authors Dr. Abobaker, Dr. Faisal Khan, Dr. Rahman, Dr. Amer Aborig, and Dr. Butt. Dr. Butt assisted in the design of the setup. I proposed the idea and concept and prepared the samples with assistance from Dr. Amer and Abobaker; they also helped conduct the experiments. However, I collected and analyzed the experimental data. Dr. Aziz evaluated the methodology and reviewed the manuscript. I wrote the original manuscript, and Dr. Aborig, Dr. Faisal Khan, and Dr . Aziz reviewed the manuscript and suggested amendments that had a significant impact on enriching this manuscript.

4.1 Abstract

Non-Darcy behavior is important for describing fluid flow in porous media in situations where high velocity occurs. A criterion to identify the beginning of non-Darcy flow is needed as well. In this study, the characteristics of the non-Darcy flow were analyzed by presenting the corresponding pressure and velocity gradient curves for each pressure. Extensive analysis indicates that many of the correlations available in the literature either have defective units or are the product of a small number of experiments. In this study, we benefit from relatively large samples, the radial flow, and the perforation in the middle of the samples. The properties of the samples were measured using mercury intrusion porosimetry. It was found that there is a direct relationship between the porosity and the grain's size; the greater the size of the grains, the greater the porosity, and vice versa. The

non-Darcy coefficient term, β, is found to be inversely proportional to the porosity and permeability. In a previous study, the β was investigated for compressible flow scenarios; however, this study calculated it for an incompressible flow. Finally, by analyzing the β values of both studies, we could deduce new novelty correlations for the β coefficient term, where the permeability, porosity, and tortuosity are included.

4.2 Introduction

Fluid particles passing through a porous bed are subject to accelerations and decelerations as alternately pass-through contraction and expansion tortuous [1]. The particle's kinetic energy is interchanged with the pressure energy during the acceleration and deceleration processes. This interchange includes significant irreversibility at the velocity where the pressure drop becomes more than proportional to the velocity [2]. Some investigators refer to this phenomenon as kinetic effects, and the researchers agree that the extra fluid motion is caused primarily by the inertial effects in the deceleration process and quiet in the absence of turbulent eddies. Some investigators have referred to this phenomenon as "non-Darcy" flow. If one assigns the extra motion of the fluid as the cause of the additional pressure loss, then the term "turbulent flow" is justified because, in actual turbulent flow in pipes, it is the extra ammunition of energy that is significant to the engineer [3]. Hence, many investigators in the field use the term "turbulent flow" to designate a condition of velocity such that increases in pressure drop for liquids or differences of squares of pressures for gases are more than proportional to increases in flow rates [4]. That is the procedure followed here; flow in porous media is present in many applications and engineering industries. The flow in porous media is essential in agricultural engineering as

it helps make the most of irrigation water. In hydrology, it is critical to the process of extracting groundwater [5]. In civil engineering, studying porous media is fundamental to building design and safety and is becoming increasingly crucial in oil and gas production [6]. Flow in porous media is a complex phenomenon because of many factors, such as the nature of fluid and porous media nature. So, there are many differences in understanding and characterizing the flow [7]. In the case of low flow velocity, Darcy's law can describe the flow in the porous media as follows.

$$Q = \frac{kA}{\mu L}\Delta P \tag{1}$$

Q is the flow rate, k is the media permeability, A is the flow rate cross-section, μ is the viscosity and sample length (L), and ΔP is the pressure drop. The non-Darcy flow is the flow that has a nonlinear relationship between flow rate and pressure difference and cannot be described by Darcy's law. The Forchheimer equation was introduced that included an extra term to address the additional pressure losses due to the inertia forces; thus, for one-dimensional flow, the Forchheimer has the following form [8]:

$$\frac{\Delta P}{\Delta X} = \frac{(\mu)}{(k)}V + \beta\rho V^2 \tag{2}$$

ΔP pressure drop, ΔX flow distance, μ viscosity, k permeability, V flow velocity, β non-Darcy coefficient, and ρ the density. Even though the flow velocity is low, some researchers still argue that the non-Darcy flow excites even in the low flow velocities. Previously, the nonlinearity between the pressure gradient and the flow rate was attributed to turbulence. Nowadays, many researchers agree that the nonlinearity is not due to turbulence only but to inertial effects too [9]. The inertia term of the Forchheimer equation included the

coefficient β, which measures the deviation from the linearity. It has been concluded that the non-Darcy effect occurs because the microscopic inertial effects alter the velocity and pressure fields. The above example implies that tortuosity should be one of the critical factors determining the non-Darcy coefficient [10]. The non-Darcy coefficient in wells is usually determined by analysis of many correlations in the literature [11]. Both empirical correlations and theoretical equations of the non-Darcy coefficient will be reviewed. For the empirical correlations, reviews will be done on one-phase and two-phase bases [12]. So far, no theoretical equations in two or more phases have been found, so the study will be limited to a one-phase case for theoretical equations [13].

The critical parameter in β correlations that predicts the non-Darcy is permeability. Ergun developed a theoretical equation by analyzing lab data collected from his experiments and data from the literature and came up with an empirical equation, which included spheres of different sizes, sand, and the following gases: carbon dioxide, nitrogen, methane, and hydrogen [14]. Comparing the Ergun empirical flow equation with the Forchheimer equation leads to [15]:

$$\beta = ab^{-1/2}(10^{-8}k)^{-1/2}\phi^{-3/2} \tag{3}$$

Where a = 1.75, b = 150 constants, k is the permeability expressed in Darcy, β is 1/cm, and ϕ is the porosity. Equation (3) analyzed for particles of different roughness and found that b = 180, while "a" ranges from 1.8 to 4 [16]. Another equation proposed by Janicek et al. [17] related the permeability and the porosity in order to predict the non-Darcy coefficient for real porous media, as shown below:

$$\beta = 1.82 \times 10^{8} k^{-5/4} \emptyset^{-3/4} \quad (4)$$

K is expressed in mD, and β in 1/cm.

However, Geertsma [18] developed an empirical relationship between the skin coefficient, permeability, porosity, and the skin factor. The dimensionally consistent equation is of the form:

$$\beta = \frac{0.005}{\emptyset^{5.5} k^{0.5}} \left[\frac{1}{(1-S_w)^{5.5} k_r^{0.5}}\right] \quad (5)$$

Additionally, he presented another correlation based on 180 β data labs from different experiments. Although the points were collected from experiments on many types of porous media and tests of liquids and gases, these laboratory data did not include data on tortuosity:

$$\beta = \frac{20.6}{\emptyset^{4.62} \sqrt{k}} \quad (6)$$

Jones [19] conducted experiments on 355 sandstone and 29 limestone cores in different core types. By analyzing the data from his experiments, he came up with a correlation to estimate the non-Darcy coefficient,

$$\beta = \frac{6.15 \times 10^{10}}{k^{1.55}} \quad (8)$$

It can be noted that the β units are not correct. From the initial assessment, we have observed that the existing correlations show a significant deviation. The first reason is the relativity of the flow direction to the porous channels (i.e., tortuosity) can affect the correlation of the non-Darcy coefficient. The second reason is that different parameters are considered when developing the correlations and the fluid used in the experiments. Umair

Khan [21] presented a study on the effects of velocity and thermal slip conditions on the stagnation-point mixed convective flow of cross liquid moving over a vertical plate entrenched in a Darcy–Forchheimer porous medium. The study concluded that the permeability parameter decelerates the drag forces and declines the heat transfer rate. Jamshaid ul Rahman [22] investigated the Darcy–Forchheimer effects on the 3D nanofluid flow with engine oil as a base fluid containing suspended carbon nanotubes mathematically. The outcome of his study indicated that a higher slip parameter boosts the axial velocity, whereas the fluid temperature lowers for a sturdier relaxation parameter. Metib Alghamdi [23] numerically examined the dynamical behavior and thermal transportation feature of an enhanced MHD convective Casson bi-phasic flow of sodium alginate-based nanofluids in a Darcy–Brinkman medium bounded by a vertical elongating slender concave-shaped surface, and the results showed that the wall heat transfer rate and the frictional effect are strengthened with the loading of nanoparticles and weakened with the mounting values of the heat source parameters. Previous studies on single-phase flow using modeling and experiments were conducted in a near wellbore and perforation tunnel [24–27]. In addition, multiphase flow studies in perforation tunnels and porous media were also conducted [11–17,28–32]. In the current study, we will examine the validity of the existing correlations reported in the literature. This study will propose a novel correlation considering sample permeability, porosity, and tortuosity. These are the essential correlation factors in developing a reliable model for β.

4.3 Experimental Methodology

The experimental method begins with the preparation of samples from sand collected from local sources. The sample preparation passes through several stages, the first of which is sieving the sand and classifying it into sizes. Then mixing each of these sizes with an adhesive substance takes place to obtain the required hardness sample, which helps to stabilize the properties during the experiment; more details will be provided in the next section. The flow experiment is carried out on seven samples that have been prepared, where the sample is placed in the chamber (Figure 1); the fluid is then injected radially into the sample, as depicted in Figure 2, and the pressure is measured.

Figure 1. Experiment Setup, Radial Flow Facility.

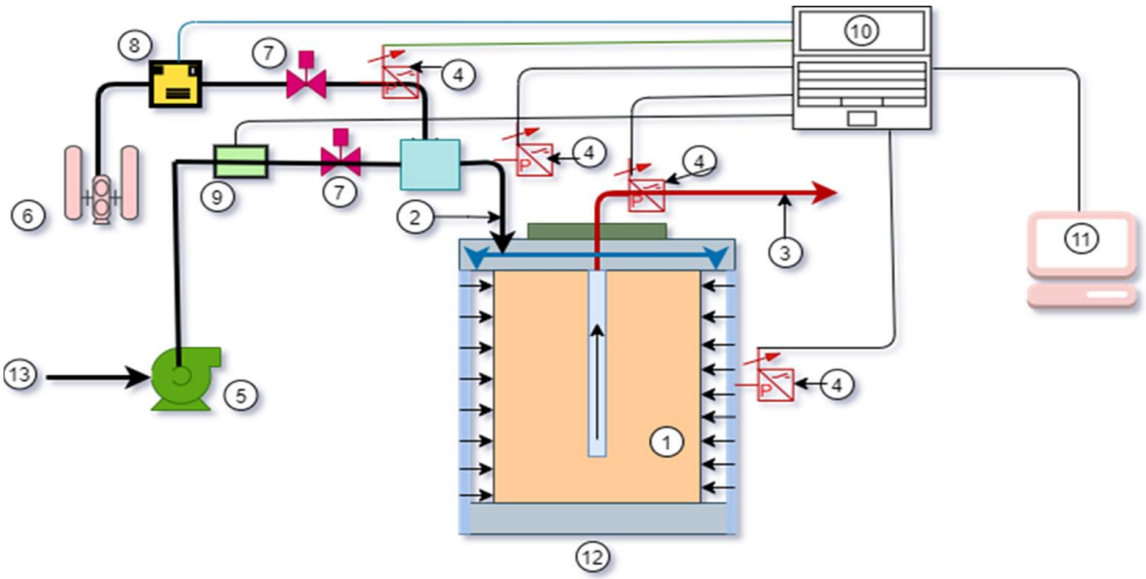

Figure 2. Schematic diagram of the experiment R.F.C. facility: 1. Sample, 2. Inlet, 3. Outlet, 4. Pressure Sensors, 5. Water pump, 6. Air compressor, 7. non-Return valves, 8. Airflow meter, 9. Water flowmeter, 10. Data Acquisition, 11. Computer, 12. Samples Chamber, 13. Waterline.

4.3.1 Experimental Setup

In the Memorial University of Newfoundland Laboratories, the experimental setup was developed to conduct experiments [33,34]. It comprises four functional units: water supply, experimentation, measurement, and data acquisition. A schematic diagram of the experimental setup is depicted in Figure 2.

As a result of the difficulties faced by non-Darcy flow tests, such as providing samples and various working fluids as well as high speeds and pressures, many researchers resort to measurements of individual cores or sand-packed models. Therefore, the resulting equations are not general. The current laboratory experiment begins with placing the sample in the sample chamber, as shown in Figures 1 and 2, and connecting all pressure sensors that are able to measure up to 300 psi; and the flow rate meters connected to the data acquisition. The flow test was repeated several times to ensure that the collected data

were correct. The experiment was designed to start with a water flow rate of 0.333 LPM, and the flow increased by 0.333 LPM each time to 6 LPM. The pressure drop data were recorded for each run, and the fluid temperature was observed and kept constant at 20 °C.

4.3.2 Porous Media Selection

This type of experiment in which the non-Darcy flow is investigated requires high fluid flow velocity. Under laboratory conditions, high pressures that can push fluids at a high flow velocity through porous media with low permeability may not be available. Therefore, the production of porous media with high permeability was resorted to in the laboratory because it is not easy to obtain real porous media with high permeability.

4.3.3 Core Preparation

Since the setup was designed to be suitable for cylindrical samples, the samples were manufactured in a cylindrical shape (Figure 3). It was taken into account that the outer surfaces of the samples are free from defects such as cracks or corroded holes; the outer surface of the samples is considered to be the inlet to the fluid flow. The appropriate outer diameter of the samples in this experiment is 15.54 cm and has a height of 31 cm. The samples have a perforated hole in the middle, 25 cm deep and 2.54 cm in diameter, and it is considered the outlet of the flow, as shown in Figure 3 above. The samples manufactured in the Memorial University Laboratories consisted of sand collected from local sources; the sand was dried and then sieved and classified according to the size of the sand grains, from the smallest to the largest. Each of these sizes was used to create the samples after mixing the sand with an adhesive liquid and placing it in specific molds to dry within 24 h. The

samples are cylindrical in shape, as well as perforated. Table 1 shows the properties of the samples that were measured in the laboratories.

Figure 3. Porous medial samples.

Table 1. The index properties for the samples

Sample No.	Permeability (mD), k	Porosity (%), $\emptyset$	Tortuosity, τ	Mean Pore Diameter M.P.D (µm)
Sample 1	2035.95	21.5	3.62	25.31
Sample 2	3981.50	23.4	3.19	32.14
Sample 3	6292.66	26.31	2.82	45.27
Sample 4	8127.04	27.94	2.27	60.61
Sample 5	12,281.50	29.3	2.10	81
Sample 6	16,320.24	31.2	1.96	100
Sample 7	26,151.72	33.2	1.7765	181.74

4.4 The Determination of a Non-Darcy Flow

From the literature, it can be noticed that a significant discrepancy exists in determining the point at which the Darcy flow turns into a transitional phase and a non-Darcy flow, which is attributed to the unique nature of the porous media. The results were different when

comparing two samples with the same permeability and porosity and when tested with the same fluid for the same flow rate. However, a Reynolds number and a Forchheimer number can be used in determining the flow type in porous media.

4.4.1 Hydraulic Gradient-Velocity

The non-Darcy flow results from increased fluid velocity, excessive momentum, and irregularities. The following formula can be used to describe the non-Darcy flow, which is known as the Izbash form [35]:

$$i = aV^b \tag{9}$$

In which a and b are constants that can be determined from the conducted experiments, V is average bulk flow velocity (m/s), and i is hydraulic gradient. The previous formula showed shortcomings in calculating all pressure values, so another side was added to Equation (9) to become a quadratic equation. The Forchheimer equation is presented as follows:

$$i = AV + BV^2 \tag{10}$$

A is a Darcy flow coefficient that depends on the properties of the porous medium, and B is a coefficient that depends on the characteristics of the porous media. Sedghi-Asl and Rahimi [36] conducted experiments on porous media with particle sizes between 55 and 79 mm as well as using six different sizes of coarse materials (2.83–56.8 mm); the experiment was carried out on a wide range of Reynolds numbers, and they obtained a quadratic relationship as follows:

$$i = \frac{bv}{2gnd^2}V + \frac{a}{2gnd}V^2 \tag{11}$$

$$f = a + \frac{b}{Re} \tag{12}$$

$$Re = \frac{Vd}{nv} \tag{13}$$

In which a, b are constants, n (-) is the porosity, f (-) is the friction factor, υ (L2 T−1) is the kinematic viscosity, Re (-) is the Reynolds number, d (L) is the grain diameter of aggregates, V(LT−1) is the bulk flow velocity, and g(LT−2) is the gravity acceleration. Additionally, Salehi et al. [37] investigated experimentally with a non-Darcy flow through a packed column test for rounded aggregates with domains between 2.83- and 56.8-mm. Ergun [14] suggested the following quadratic equation for both Darcy and non-Darcy flow regimes:

$$i = \frac{150v(1-n)^2}{gn^3d^2}V + \frac{1.75(1-n)}{gn^3d}V^2 \tag{14}$$

Mc Corquodale et al. [38] presented the following relationship by means of 1,250 experimental data as

$$i = \frac{70v}{R^2gn}V + \frac{0.81}{Rgn^{\frac{1}{2}}}V^2 \tag{15}$$

Where R is the hydraulic mean radius, which is defined as

$$R = \frac{nd}{6(1-n)r_e} \tag{16}$$

In which (r_e) is the shape factor efficiency, which for spherical grains is equal to 1, and which represented the following relationship by means of 300 experimental data:

$$i = \frac{144v(1-n)^2}{gn^3d^2}V + \frac{2.4(1-n)}{gn^3d}V^2 \tag{17}$$

Kadlec and Knight [39] also suggested the following equations:

$$i = \frac{255v(1-n)^2}{gn^{3.7}d^2}V + \frac{2.4(1-n)}{gn^3 d}V^2 \quad (18)$$

4.5 Experimental Results and Analysis

In this section, the results and analysis of data obtained from laboratory experiments will be presented. The flow results will be analyzed, and the non-Darcy flow will be verified, as well as the interaction between the velocity and the hydraulic gradient, to arrive at a proper formula for non-Darcy's coefficient.

4.5.1 Hydraulic Gradient-Velocity

One of the methods used to determine whether the flow is Darcy or non-Darcy is the relationship between hydraulic gradient (i) and flow velocity (V); Figures 4–7. The flow can be considered a Darcy flow if the relationship is linear, but if the relationship is non-linear, this indicates the presence of a non-Darcy flow. The following figures show the nonlinear relationship between the flow velocity and the hydraulic gradient.

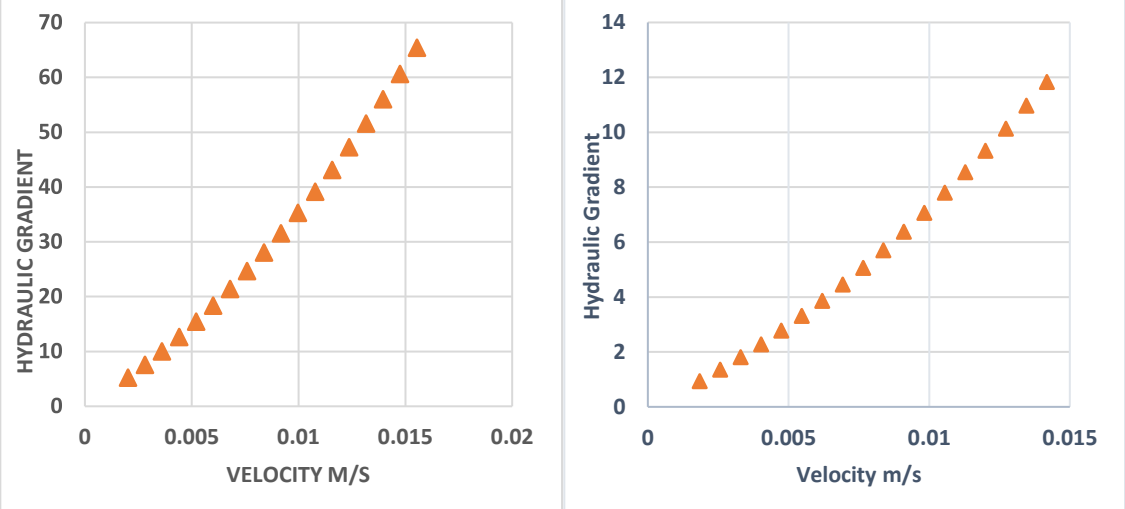

Figure 4. Hydraulic Gradient vs. Velocity for samples 1 and 2, respectively.

Testing and plotting the relationship between the velocity and the hydraulic gradient makes it easy to observe whether the relationship is linear or nonlinear. It can be noted that all samples have a nonlinear relationship, even though in varying proportions, as the samples with high permeability and porosity have less resistance and fewer pressure losses, and therefore the flow behavior is close to that of the Darcy flow.

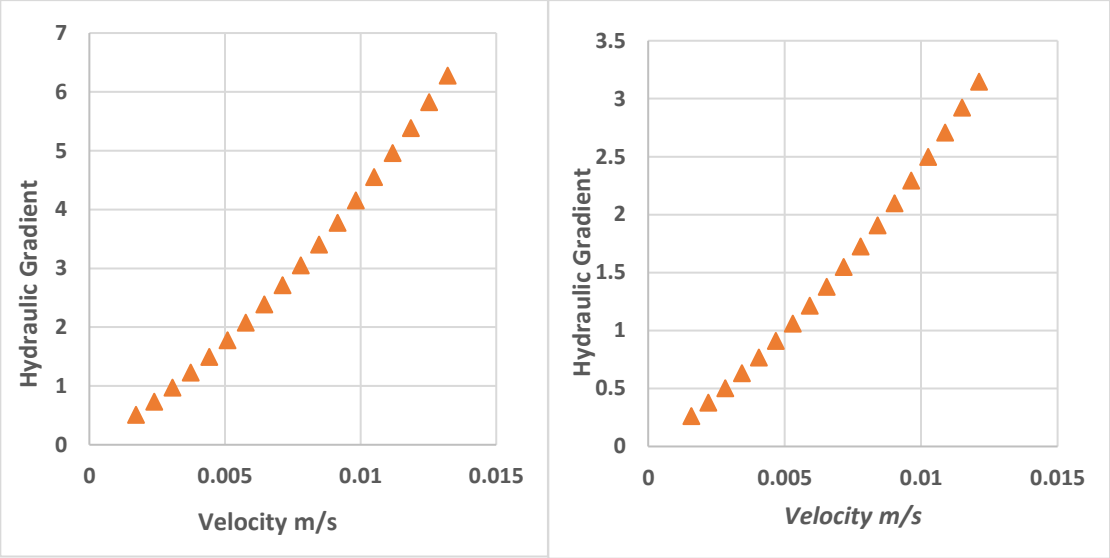

Figure 5. Hydraulic Gradient vs. Velocity for samples 3 and 4, respectively.

The figures of all flow samples clearly show the relationship between the velocity and the hydraulic gradient. It is easy to see that all samples' relationships are nonlinear, although the variance varies from sample to sample. Samples with low porosity and permeability have more curved lines, indicating that the flow is moving away from the Darcy flow performance compared to samples with high porosity and permeability.

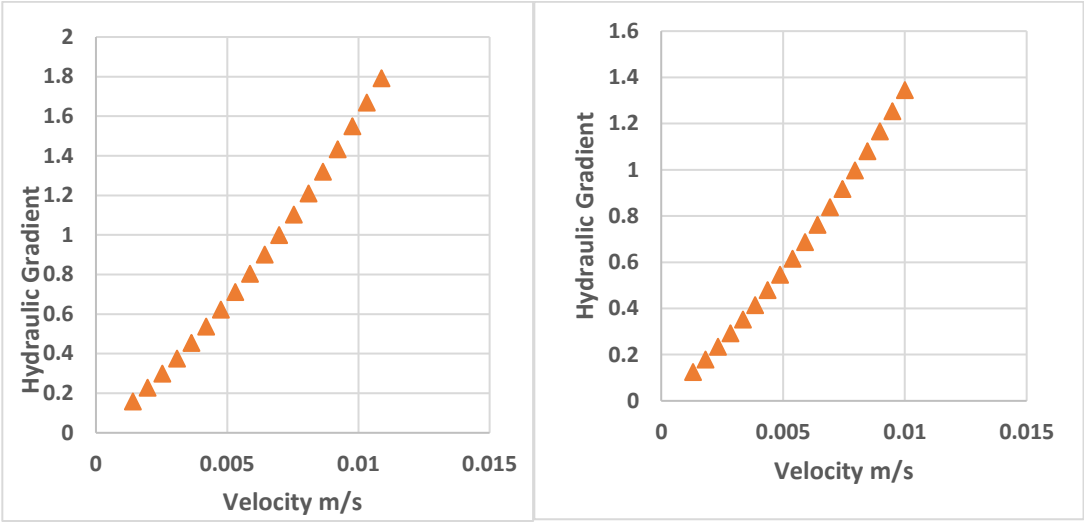

Figure 6. Hydraulic Gradient vs. Velocity for samples 5 and 6.

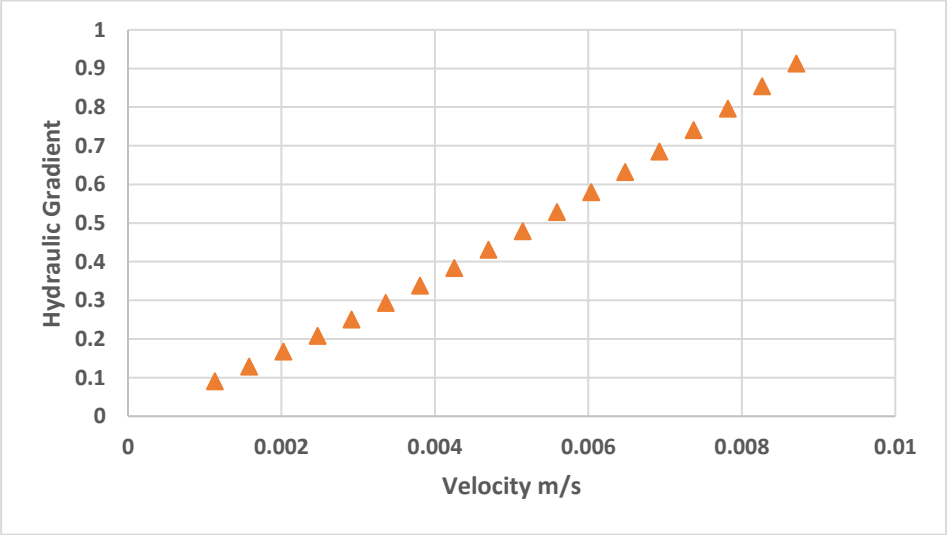

Figure 7. Hydraulic Gradient vs. Velocity for samples 7.

4.5.2 The Flow Rate and Pressure Gradient

Seven large cylindrical cores were experimentally tested; the results are displayed in Figure 8, where the flow rate and pressure gradients are the abscissa and ordinate, respectively. The Figure shows that the pressure gradient and flow rate have a better linear relationship when the flow rate is low. As the flow rate increases, the curve proves a departure from

linearity and tilts towards the pressure gradient axis, i.e., there is an obvious non-Darcy flow when the flow rate is higher.

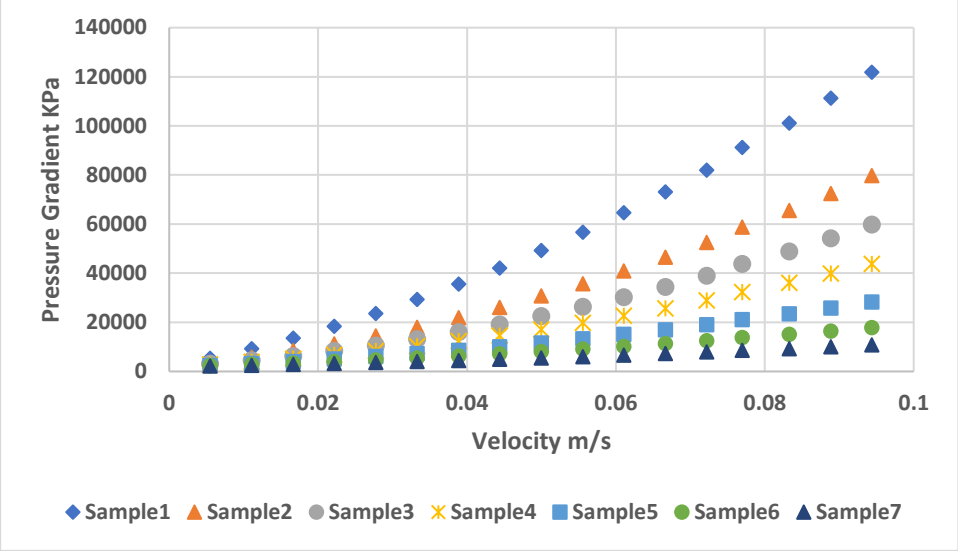

Figure 8. Pressure Gradients vs. Velocity.

4.6 Porosity Effect

The porous media porosity plays a significant role in determining the non-Darcy coefficient. The non-Darcy coefficient is a function of the porosity derived from the Mercury Intrusion Porosimeter (M.I.P.) test, as illustrated in Figure 9. The graph indicated that the coefficient is inversely proportional to the porosity. Significantly, the coefficient decreases sharply with the increase in the mean pore diameter and seems to be conversing at a lower limit.

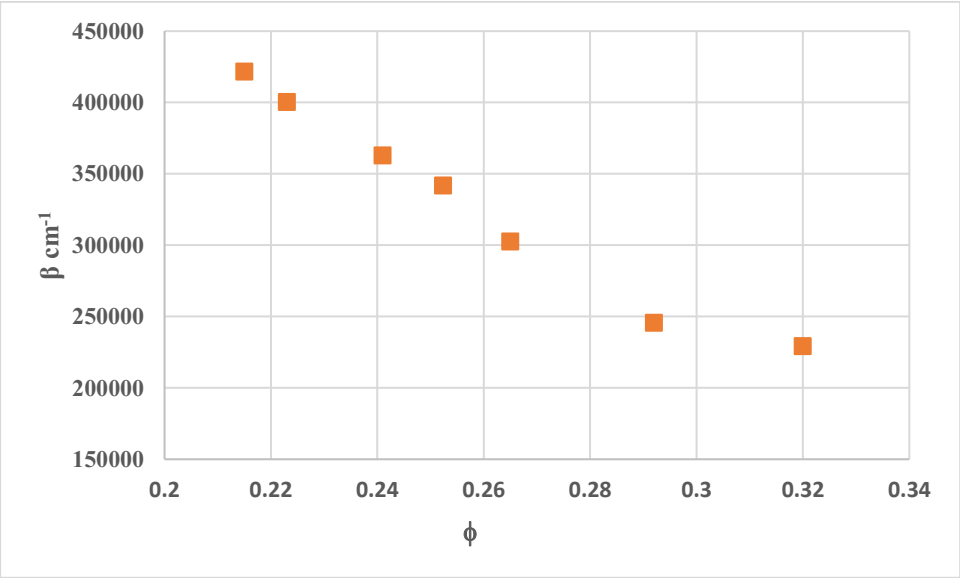

Figure 9. Non-Darcy coefficient vs. porosity.

Porosity is one characteristic that determines whether the flow is Darcy or non-Darcy. Therefore, it found that most coefficients of Darcy's empirical equations are based mainly on porosity and permeability. In general, it can be said that there is a direct relationship between the porosity and the grain's size; the greater the size of the grains, the greater the porosity, and vice versa. Synthetic sample porous media may deviate from this rule, as using pistons to compress samples or mixing more than one size of grains may make the relationship between grain size and porosity inverse. The relationship between porosity and grain size is presented in Figure 10, as each sample used a one-grain size, and no pressing tools were used during the manufacturing stages.

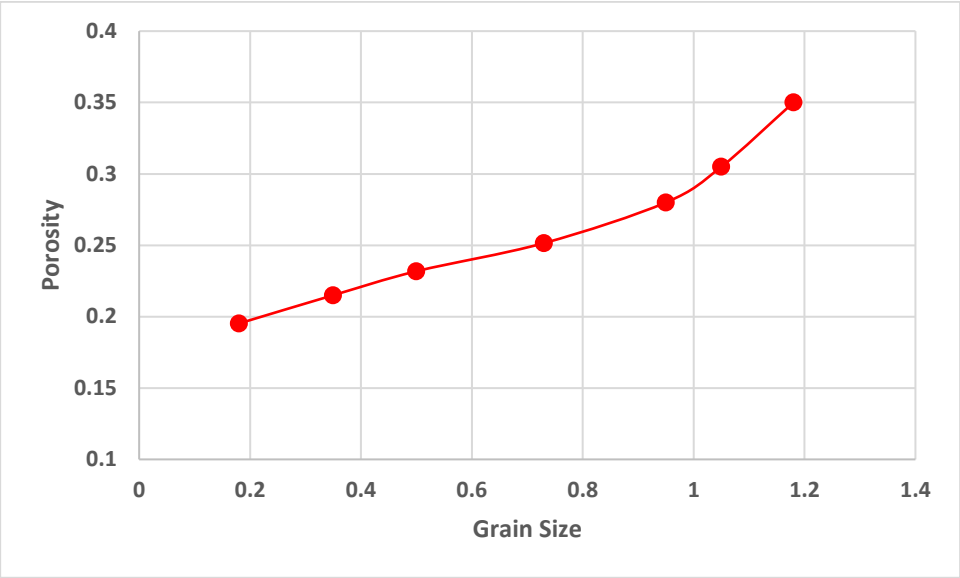

Figure 10. Relationship between the porosity of the samples and the grain size.

4.7 Correlation of Non-Darcy Coefficient

The non-Darcy coefficient β can be expressed with the hydraulic conductivity and porosity in another form and shown as follows by Yuedong [40]:

$$\beta = \frac{c}{\sqrt{k}\varphi^{1.5}} \tag{19}$$

This paper used water as a working fluid, and non-Darcy's coefficient was calculated in the seven synthetic

samples. In previous work, the air was used [41], the non-Darcy flow was characterized, and the calculation of the non-Darcy coefficient was calculated. In general, the non-Darcy coefficient β is determined based on the following expression:

$$\beta = \frac{a}{k^c \emptyset^b} \tag{20}$$

If both sides are logarithm taking, draw the relationship between Log(βk^0.5) and (log Ø) as in Figure 11. It is possible to put the relationship as follows, converting the natural logarithm to the base ten logarithms.

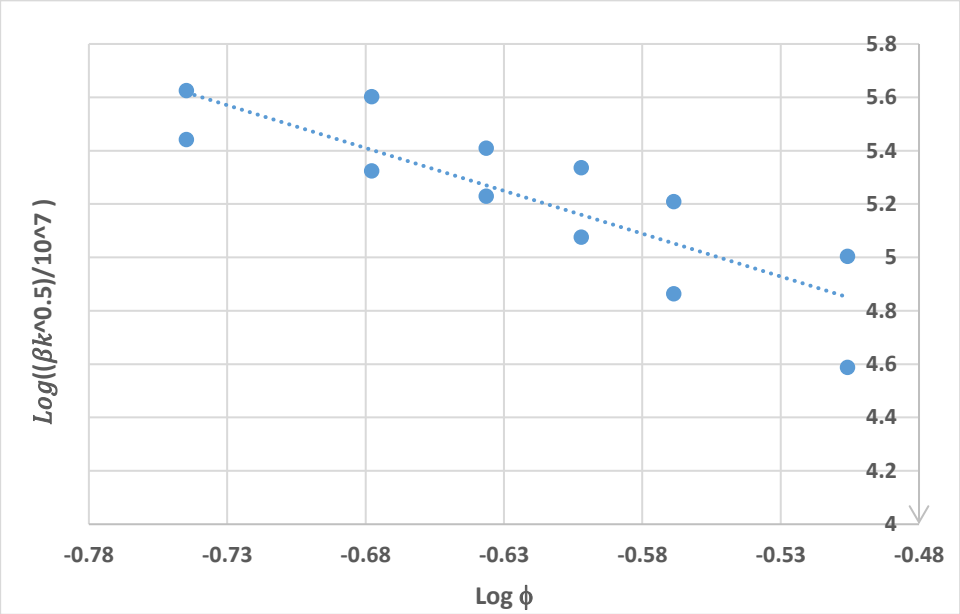

Figure 11. The non-Darcy coefficient for the seven samples resulted from two different air and water experiments.

$$Log\left(\frac{\beta k^{0.5}}{10^7}\right) = log\emptyset^{-2.0} - log31622.77 \tag{21}$$

With further simplifications, the final form is:

$$\beta = \frac{4.5}{k^{0.5}\emptyset^2} \tag{22}$$

Although it is considered a preliminary study, it produced reliable correlations for calculating the non-Darcy flow coefficient. The units in this equation are identical to the non-Darcy coefficient unit.

4.8 Tortuosity

Tortuosity is an important parameter in the oil and gas industry. The concept of tortuosity is used to characterize the structure of porous media, estimate their hydraulic conductivity, and study the travel time and length for tracer dispersion. Therefore, it is essential to include tortuosity within the correlation. The general expression for the non-Darcy coefficient with respect to tortuosity is:

$$\frac{\beta k^{0.5}}{\tau} = \frac{a}{\emptyset^{b}} \tag{23}$$

where τ is the tortuosity.

The tortuosity of the samples was obtained from the mercury intrusion porosimetry (M.I.P.) as given in Table 1; using the data of β, φ, k, and τ Figure 12 can be generated, and the obtained correlation is as follows:

$$\beta = \frac{6.5\,\tau}{k^{0.5}\emptyset^{4.4}} \tag{24}$$

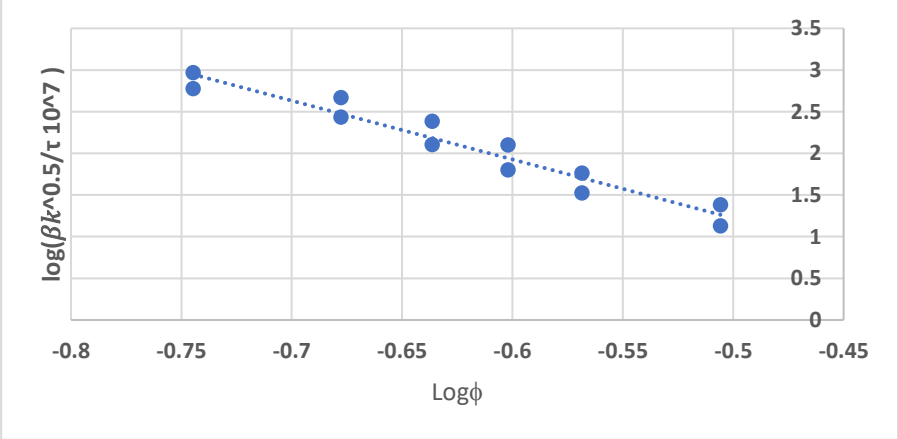

Figure 12. The non-Darcy coefficient with the effect of tortuosity for the seven samples resulted from two different air and water experiments.

Finally, both obtained novelty correlations, as illustrated in Equations (22) and (24), not only distinguished that they are consistent in terms of units; but in addition, they are correct compared to many correlations found in the literature. It was noted that many of them are incorrect in terms of units. However, our reliable experimental results, as shown in Figures 13 and 14, were obtained based on radial flow experiments and large samples.

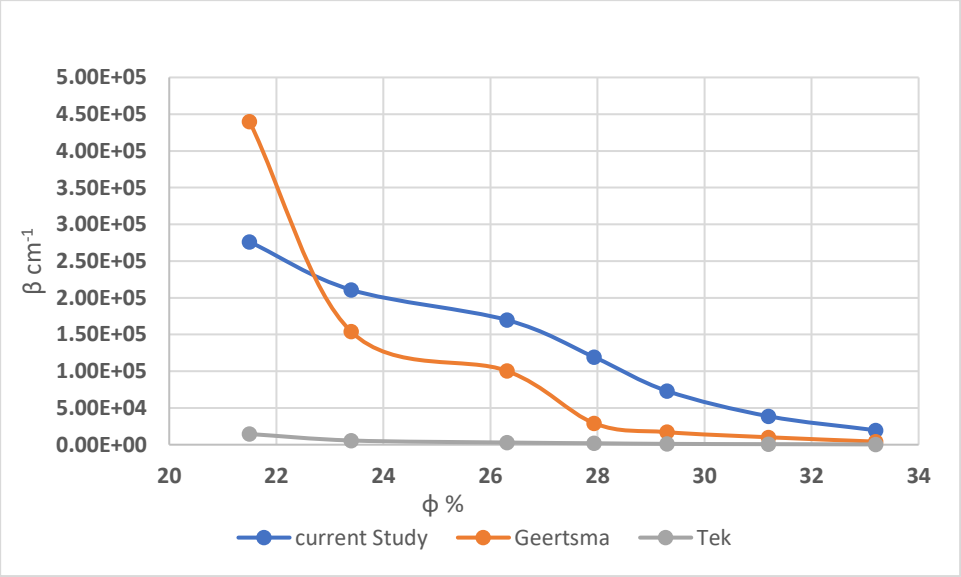

Figure 13. Comparison of a correlation equation (23) with Geertsma and Tek correlations.

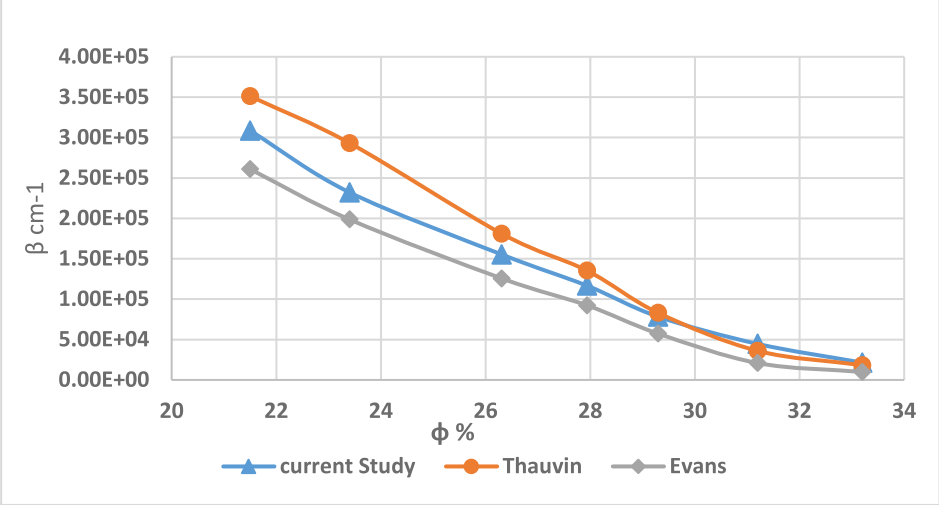

Figure 14. Comparison of a correlation equation (24) including tortuosity effect with Thauvin and Evans correlations.

4.9 Conclusions

In this study, the non-Darcy flow was characterized by means of the hydraulic gradient using seven large synthetic porous media. In addition, non-Darcy co-efficient data were collected from our experiment. As a result, imperative correlations were generated with respect to unit consistency and the influence of porosity and tortuosity.

- There are many methods for calculating the non-Darcy coefficient in the literature using flow velocity and the combined action of the displacement medium (liquid) and the porous media. This includes using the Reynolds number, the Forchheimer number or analyzing pressure and flow data.

- The data were collected using seven large samples in this paper, and the flow was radially considered uncommon in the literature. In total, 358 experiments were conducted. Water and air were used as operating fluids.

- This study produced two reliable correlations, one of which considered tortuosity an important parameter. Many researchers have recently argued that it should be included in the correlations. This work can be extended by experimenting with other fluids such as oil, CO2, etc. Additionally, more samples with different porosity and permeabilities will produce more β points.

References

[1] Andrade, J.S.; Costa, U.M.; Almeida, M.P.; Makse, H.A.; Stanley, H.E. Inertial Effects on Fluid Flow through Disordered Porous Media. *Phys. Rev. Lett.* 1999, *82*, 5249–5252.

[2] Hill, R.J.; Koch, D.L.; Ladd, A.J.C. The First Effect of the Fluid Inertia on Flows in Ordered and Random Arrays of Sphers. *J. Fluid Mech.* 2001, *448*, 213–241.

[3] Cheng, H.; Papanicolaou, G. Flow past periodic arrays of spheres at low Reynolds number. *J. Fluid Mech.* 1997, *335*, 189–212.

[4] Wu, Y.-S.; Lai, B.; Miskimins, J.L.; Fakcharoenphol, P.; Di, Y. Analysis of Multiphase Non-Darcy Flow in Porous Media. *Transp. Porous Media* 2011, *88*, 205–223.

[5] Cattaneo, L.; Comunian, A.; De Filippis, G.; Giudici, M.; Vassena, C. Modeling Groundwater Flow in Heterogeneous Porous Media with YAGMod. *Computation* 2016, *4*, 2–19.

[6] Ghahri, P.; Jamiolahmady, M. A new, accurate and simple model for calculation of productivity of deviated and highly deviated well – Part I: Single-phase incompressible and compressible fluid. *Fuel* 2012, *97*, 24–37.

[7] Ni, X.; Kulatilake, P.; Chen, Z.; Gong, P.; Kong, H. Experimental Investigation of Non-Darcy Flow in Sandstone. *Geotech. Geol. Eng.* 2016, *34*, 1835–1846.

[8] Akihiro, T.; Xiaopeng, Z.; Taku, T.; Mitsuru, K. Topology optimization of a porous unit cell in a fluid flow considering Forchheimer drag. *Int. J. Comput. Fluid Dyn.* 2020, *34*, 50–60.

[9] Ovalle-Villamil, W.; Sasanakul, I. Investigation of Non-Darcy Flow for Fine Grained Materials. *Geotech. Geol. Eng.* 2019, *37*, 413–429.

[10] Partha, K.; Vimal, K.; Lausanne, M. Experimental and numerical investigation of fluid flow hydrodynamics in porous media: Characterization of pre-Darcy, Darcy and non-Darcy flow regimes. *Powder Technol.* 2016, *303*, 278–291.

[11] Yang, Y.; Huiqing, L.; Ling, X.; Meng, Z. Experimental study of non-darcy two-phase flow in a fractured—Vuggy medium. *Chem. Technol. Fuels Oils* 2016, *52*, 36–40.

[12] Wheeler, M.; Balhoff, M. A Predictive Pore-Scale Model for Non-Darcy Flow in Porous Media. *SPE J.* 2009, *14*, 579–587.

[13] Hassanizadeh, S.M.; Gray, W.G. High-Velocity Flow in Porous Media. *Transp. Porous Media* 1987, *2*, 521–531.

[14] Ergun, S.; Orning, A. Fluid Flow through Randomly Packed Columns and Fluidized Beds. *Ind. Eng. Chem.* 1949, *41*, 1179–1184.

[15] Dacun, L.; Robert, S.; Tom, E.; Reid, G. Modeling and Simulation of the Wafer Non-Darcy Flow Experiments. In Proceedings of the SPE Western Regional Meeting, Bakersfield, CA, USA, 26–30 March 2001.

[16] Macdonald, F.; Mow, E.S.K.; Dullien, L. Flow through Porous Media-the Ergun Equation Revisited. *Ind. Eng. Chem. Fundam.* 1979, *18*, 199–208.

[17] Janicek, J.; Katz, D. *Applications of Unsteady State Gas Flow Calculations*; University of Michigan, Ann Arbor, MI, USA, 1955.

[18] Geertsma, J. Estimating the Coefficient of Inertial Resistance in Fluid Flow Through Porous Media. *Soc. Pet. Eng. J.* 1974, *14*, 445–450.

[19] Jones, S.C. Using the Inertial Coefficient, B, To Characterize Heterogeneity in Reservoir Rock. In Proceedings of the SPE Annual Technical Conference and Exhibition, Dallas, TX, USA, 27–30 September 1987.

[20] Wang, X.; Thauvin, F.; Mohanty, K.K. Non-Darcy flow through anisotropic porous media. *Chem. Eng. Sci.* 1999, *54*, 1859–1869.

[21] Khan, U.; Zaib, A.; Khan, I.; Nisar, K.S.; Baleanu, D. Insights into the Stability of Mixed Convective Darcy–Forchheimer Flows of Cross Liquids from a Vertical Plate with Consideration of the Significant Impact of Velocity and Thermal Slip Conditions. *Mathematics* 2020, *1*, 8.

[22] Rahman, J.U.; Khan, U.; Ahmad, S.; Ramzan, M.; Suleman, M.; Lu, D.; Inam, S. Numerical Simulation of Darcy–Forchheimer 3D Unsteady Nanofluid Flow Comprising Carbon Nanotubes with Cattaneo–Christov Heat Flux and Velocity and Thermal Slip Conditions. *Processes* 2019, *7*, 687.

[23] Alghamdi, M.; Wakifc, A.; Thumma, T.; Khan, U.; Baleanu, D.; Rasool, G. Significance of magnetic field strength and heat source variability on the radiative-convective motion of sodium alginate-based nanofluid within a Darcy-Brinkman porous structure bounded vertically by an irregular slender surface. *Case Stud. Therm. Eng.* 2021, *28*, 101428.

[24] Rahman, M.A.; Mustafiz, S.; Koksal, M.; Islam, M.R. Quantifying the skin factor for estimating the completion efficiency of perforation tunnels in petroleum wells. *J. Pet. Sci. Eng.* 2007, *58*, 99–100.

[25] Rahman, M.A.; Mustafiz, S.; Biazar, J.; Koksal, M.; Islam, M.R. Investigation of a novel perforation technique in petroleum wells—perforation by drilling. *J. Frankl. Inst.* 2007, *344*, 777–789.

[26] Zheng, L.; Rahman, M.A.; Ahammad, M.J.; Butt, S.D.; Alam, J.M. Experimental and Numerical Investigation of a Novel Technique for Perforation in Petroleum Reservoir. In Proceedings of the SPE International Conference and Exhibition on Formation Damage Control, Lafayette, LA, USA, 24–26 February 2016.

[27] Abobaker, E.; Elsanoose, A.; Khan, F.; Rahman, M.A.; Aborig, A.; Noah, K. Quantifying the partial penetration skin factor for evaluating the completion efficiency of vertical oil wells. *J. Pet. Explor. Prod. Technol.* 2021, *11*, 3031–3043.

[28] Rabbani, H.; Khan, M.; Qureshi, M.F.; Rahman, M.A.; Seers, T.; Lal, B. Analytical Modelling of Gas Hydrates in Porous Media. In Proceedings of the Offshore Technology Conference Asia, Kuala Lumpur, Malaysia, 22–25 March 2022.

[29] Ahammad, M.J.; Alam, M.J.; Rahman, M.A.; Butt, S.D. Numerical simulation of two-phase flow in porous media using a wavelet-based phase-field method. *Chem. Eng. Sci.* 2017, *17*, 230–241.

[30] Rabbani, S.; Osman, H.; Almaghrabi, Y.; Rahman, A.; Seers, M. The Control of Apparent Wettability on the Efficiency of Surfactant Flooding in Tight Carbonate Rocks. *Processes* 2019, *7*, 684–694.

[31] Ding, L.; Cui, L.; Jouenne, S.; Gharbi, O.; Pal, M.; Bertin, H.; Rahman, M.A.; Romero, C.; Guérillot, D. Estimation of Local Equilibrium Model Parameters for Simulation of the Laboratory Foam-Enhanced Oil Recovery Process Using a Commercial Reservoir. *ACS Omega* 2020, *5*, 23437–23449.

[32] Shachi; Yadav, B.K.; Rahman, M.A.; Pal, M. Migration of CO_2 through Carbonate Cores: Effect of Salinity, Pressure, and Cyclic Brine-CO_2 Injection. *J. Environ. Eng.* 2020, *146*, 04019114.

[33] Ahammad, J.; Rahman, M.A.; Butt, S.D.; Alam, J.M. An Experimental Development to Characterise the Flow Phenomena at the Near-Wellbore Region. In Proceedings of the ASME 2019 38th International Conference on Ocean, Offshore and Arctic Engineering, Glasgow, Scotland, UK, 9–14 June 2019.

[34] Elsanoose, A.; Abobaker, E.; Khan, F.; Rahman, M.A.; Aborig, A.; Butt, S.D. Experimental Investigation of Single Flow through Porous Media Around Perforation Tunnel. In Proceedings of the 7th Thermal and Fluids Engineering Conference, Las Vegas, NV, USA, 15–18 May 2022.

[35] Wen, Z.; Huang, G.; Zhan, H. Non-Darcian flow to a well in an aquifer–aquitard system. *Adv. Water Resour.* 2008, *31*, 1754–1763.

[36] Sedghi-As, M.; Rahimi, H. Adoption of Manning's equation to 1D non-Darcy flow problems. *J. Hydraul. Res.* 2011, *49*, 814–817.

[37] Salahi, M.-B.; Sedghi-Asl, M.; Parvizi, M. Nonlinear Flow through a Packed-Column Experiment. *J. Hydrol. Eng.* 2014, *9*, 04015003-1–04015003-9.

[38] McCorquodale, J.A.; Hannoura, A.-A.A.; Nasser, M.S. Hydraulic Conductivity Of Rockfill. *J. Hydraul. Res.* 2010, *16*, 123–137.

[39] Kadlec, R.; Knight, R. *Treatment Wetlands*; Lewis Publishers: Boca Raton, FL, USA, 1996.

[40] Yao, Y.; Li, G.; Qin, P. Seepage features of high-velocity non-Darcy flow in highly productive reservoirs. *J. Nat. Gas Sci. Eng.* 2015, *24*, 1732–1738.

[41] Elsanoose, A.; Abobaker, E.; Khan, F.; Rahman, M.A.; Aborig, A.; Butt, S.D. Estimating of Non-Darcy Flow Coefficient in Artificial Porous Media. *Energies* 2022, *15*, 1197.

Chapter 5

Investigation of Multi-phase flow in porous media around perforation tunnel Near Wellbore region, Experimental and Numerical Study

Preface

A version of this chapter has been published in OMAE 2021- 62915. I am the primary author of this manuscript, along with co-authors Dr. Abobaker, Dr. Faisal Khan, Dr. Rahman, Dr. Amer Aborig, and Dr. Butt. Dr. Butt assisted in the design of the setup. I proposed the idea and concept and prepared the samples with assistance from Dr. Amer and Abobaker; they also helped conduct the experiments. However, I collected and analyzed the experimental data. Dr. Aziz evaluated the methodology and reviewed the manuscript. I wrote the original manuscript, and Dr. Aziz reviewed the manuscript and suggested amendments that significantly impacted this manuscript.

5.1 Abstract:

Understanding the multi-phase flow behavior in the porous media near the wellbore region is essential for increasing wells' productivity and recovery. An experimental and numerical study of multi-phase flow in porous media near a perforation tunnel is presented. The effect of properties on the flow, such as porosity and permeability, are crucial for increasing oil and gas production. Five synthetic samples were created at Memorial university labs, the sample dimensions are 30.48 cm high and 15.54 cm diameter, and a perforation tunnel has a 25.54 cm depth and 2.54cm diameter. The air and water were injected into the sample radially at different flow rates, the water flow rate ranged from 1 to 3 LPM, and the air was 3 to 9 LPM. The simulation using ANSYS-Fluent 18.1 commercial software simulates the

volume of fluid method VOF coupled with the different turbulent models used to simulate the flow. The results showed that the pressure buildup in the porous media is greatly affected by the gas flow rate and permeability. The porosity have less effect on the pressure buildup profile in the porous media. The gas flow rate is the dominant factor for the breakthrough of a fluid in a core sample. Incorporating the gas flow in a porous system will reduce hydrostatic pressure loss, and less time is required to activate the breakthrough time.

5.2 Introduction

Multi-phase flow in porous media is encountered in chemical, petroleum, groundwater, soil contamination, subsurface remediation, and environmental engineering problems. The development in modeling and characterizing the multi-phase flow in porous media over a hierarchy of scales (pore-to-core, core-to-reservoir) showed encouraging theoretical and experimental results. The numerical and mathematical models are based on porous media's properties, including permeability, pore size, and other properties [1]. The permeability of porous media is an important parameter where its value determines the flow's type and behavior. It is an important parameter that helps to understand the behavior of transporting the gas mass in tight porous media. Relative permeability combines the properties of porous media, and fluids passing through the media are employed in some models; it is reasonable to consider wettability as an element that impacts the relative permeability. Wettability is a property related to the material surface nature, so the change in wettability effect on how the relative permeability changes the surfaces become more hydrophobic, the relative permeability of water increases significantly [2]. The determination of the permeability in porous media is combination of mathematical and

experimental methods under steady-state conditions at different pressure. Several factors, including absorption and slippage at the surfaces, influence permeability. Therefore, the actual and apparent permeability can be calculated using models derived from the laboratory experiment [3] [4] [5] [6] [7]. Porous media is not always homogenous, so it is no easy task to drive a mathematical model to represent two-phase flow in heterogeneous porous media because the size and path of the pores are not uniform. [8]. Therefore, most mathematical models presented in heterogeneous porous media are found for single-phase flow [9] [10]. Increasing oil reservoir production is a major goal for all oil producers; therefore, the interest in horizontal wells increased. The horizontal wells are characterized by their high productivity, especially in low reservoir pressure drawdown Figure 1. The method used in drilling the oil wells plays an important role in the left side effect on the porous media area surrounding the well. Rahman et al. compared the perforation by drilling technique with the traditional perforation technique by shooting (PS) for single-phase flow. Further, Rahman et al. studied the skin effect due to perforation with the same approach. In both works, it is found that during the PS technique, fine particles get redistributed around the perforation tunnel. The redistribution reduces the pore throat size, which is liable for permeability reduction significantly. As a result, the flow rates decrease at the same level of differential pressure. However, the reduction of permeability by the traditional perforation techniques has not been thoroughly investigated with the multi-phase flow in petroleum production engineering, especially in gas reservoirs. Rahman and Zheng investigated numerically and experimentally the formation damage of petroleum wells due to shooting in well completion [11] [12] [13]. The experimental study presented by Ahammad considered one-phase flow, while the numerical study investigated two-phase

flow. The first is based on ANSYS-CFX and the second is a computational methodology based on the weight residual collocation method. The effects of different Petro-physical properties, such as permeability, porosity, fluid viscosity, flow rates, and injection pressure, are analyzed in the simulations. In his numerical study, Ahammad concluded that the pressure buildup in the porous media is greatly affected by the gas flow rate, the media's permeability, and the fluid's temperature. The wellbore pressure and porosity have less effect on the pressure buildup profile in a porous media; the dominant factor for the breakthrough of a fluid in a core sample is the gas flow rate. Incorporating the gas flow in a porous system will reduce hydrostatic pressure loss, and less time is required to activate the breakthrough time [14]. The current workis a continuation of [14] work, and an experimental investigation will be presented to extend one phase of the experiment into two phases of flow, as will using different synthetic samples. As shown in Fig. 1, the horizontal oil wells are drilled horizontally. The wells' production can be increased by drilling perforations on both sides of the well's top and bottom sides.

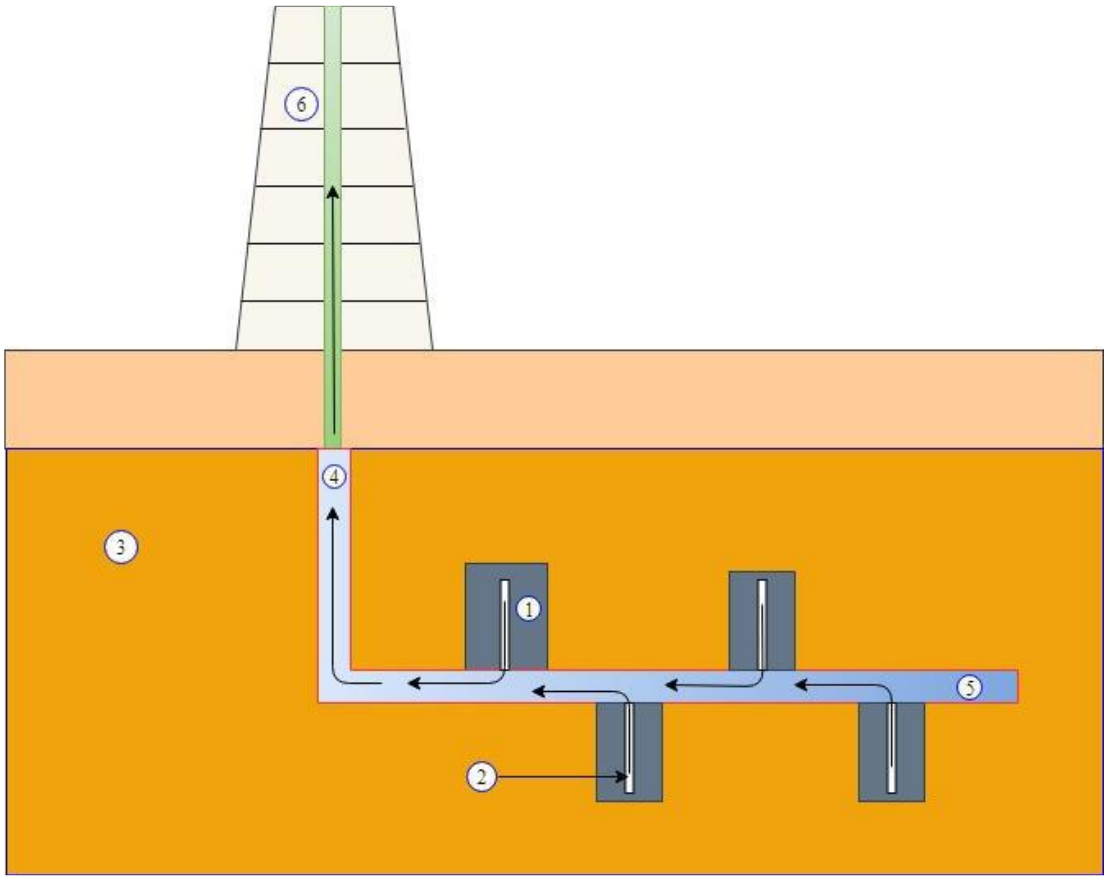

Figure 1. Horizontal Wellbore, 1, formation damage zone. 2, Perforation tunnel. Three undamaged zones. 4, Vertical Wellbore. 5, Horizontal Wellbore.

5.3 Experimental Procedure:

The experimental procedure of this work is divided into two stages, the first stage is the preparation of samples from sand and epoxy, and the second part is conducting two-phase flow experiments on the Radial Flow Cell facility.

5.3.1 Preparation of the Samples:

In the laboratory, five synthetic samples were created from sand collected from local sources. Using a hot-air oven, the sand was then dried in the civil engineering lab. The oven

is thermostatically controlled at temperatures between 105° C and 110° C. The sand was dried for 24 hours and then sieved Figure 2.

Figure 2. Sieving and Classification of the sand

The sand was then analyzed and categorized to measure the size of the sand grains quantitatively. At this stage, the sand was ready to create the samples. The sand and epoxy were mixed in different quantities (depending on the size of the sand) by using an electric mixer for 10 minutes. The mixture is then placed in a plastic container, and an electric vibrator is used to ensure the distribution of grain with the epoxy glue (Fig. 3). The sample dimensions are 30.48 cm high, 15.54 cm diameter, and a perforation tunnel has a 25.54 cm depth and 2.54cm diameter.

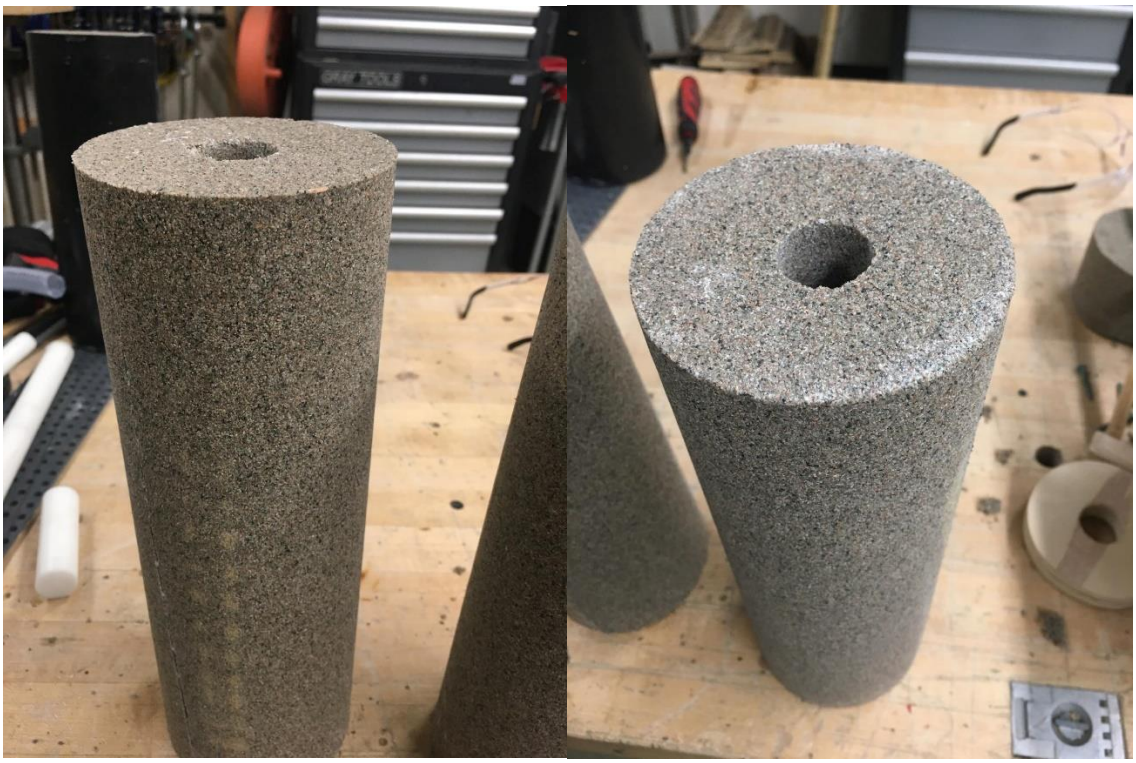

Figure 3. Synthetic Porous Media Samples

Table 1. The index properties for the samples.

Sam No	Permeability (mD)	Porosity (%)	Tortuosity	MPD (µm)
Sample 1	2035.95	21	3.62	25.31
Sample 2	6292.66	26	2.82	45.27
Sample 3	8127.04	27	2.27	60.61
Sample 4	16320.24	31	1.96	100
Sample 5	26151.72	33	1.7765	181.74

5.3.2 Performing the Flow Experiment

At this stage, five synthetic porous media samples were prepared: the next step is to conduct experiments. RFC Figure 4 [15] has been updated to be suitable for conducting multi-phase flow experiments, as five pressure sensors have been repaired and calibrated with pressure sensors from other experiments. Two pressure sensors were placed on the inlet and outlet, and the rest was placed on the fluid mixing lines. With help from the university's technical department, an air flowmeter was repaired and successfully calibrated. Also, another two lines were added to make the experiment ready to perform experiments on three phases flow. The experiment procedure begins by placing and fixing the sample in the cylinder, connecting the waterline, and connecting the air compressor with the mixing lines. The pressure sensors and flow meters are connected to the data acquisition to monitor the flow rate and record the pressure data during the experiment. The water flow rate was chosen to be from 1 to 3 liters per minute, and the airflow rate was 3 to 9 liters per minute. The main objective is to test the effect of changing the air flow rate on the pressure data and the shape of the pressure curve.

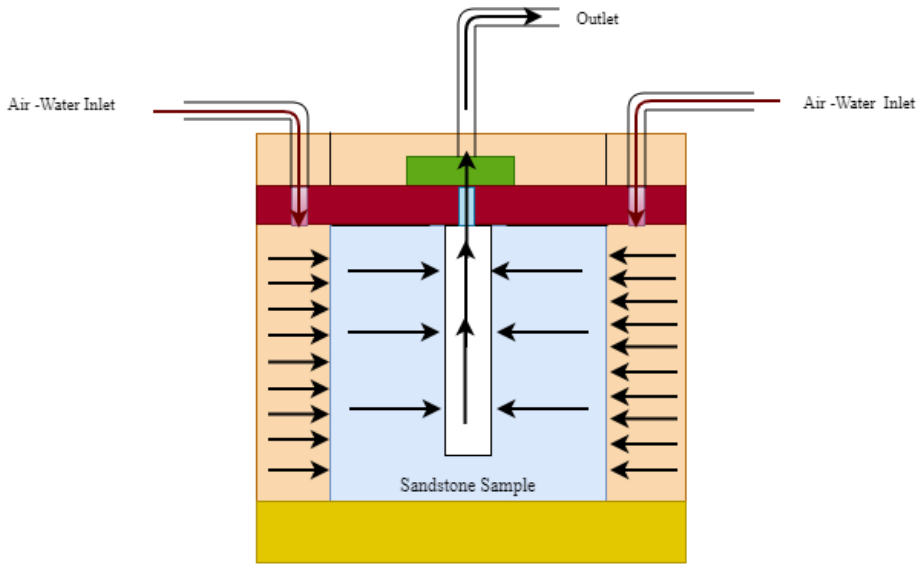

Figure 4. RFC facility

5.4 Numerical Procedure

ANSYS 18.1 FLUENT (3D) was used to simulate the multiphase flow pattern in the porous media. For the multi-phase flow model, the volume of fluid method coupled with the RNG k-ε turbulence model has been applied to solve the turbulent air-water flow pattern. The volume of fluid method (VOF) is designed for immiscible fluids where it can predict the situation of the interface between the immiscible fluids during the flow time. The k-ε turbulence model is the most common turbulent model used in the computational fluid dynamics field. The k-ε turbulence model derived from Reynolds Averaged Navier Stokes (RANS) equations is often applied for simulating multiphase flows, with greater or lesser success rates inaccuracy. Fig. 5 shows the geometry of the area surrounding the perforation; the geometry of a cylindrical core sample with a perforated hole at the center is used for the numerical simulations. The sample dimensions are 30.48 cm high, 15.24 cm radius, 2.54 cm radius of the perforation, and 25.4 the depth of the perforation.

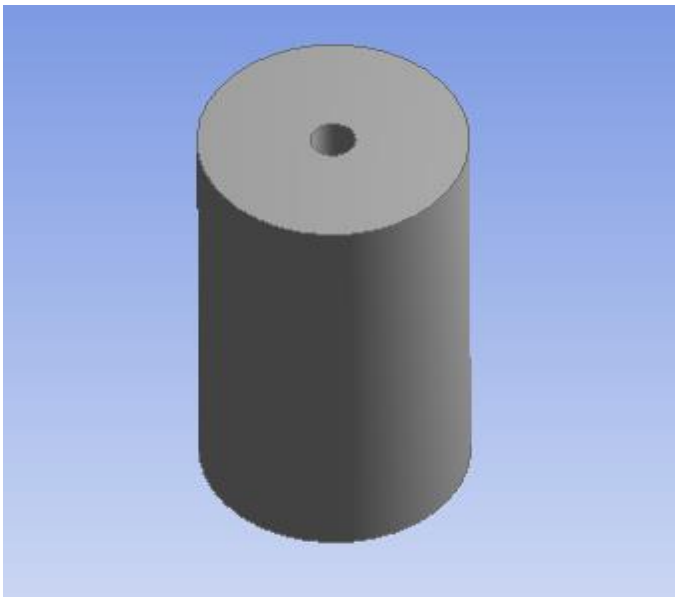

Figure 5. The sample geometry

5.4.1 CFD Simulation Technique

ANSYS is a well-known commercial software that assists in modeling fluid flow and other related fluid phenomena. ANSYS Fluent is a high-performance simulation tool that has been applied to solve wide-ranging fluid flow problems with reliable and accurate solutions. ANSYS fluent 18.1 for numerical simulations through a perforated tunnel in a reservoir well. A finite volume mesh with a smaller grid size and higher smoothing is used for more accurate results; the total number of the grid is 32000. The representation of the perforation in the formation pay zone and the simulated sample is presented in Fig. 6, with the cross-section of the domain mentioning possible damage. The validation of the CFD simulations for the perforation by drilling is performed with the experimental results. For meshing, ANSYS is used to generate a hexahedral mesh with no inflation Fig 6.

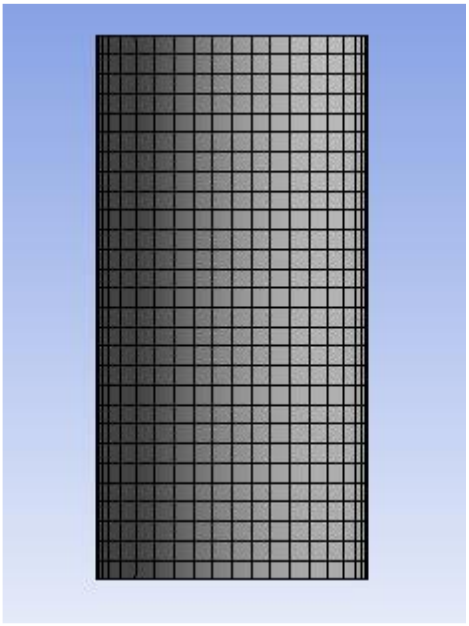

Figure 6. The Mesh distribution.

5.4.2 Governing Equations

fluids are entering from the reservoir to the perforated tunnel, so this is convenient to consider non-Darcy flow [16]. In the homogeneous multiphase flow system, a common flow field has the same characteristics as all fluids and other relevant fields, such as temperature. Therefore, the homogeneous model assumes that the transported quantities for that process remain the same for all phases. For porous regions in multiphase flow, ANSYS FLUENT calculations rely on volumetric flow rate. If we then assume isotropic porosity and multiphase flow, momentum and continuity equations describing two-phase flow in a porous region could be expressed, respectively, as (ANSYS, 2016)

$$\frac{\partial}{\partial t}(\gamma \alpha_q \rho_q) + \nabla(\gamma \alpha_q \rho_q \vec{v}_q) = \gamma \sum_{p=1}^{n} (\dot{m}_{pq} - \dot{m}_{qp}) + \gamma S_q \qquad (1)$$

$$\frac{\partial}{\partial t}\left(\gamma\alpha_q\rho_q\vec{v}_q\right)+\nabla\left(\gamma\alpha_q\rho_q\vec{v}_q\vec{v}_q\right)$$

$$=-\gamma\alpha_q\nabla.(p-p_c)+\nabla.\left(\gamma\bar{\tau}_q\right)+\gamma\alpha_q\rho_q\vec{B}_f$$

$$-\left(\alpha_q^2\gamma^2\frac{\mu_q\vec{v}_q}{KK_{r,q}}+\alpha_q^3\gamma^3\frac{C_{2\rho}\left|\vec{v}_q\right|\vec{v}_q}{2}\right)+\gamma\sum_{p=1}^{n}(\vec{F}_{pq}^{D}+\vec{F}_{pq}^{TD}+\dot{m}_{pq}\vec{v}_{pq}$$

$$+\dot{m}_{qp}\vec{v}_{qp})+\gamma(\vec{F}_q+\vec{F}_q^{L}+\vec{F}_q^{vm}) \quad (2)$$

Darcy and Forchheimer's forces are coupled with the momentum sink through *Fi*. The boundary conditions are the same as the experimental runs. The outer surface of the samples is considered the inlet, while the perforation is the outlet. The water's initial velocity ranged from 1 to 3 LPM while the air from 3 to 12 LPM. The air is considered an ideal gas, while the water is incompressible.

5.5 Results and Discussion

This research investigated a specific liquid and gas volume that was injected into the samples to determine the differential pressure of these samples and the time needed to achieve a steady state under various tested boundary conditions. The distribution of the injection build-up pressure for the two-phase flow through the perforation tunnel is shown in Figure 7. The comparison between the experimental, numerical, and two correlations results with the same flow boundary conditions is shown in Figure 8. The experimental data and numerical results are in good agreement.

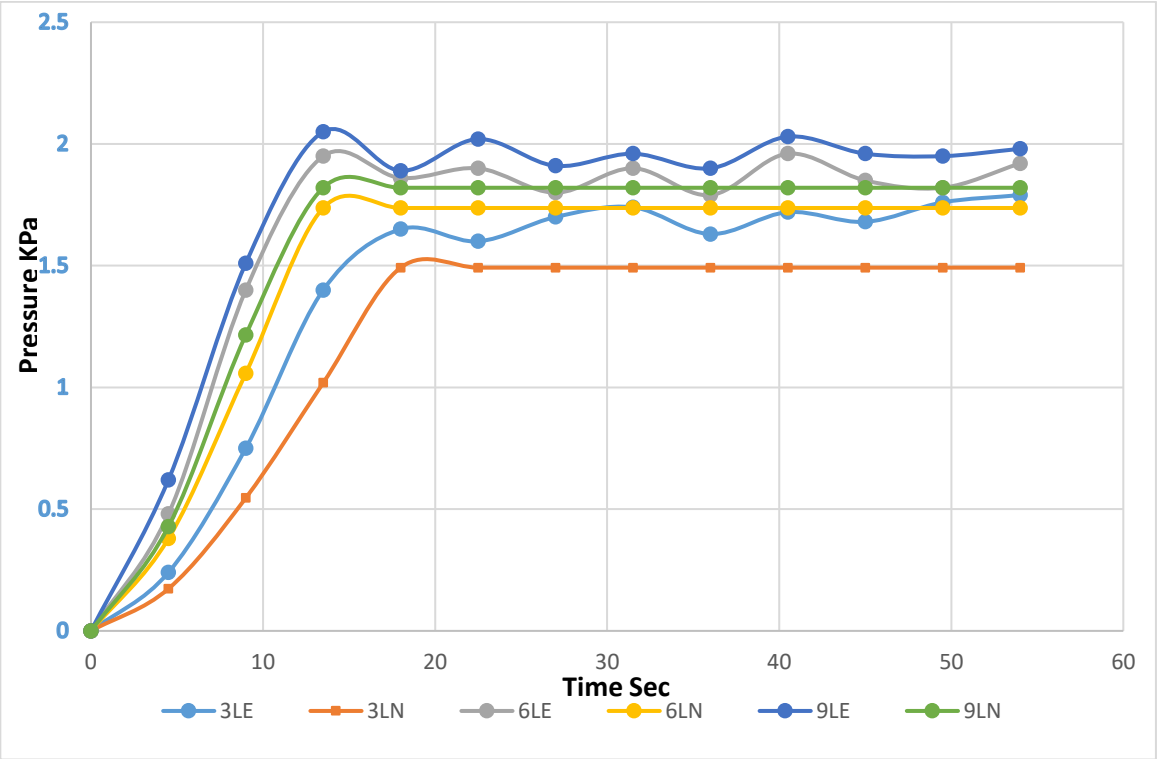

Figure (7) Sample No 5 k= 26 D 1LPM Water and 3-9LPM Air.

The addition of more water will eventually result in the formation of bubbles. This causes an intensification of the Jamin effect, where capillary pressure hinders the flow of bubbles and droplets past the narrow throat. The Jamin effect can critically impact two-phase flows occurring in reservoir porous substances at specific velocities.

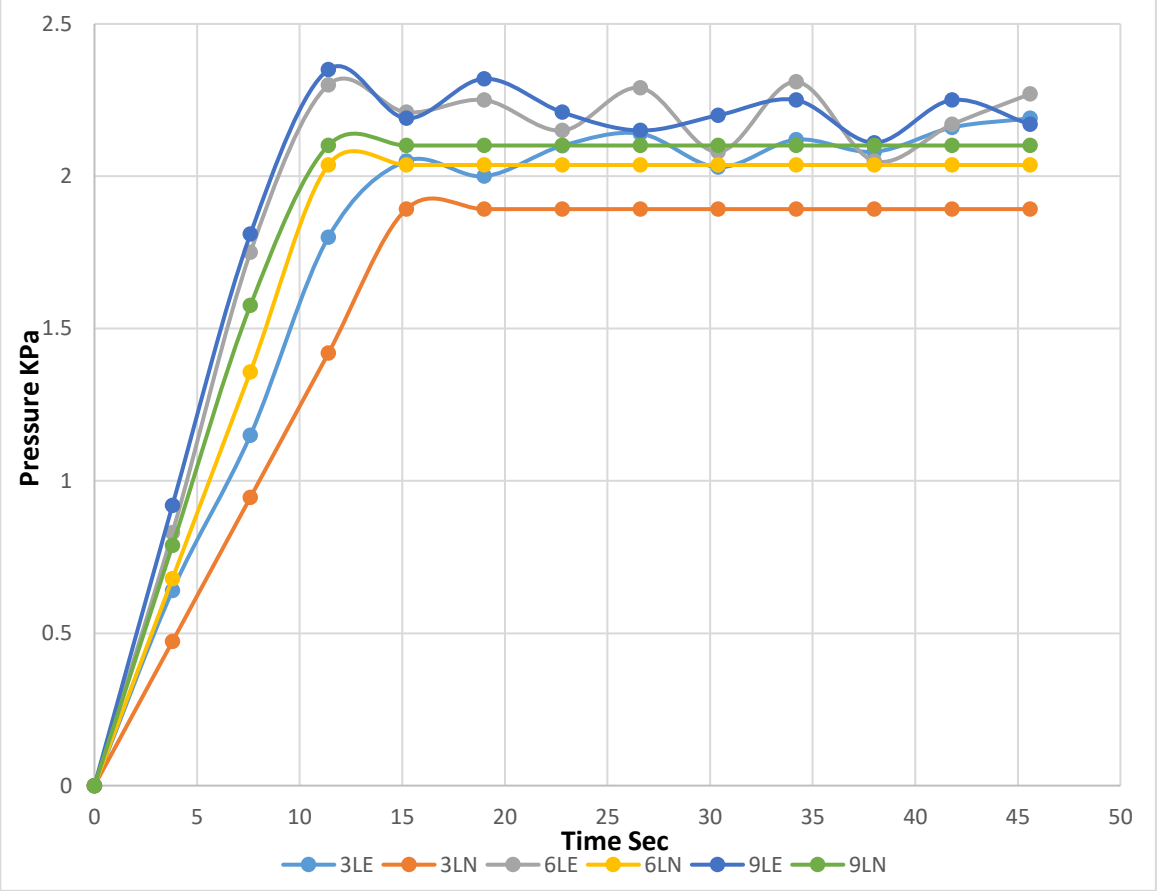

Figure (8) Sample No 5 k= 26 D 2LPM Water and 3-9LPM Air.

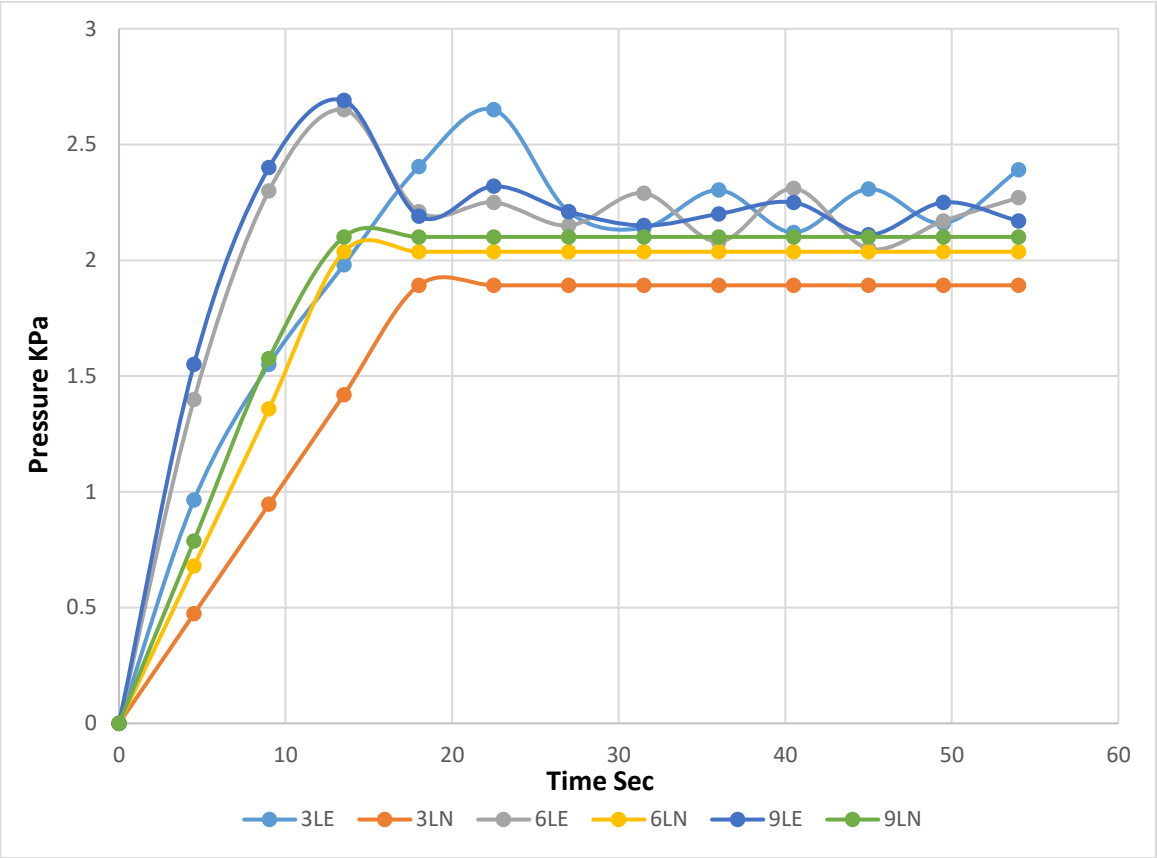

Figure (9) Sample No 5 k= 26 D 3LPMWater and 3-9LPMAir

5.5.1 Porosity Effect

Figure 10 describes how porosity influences the injection pressure for the mixture fluid. The porosity has fewer effects on the pressure after the steady-state condition is achieved. This is because porosity does not influence the injection pressure of any mixture of fluids. However, the porosity affects the pressure profile before the steady state for a lower porosity sample. The pressure profile achieves a higher value in the case of the low porosity sample compared to the other high porosity samples. The Jamin effect is dominant in the case of a low porosity sample before the steady-state condition is achieved.

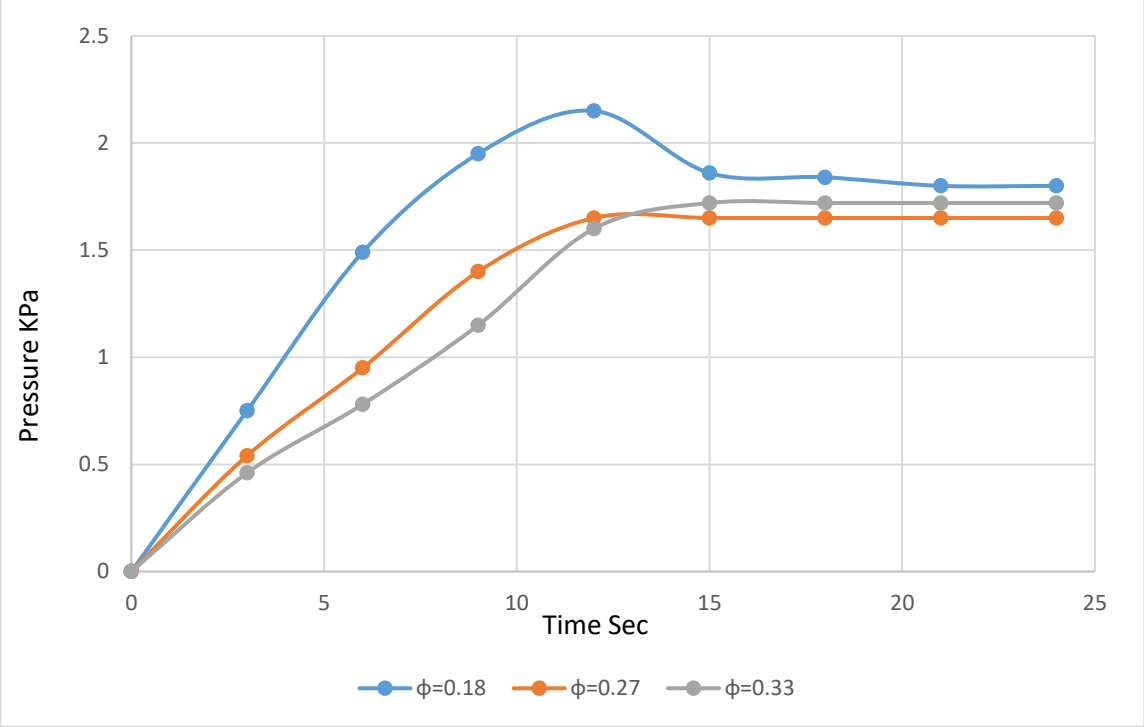

Figure 10 Porosity Effect on the pressure profile.Water 1LPM, Air 6 LPM

5.5.2 The effect of airflow rate on the pressure profile

The experimental results showed that the water flow rate affects steady-state flow while the airflow rate determines the pace of reaching the steady state. Figure (11) show the experimental results of the pressure profile of air-water two-phase flow. The water flow rate was fixed at 2 LPM while the airflow rate ranged from 3 – 12 LPM; the experimental run was on sample No 5, the permeability was 26 Darcy, and the porosity was 28 %. The time required for reaching steady-state conditions will be shorter with the higher airflow rate. Air helps to reduce the frictional pressure and static pressure loss in the porous medium.

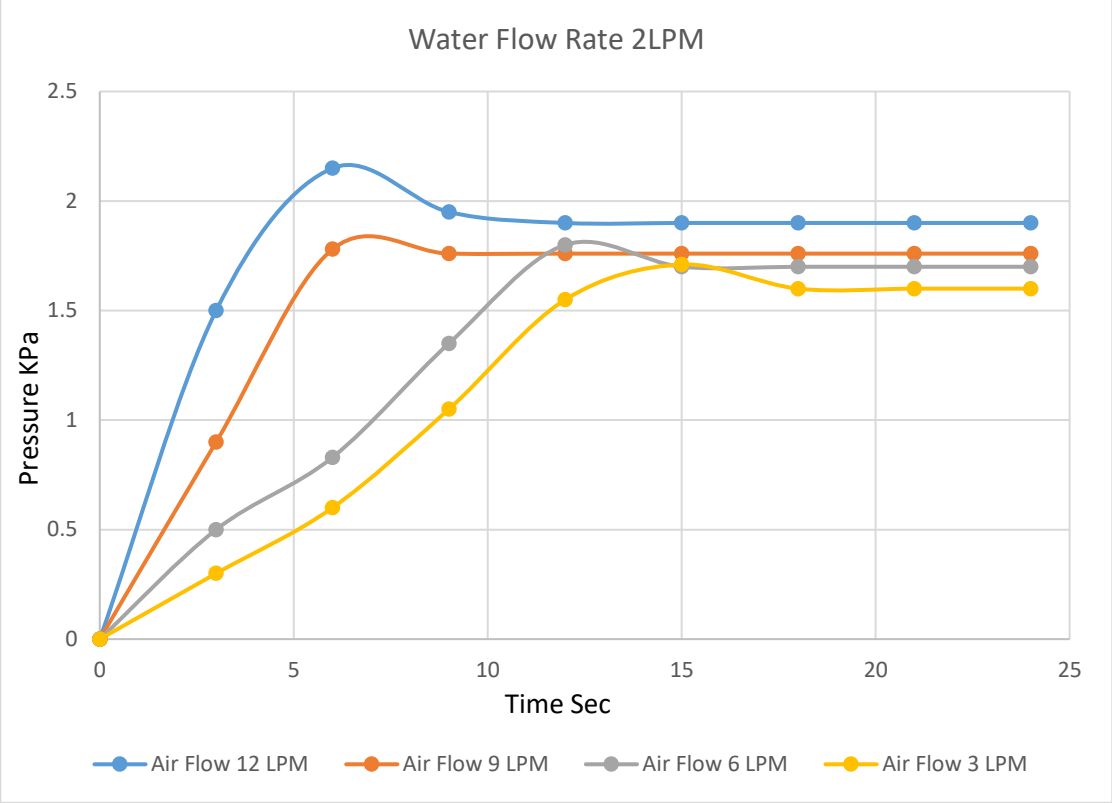

Figure (11) The effect of the airflow rate on the pressure profile, Sample 3.

5.5.3 Pressure distribution contours

Figure (12) illustrates the pressure distribution during the simulation starting at 2 sec from the beginning of the air-water injection. It can be seen that the pressure distribution starts to be uniform. With progressing in time, the effect of perforation depth does not reach the bottom of the sample begins to appear. When the flow reaches a steady state, the pressure at the bottom looks higher, as the perforation sealing causes the flow to tend to the top; as a result, the pressure rises.

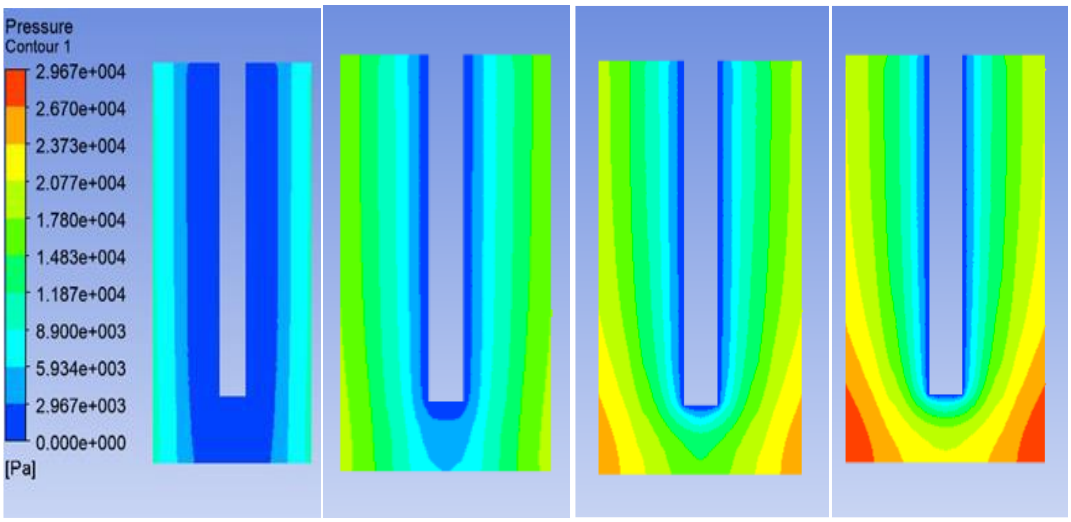

Figure (12) Pressure distribution during the simulation. Duration of 22 Sec

5.6 Conclusion

an experimental and numerical study of two-phase flow in porous media near a perforation tunnel is presented. The effect of properties, such as porosity and permeability, are crucial for increasing oil and gas production. Two-phase flow through a cylindrical porous media with a perforation tunnel sample experimentally and numerically tested. The proportion or fraction of the two phases is considered for calculating the mixture density. The two-phase flow was investigated considering the water flow rate as constant and changing the flow rate of air. A radial Flow Facility (RFC) was used to conduct the study's experimental part. ANSYS is a well-known commercial software that assists in modeling fluid flow and other related fluid phenomena. ANSYS Fluent is a high-performance simulation tool that has been applied to solve wide-ranging fluid flow problems with reliable and accurate solutions. The results showed that the pressure buildup in the porous media is greatly affected by the gas flow rate and its permeability. The wellbore pressure

and porosity have less effect on the pressure buildup profile in the porous media. The gas flow rate is the dominant factor for the breakthrough of a fluid in a core sample.

REFERENCES

[1] T. Xiao-Hua, L. Xiao-Ping, L. Jian-Yi and Z. Guang-Dong, "Analysis of permeability for transient two-phase flow in fractal porous media," JOURNAL OF APPLIED PHYSICS, pp. 113502/1-113502/6, 2014.

[2] A. Beltrán, D. Hernández-Díaz, O. Chávez, A. García, B. Mena and R. Zenit, "Experimental study of the effect of wettability on the relative permeability for air–water flow through porous media," International Journal of Multiphase Flow, vol. 120, p. 103091, 2019.

[3] J. Wang, L. Yu, and Q. Yuan, "Experimental study on permeability in tight porous media considering gas adsorption and slippage effect," Fuel, vol. 253, p. 561–570, 2019.

[4] Z. Zhu, R. Nathan, and Q. Wu, "An experimental study of the lubrication theory for highly compressible porous media with and without lateral leakage," Tribology International, vol. 127, p. 324–332, 2018.

[5] M. Fahad, F. Hussain, S. S. Rahman, and Y. Cinar, "Experimental investigation of upscaling relative permeability for two-phase flow in fractured porous media," Journal of Petroleum Science and Engineering, vol. 149, p. 367–382, 2017.

[6] Boubaker, S. Harmand, and V. Platel, "Experimental study of the liquid/vapor phase change in a porous media of two-phase heat transfer devices," Applied Thermal Engineering, vol. 143, p. 275–282, 2018.

[7] M. J. Ahammad, J. M. Alam, M. Rahman, and S. D. Butt, "Numerical simulation of two-phase flow in porous media using a wavelet-based phase-field method," Chemical Engineering Science, vol. 173, p. 230–241, 2017.

[8] A. Szymkiewicz, R. Helmig and H. Kuhnke, "Two-Phase Flow in Heterogeneous Porous Media with Non-Wetting Phase Trapping," Transp Porous Med, vol. 86, p. 27–47, 2011.

[9] F. F. Rocha, F. S. Sousa, R. F. Ausas, G. C. Buscaglia and Felipe Pereira, "Multiscale of mixed methods for two-phase flows in high-contrast porous media," Journal of computational physics, vol. 409, p. 109316, 2020.

[10] D. Dua, Y. Li, D. Zhang, X. Dong, F. Wang, and K. Chao, "Experimental study on the inlet behavior of CO2 foam three phase displacement processes in porous media," Experimental Thermal and Fluid Science, vol. 103, p. 247–261, 2019.

[11] L. Zheng, M. Rahman, M. Ahammad, S. Butt and J. Alam, "Experimental and Numerical investigation of a novel technique for perforation in petroleum reservoir," in SPE International Conference and Exhibition on Formation. Damage Control. Society of Petroleum Engineers., 2016.

[12] M. Rahman, S. Mustafiz, J. Biazar, M. Koksal, and M. Islam, "Investigation of a novel perforation technique in petroleum wells—perforation by drilling," Journal of J. Frankl. Institute, vol. 344, p. 777–789, 2007a.

[13] M. Rahman, S. Mustafiz, M. Koksal, and M. Islam, "Quantifying the skin factor for estimating the completion efficiency of perforation tunnels in petroleum wells.," vol. 58, no. 1, p. 99–110, 2007b.

[14] M. Ahammad, M. Rahman, L. Zhang, J. Alam, and S. Butt, "Numerical investigation of two-phase fluid flow in a perforation tunnel," Journal of Natural Gas Science and Engineering 606–611, vol. 55, p. 606–611, 2018.

[15] J. Ahammad, M. A. Rahman, S. D. Butt, and J. M. Alam, "Aa Experimenta Development To Characterise The Flow Phonomena At The Near-Wellbore Region," in Conference on Ocean, Offshore and Arctic Engineering, Glasgow, Scotland, UK, 2019.

[16] H. Belhaj, K. Agha, A. Nouri, S. Butt, H. Vaziri and M. Islam, "Numerical Simulation of Non-Darcy Flow Utilizing the New Forchheimer's Diffusivity Equation," in SPE conference, Bahrain, 2003.

Chapter 6

Conclusion and future work

This study's overall objective is to present a better understanding of the fluid flow behavior in porous media and pressure gradient as a function of single and two-phase flow rate conditions. The presence of inertia forces characterizes the non-Darcy flow; the Forchhiemer equation is the mathematical model used that represents the relationship between the pressure and inertia forces. The non-Darcy or the inertia coefficient β is the key constant representing the inertial resistance in a porous medium and depends on the pore geometry and fluid properties. Therefore, the study assessed how different porous media properties index and the flow conditions affect the non-Darcy flow. In addition, the pressure and flow data and synthetic porous media properties were used to introduce correlations through which the non-Darcy flow coefficient can be calculated. The study methodology included sample preparation, updating the experimental setup, conducting the flow experiments, analyzing the collected data, verifying the non-Darcy flow, and finally investigating the two-phase flow.

A new technique has been presented to prepare homogenous synthetic samples used in this study and can be applied in hydrocarbon recovery projects. The sand was mixed with epoxy in appropriate quantities so that the samples acquired a suitable hardness and, at the same time, the epoxy did not close the pores of the porous media.

Mercury intrusion porosimetry (MIP) and scanning electron microscopy (SEM) have been used first to characterize and analyze the pore morphology and index properties of the

synthetic samples. The experimental results indicated that mixing and grain size strongly affects weak solidified index characteristics.

An experimental study investigated the single-phase flow in porous media around a perforation was presented. Compressible and incompressible fluids experimented on a wide range of flow rates. Different approaches were used to detect the non-Darcy flow; for the compressible flow, the square pressure differences vs. the flow rate curve, and Reynolds number vs. friction factor for incompressible flow. The results showed that the non-Darcy flow behavior exists in the flow rate range used in this experiment.

The non-Darcy coefficient is essential to the Forchhiemer equation, representing the inertia forces. Therefore, an experimental study was conducted to calculate the non-Darcy coefficient, seven synthetic porous media were prepared, and the air was used in the flow experiments. The study concluded that the non-Darcy coefficient decreases with the median pore diameter and porosity increase. The existence of a non-Darcy flow was confirmed for all the investigated samples. The Forchheimer numbers for airflow at varied flow rates are determined using experimentally measured superficial velocity, permeability, and non-Darcy coefficient.

The non-Darcy flow in incompressible flow was analyzed. The data were collected using seven large samples, and the flow was radially injected, which is uncommon in the literature; the flow rate ranges from 0.33 to 6 LPM. The hydraulic gradient was employed to determine the non-Darcy flow in the samples where the water (incompressible) was used in the experiment runs. The hydraulic gradient vs. velocity curve revealed that the non-Darcy flow is more apparent in the samples with low permeability; however, as the

permeability increases, the flow tends toward the Darcy flow. This study produced two reliable correlations, one of which considered tortuosity a critical parameter.

The study also aimed to enhance oil recovery by modeling a two-phase flow in the near-wellbore region, thereby expanding industry knowledge about wells' performance. An experimental procedure investigated two-phase flow behavior through a cylindrical perforation tunnel. The experimental data were validated to the numerical results, and the comparison of results was in good agreement. The numerical analysis demonstrated each investigated parameter's effect. The permeability, flow rate, and viscosity of the liquid significantly affect the injection pressure build-up profile, and porosity and gas flow rate substantially affect the time required to attain steady-state conditions.

Future Work

This study can be extended to many applications related to flow in porous media. The RFC is unique because it enables us to inject the fluids radially, which is close to the real situation in the near wellbore region. The experimental setup has been updated to be suitable for three-phase flow experiments, opening many research doors in this field. In addition, in this research, the sample preparation technique was developed where samples can be easily prepared without needing real samples, which cost a lot. It isn't easy to obtain real samples with suitable permeability for laboratory experiments. This work can extend the testing of other fluids, such as nitrogen, carbon dioxide, and oil, that we could not test due to the pandemic and lack of time and funding. Non-Newtonian fluids, which are involved in many engineering applications, are another option that can be tested on this

device. Chemical and hazardous materials used in cleaning and removing impurities are one of the hot research topics possible on this device if it is correctly updated.

Appendix

1. Uncertainty Calculation for Chapter 5

The sixth chapter presented a laboratory study on biphasic flow. Water and air were mixed with different flow rates, and the pressure data was recorded each time. The water flow rate ranged from 1 to 3 liters per minute, while the air flow rate ranged from 3 to 12 liters per minute. In all, 180 laboratory experiments were performed. The following is the uncertainty calculation for the five samples at a water flow rate of 2 liters per minute and air at 9 liters per minute.

The uncertainty in the results can be estimated from the uncertainties in the primary measurements. Assume that experimental measurement of independent variables, $V_1, V_2, , V_3, \dots, V_n$ are taken, then replicate the measurement's mean value V_m may be expressed as

$$V_m = \frac{V_1, V_2, , V_3, \dots, V_n}{n} = \frac{\sum_{i=1}^{n} V_i}{n} \quad (1)$$

In statistical parlance, the term "uncertainty" is associated with a measurement that refers to the expected variation of the value derived from an average of several readings from the true mean of the data set or readings. In other words, the uncertainty can be considered the standard deviation of the data set's mean. The formula for uncertainty can be derived by summing squares of deviation of each variable from the norm, then dividing the result by the product of the number of readings and the number of readings minus one, and then

computing the square root of the outcome. Mathematically, the Uncertainty Formula is represented as, Where

$$U = \sqrt{\frac{\sum_{i=1}^{n}(V_i - V_m)}{n * (n-1)}} \quad (2)$$

Where U is the uncertainty, V_i is a reading, V_m

The uncertainty in the experimental measurements of temperature, pressure, and flow rate are summarized in Table 1.

Table 1. Uncertainty in Measurements

Measurement	**Uncertainty** Pressure [Pa]
Sample 1	$\pm 0.1\%$
Sample 2	$\pm 0.42\%$
Sample 3	$\pm 0.18\%$
Sample 4	$\pm 0.25\%$
Sample 5	$\pm 0.9\%$

CFD Calculations Mesh Independence

In the fifth chapter, laboratory results were compared with numerical simulations. The volume of Fluid The numerical simulation method was used to produce the numerical model in the ANSYS software. Ensuring that the numerical simulation results are independent of the grid number is essential. The different mesh numbers are used to simulate the flow rate through sample 4, the airflow rate is 9 LPM, and the water flow rate is 1 LPM. The mesh number has been chosen to be 45k, 50k, and 55k. Figure 1 shows the results of the pressure calculations in sample 5.

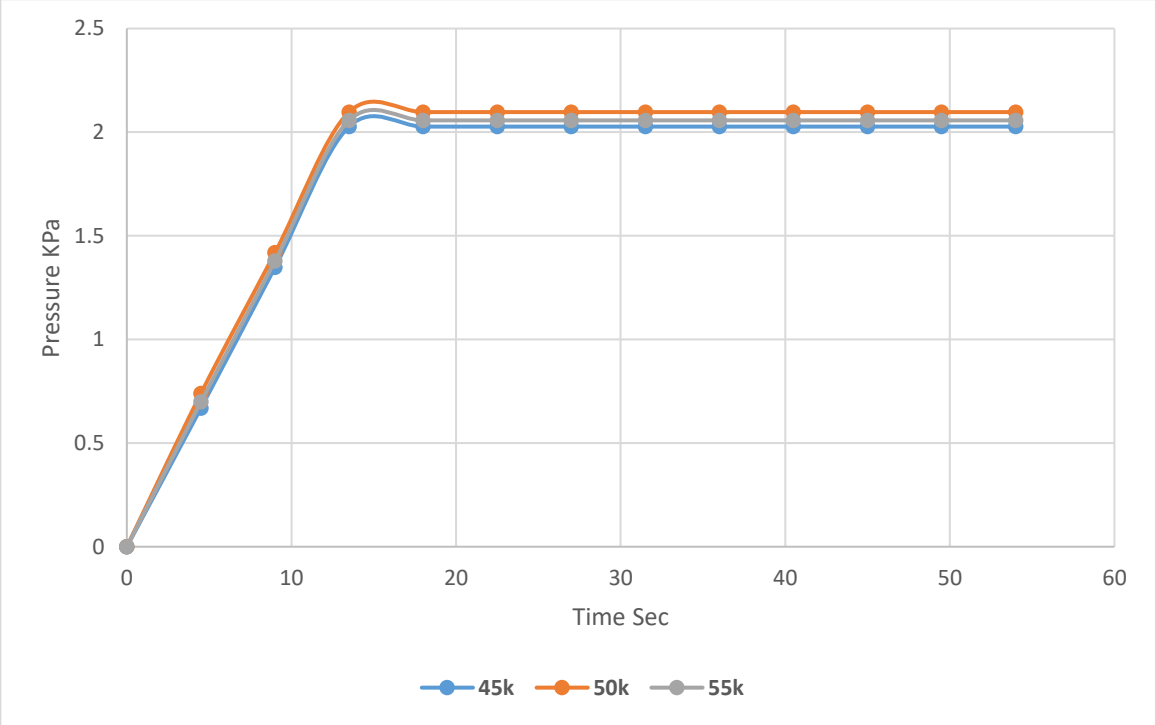

Figure 1. Mesh independency calculations

As can be seen, increasing the mesh number has a minimal effect on the numerical simulation, where the change is about ± 0.06%.